Mantle Melting Processes: Evidences from Ophiolites, Large Igneous Provinces, and Intraplate Seamounts.

María del Pilar Madrigal Quesada

Dissertation submitted to the faculty of the Virginia Polytechnic Institute and State University in partial fulfillment of the requirements for the degree of

Doctor of Philosophy

In

Geosciences

Esteban Gazel, Chair

Jonathan E. Snow

Mark J. Caddick

D. Sarah Stamps

May 2nd, 2016

Blacksburg, Virginia

Keywords: Santa Elena Ophiolite, mantle geochemistry, mantle petrology, melting processes, isotope geochemistry, major and trace element geochemistry, large igneous provinces, ophiolites, seamounts.

Mantle melting processes: evidences from ophiolites, large igneous provinces, and intraplate seamounts.

Pilar Madrigal

ABSTRACT

Melting processes in the mantle have a key role in plate tectonics and in the most colossal phenomena in the Earth, like large igneous provinces, mantle plume upwellings, and the constant growth of the planet's tectonic plates. In this study we use the geochemical and petrological evidence preserved in ophiolites, large igneous provinces, and intraplate seamounts to understand causes, timing and implications of melting in these different tectonic environments.

We studied melting at extensional environments, in mid-ocean ridges and back-arc basins, preserved in ophiolites. The Santa Elena Ophiolite in Costa Rica comprises a well-preserved fragment of the lithospheric mantle that formed along a paleo-spreading center. Petrological models of fractional crystallization suggest deep pressures of crystallization of >0.4 GPa for most of the samples, in good agreement with similar calculations from slow/ultra-slow spreading ridges and require a relatively hydrated (~0.5 wt% H_2O) MORB-like source composition. Our findings suggest a complex interplay between oceanic basin and back-arc extension environments during the Santa Elena Ophiolite formation.

Secondly, we analyzed large igneous provinces and their mechanisms of formation. As the surface expression of deep mantle processes, it is essential to understand the time frames and geodynamics that trigger these massive lava outpourings and their impact to life in the planet. We analyze the record and timing of preserved fragments of the Pacific Ocean Large Igneous Provinces to reconstruct the history of mantle plume upwellings and their relation with a deep-rooted source like the Pacific Large Low Shear Velocity Province during the Mid-Jurassic to Upper Cretaceous.

Lastly, we explore the occurrence of low-volume seamounts unrelated to mantle plume upwellings and their geochemical modifications as they become recycled inside the mantle, to answer questions related to the nature and origin of upper mantle heterogeneities. We present evidence that an enriched mantle reservoir composed of recycled seamount materials can be formed in a shorter time period than ancient subducted oceanic crust, thought to be the forming agent of the HIMU mantle reservoir endmember. A "fast-forming", enriched reservoir could explain some of the enriched signatures commonly present in intraplate magmas not related with an active mantle plume upwelling.

Dedicated to my Mom, Milagro

Acknowledgements

First and foremost, I want to thank Esteban Gazel for encouraging me to pursue a scientific career, and to go the extra mile in everything that I do. I would not be here if it wasn't for your support and patience. I will be forever grateful for this opportunity and can only hope to help my future students advance their careers in the same way that you did.

Thanks to Sarah Stamps, Mark Caddick and Jon Snow who were there with insightful discussions and helped me improve my work and gave me ample professional advice. Thank you to our collaborators: Percy Denyer, Drew Coleman, Brian Jicha, Ian Smith, Michael Bizimis, Ricardo Sanchez.

I want to acknowledge Esther Schwarzenbach and Kennet Flores who have been terrific mentors and collaborators. Special thanks to the VT Volcanoes Group: Sarah, Jarek, Lowell, Lisa, Ty, Denis and our honorary members, Besim and Claudia, who actually witnessed the evolution of my projects since the beginning and were always ready to give great input to the process. These years at VT would not have been the same without them.

But above all, I want to thank my family, Renee, Sarita, Gaby, Jose Pablo, Marianito, Drew and friends who supported me through, possibly, the hardest moments of my life, while trying to thrive in Grad School. Specially Drew, who keeps me sane and hopeful still today. My love to all.

To my mom, Milagro, infinite thanks. She gave me purpose and kept me dreaming about all the possibilities that lie in the future, until the end. You are still my engine, and this is only the beginning.

Attributions

Several co-authors contributed during the research and writing of the manuscripts that constitutes this dissertation.

Chapter 1 was published as Madrigal, P., Gazel, E., Denyer, P., Smith, I., Jicha, B., Flores, K.E., Coleman, D., Snow, J., 2015. A melt-focusing zone in the lithospheric mantle preserved in the Santa Elena Ophiolite, Costa Rica. Lithos 230, 189-205. P. Madrigal was responsible for sample analysis, project development, writing the manuscript. E. Gazel helped with the project conception, data analysis, writing the manuscript. P. Denyer contributed with the project conception and field work. I. Smith, B. Jicha, D. Coleman, helped with the analytical work. J. Snow and K. Flores aided with interpretations and manuscript revisions.

Chapter 2 was submitted as Madrigal P., Gazel E., Flores, K., Jicha, B., Bizimis, M., (in rev.). Record of the Pacific LLSVP upwellings in the Cretaceous. *Submitted to Nature Communications.* P. Madrigal contributed to project conception, sample and data analysis, interpretations and manuscript writing. E. Gazel and K. Flores aided with insightful discussions and were responsible for project conception, interpretations and manuscript writing. K. Flores created the kinematic paleotectonic models. B. Jicha and M. Bizimis aided with the analytical work and manuscript revisions.

Chapter 3 is currently under preparation for submission. P. Madrigal and E. Gazel are responsible for project conception and development, data analysis and modelling, and manuscript writing. J. Snow collaborated with revisions and comments.

Table of contents

List of figures

Introduction

The Earth's mantle is in a constant state of changing and the melting processes occurring at all depths in the mantle can attest for this dynamism. Melting occurs by the means of changes on the physical and chemical conditions of portions of the mantle: increases in temperature, decreases in pressure, a change in composition that lowers the mantle solidus. It is no surprise then, that melting seems to be favorable at locations where either decompression (mid-ocean ridges), thermochemical anomalies (mantle plumes) or H_2O input (subduction zones) are responsible for the mechanisms of melting.

Nevertheless, there are circumstances where melting occurs in a less understood manner, either because of physical inaccessibility or restricting time scales. For example, at slow-spreading ridges where magma is generated at high depths; at locations where a mantle plume impacts the lithosphere to create a large igneous province in short periods of time (<5Ma); or at low-volume, monogenetic volcanic seamounts unrelated to mantle plume upwellings.

This study aims to contribute to the understanding of how melting occurs in these atypical settings by exploring the geochemical and petrological characteristics of melting products from concrete locations and comparing them to other examples worldwide.

Chapter I concerns the study of the melt focusing zone preserved at the Santa Elena Ophiolite in Costa Rica. For this study I collected geochronological, geochemical, and structural data from the diabase intrusions that crosscut the peridotite to interpret the origin of the ophiolite. This chapter culminated in a publication in the journal Lithos in 2015:

MADRIGAL, P., GAZEL, E., DENYER, P., SMITH, I., JICHA, B., FLORES, K.E., COLEMAN, D., SNOW, J., 2015. A melt-focusing zone in the lithospheric mantle preserved in the Santa Elena Ophiolite, Costa Rica. Lithos 230, 189-205.

Chapter II covers the study of the link between deep mantle dynamics, melting during large igneous province (LIP) events, and the implications of these phenomena for life in the planet. For this, I collected geochronological and geochemical data from accreted LIP terranes at the margins of Nicoya Peninsula in Costa Rica. To assess the provenance of these LIP fragments we created a series of kinematic models that show the paleotectonic evolution of these terranes. Our kinematic models suggest a clear relationship between the emplacement of LIPs, the location of mid-ocean ridges, and potential pulses of deep mantle upwellings, which is also confirmed by our petrological models, created for LIPs globally. This chapter is currently under review in the journal *Nature Communications.*

MADRIGAL P., GAZEL E., FLORES, K., JICHA, B., BIZIMIS, M., (in rev.). Record of the Pacific LLSVP upwellings in the Cretaceous. *Submitted to Nature Communications.*

Chapter III aims to understand the nature of heterogeneities ubiquitous to the upper mantle. Pockets of more enriched recycled material in the upper mantle tend to melt preferentially compared to the surrounding peridotite. These heterogeneities are sampled by mid-ocean ridges, creating enriched MORB signatures (EMORB), or by low-volume intraplate magmatic processes. We collected geochemical and geochronological data from non-plume related seamounts accreted to the margins of the Santa Elena Peninsula in Costa Rica, as a proxy for the composition of subducted seamounts that later become these low-volume heterogeneities in the upper mantle. We modeled the progressive enrichment of their isotopic evolution to suggest that the recycling times of these seamounts are ~200 Ma-500 Ma. In this time interval, subducted seamounts can become

as enriched as HIMU-type reservoirs. Our binary mixing models suggest that an enriched non-plume seamount reservoir in the upper mantle may be responsible for the isotopic diversity observed in global examples of ocean island basalts and EMORB. This chapter will be submitted to Earth and Planetary Science Letters.

Chapter 1: A melt-focusing zone in the lithospheric mantle preserved in the Santa Elena Ophiolite, Costa Rica

Abstract

The Santa Elena Ophiolite in Costa Rica is comprised of a well-preserved fragment of the lithospheric mantle that formed along a paleo-spreading center. Within its exposed architecture, this ophiolite records a deep section of the melt transport system of a slow/ultra-slow spreading environment, featuring a well-developed melt-focusing system of coalescent diabase dikes that intrude the peridotite in a sub-vertical and sub-parallel arrangement. Here we present an integrated analysis of new structural data, $^{40}Ar/^{39}Ar$ geochronology, major and trace element geochemistry and radiogenic isotopes data from the diabase dikes in order to elucidate the tectonic setting of the Santa Elena ophiolite. The dikes are basaltic and tholeiitic in composition. Petrological models of fractional crystallization suggest deep pressures of crystallization of >0.4 GPa for most of the samples, which is in good agreement with similar calculations from slow/ultra-slow spreading ridges and require a relatively hydrated (~0.5 wt% H_2O) MORB-like source composition. The diabase dikes share geochemical and isotope signatures with both slow/ultra-slow spreading ridges and back-arc basins and indicate mixing of a DMM source and an enriched mantle end-member like EMII. The $^{40}Ar/^{39}Ar$ geochronology yields an age of ~131 Ma for a previous pegmatitic gabbroic magmatic event that intruded the peridotite when it was hot and plastic and an age of ~121 Ma for the diabase intrusions, constraining the cooling from near asthenospheric conditions to lithospheric mantle conditions to ~10 Ma. Our findings suggest a complex interplay between oceanic basin and back-arc extension environments during the Santa Elena Ophiolite formation. We propose an alternative hypothesis for the origin of Santa Elena as an obducted fragment of an oceanic core complex (OCC).

1. Introduction

To understand the evolution of our planet, it is fundamental to constrain melt generation and transport processes that occur in the mantle. In an extensional environment, when the upper mantle crosses its solidus through decompression, melting initiates as an inter-granular network of melt (Karato and Jung, 1998; Kelemen et al., 2000; Faul, 2001; Dasgupta and Hirschmann, 2006). Then, physical and chemical changes during reactive melt transport allow segregation of the partial melts increasing the porosity of the upper mantle host (Kelemen et al., 1997; Kelemen et al., 2000; Spiegelman et al., 2001). At extensional environments like mid-ocean ridges (Fig. 1.1), basaltic melts separate from the peridotite residue and react with the lithospheric mantle as they rise buoyantly through this network of melt (Kelemen et al., 2000; Bouilhol et al., 2011). After these ascending melts coalesce and evolve beneath the ridge axis they erupt to produce new oceanic crust (O'Hara, 1985).

Because it is difficult to reach deep segments of extensional regimes (i.e. mid-ocean ridges, fore-arc basins, back-arc basins) we rely on more accessible geologic features as analogous to these environments, such as ophiolites. Ophiolites consist of ultramafic and mafic mantle lithologies that formed along spreading centers and get subsequently obducted or exposed onto continents by tectonic processes. Conceptually, ophiolite assemblages are composed from bottom to top, of peridotite (including lherzolite, harzburgite and dunite) variably altered to serpentinite; gabbro and diabase intrusions; and extrusive sequences of pillow lavas and massive flows that are typically overlain by deep-sea sediments (Coleman, 1971; Dewey and Bird, 1971; Dewey, 1976; Steinmann et al., 2003; Dilek and Furnes, 2011, 2014). Although such lithological associations have commonly been attributed to mid-ocean ridge or back-arc origin, other interpretations for ophiolite origins also exist, such as supra-subduction zone (SSZ) ophiolites, plume-related

ophiolites and continental margin ophiolites (see Dewey and Casey, 2011; Dilek and Furnes, 2014 and references therein).

Based on geochemical affinities and order of mineral crystallization, Dilek and Furnes (2011) developed a first order classification, separating ophiolites as subduction-related and subduction-unrelated types. Within their classification, mid-ocean ridge (MOR) type ophiolites show geochemical consistency with normal mid-ocean ridge basalt (MORB). Depending on the proximity to features like mantle plumes, the geochemical affinity may fluctuate from MORB all the way to enriched MORB (EMORB). In contrast, subduction-related ophiolites show a progressive geochemical affinity from MORB-like to Island Arc Tholeiite (IAT) and Boninite in the later stages of SSZ ophiolites (Dilek and Furnes, 2011).

Even though the geochemical affinities expected in ophiolites are well-established, secondary processes occur after the formation of new oceanic crust must also be considered. Hydrothermal systems that transport heat from the magma lenses to the surface interact with the crust resulting in hydrothermal alterations and ocean floor metamorphism (Pearce, 2008; Pearce, 2014 and references therein). Enrichments in large ion lithophile elements (LILE) that are usually attributed to an arc-related fluid interaction between the subducting slab and the mantle wedge, could easily be mistaken with seawater interaction and contamination during the emplacement of hot oceanic crust, and vice versa (Boudier et al., 1988; Nicolas and Boudier, 2003). Therefore, the discrimination between MOR-type ophiolites and SSZ ophiolites has to be done carefully and by integrating several geochemical tools. Consequently, in order to accurately assess the geochemical fingerprinting of ophiolites, it is necessary to look at the fluid-immobile element data. Fluid-immobile elements remain unaltered during weathering and low-temperature alteration. These elements are characterized by high to intermediate charge/radius ratios and include most of the

rare-earth elements (REE) and high field strength elements (HFSE) (Pearce, 2014). The concentration of these elements is controlled by the chemistry of the magma source and the crystallization processes that occur during the magmatic evolution. Several authors have worked on creating fluid-immobile element proxies, which are compared to element ratios that correlate with a specific geological process (Cann, 1970; Pearce and Cann, 1971; Floyd and Winchester, 1975; Pearce, 1975; Shervais, 1982; Sun and McDonough, 1989; Pearce, 2008).

Another useful parameter for ophiolite characterization is its preserved architecture. Variations of the magma supply and spreading rates can modify the architecture of the new oceanic lithosphere (Nicolas and Boudier, 2003; Dilek and Furnes, 2011). Ishiwatari (1985) linked petrological and compositional features of ophiolites to their genesis and to variations in the spreading rates (Fig. 1.1). In this regard, the structure and composition of an ophiolite can aid to the elucidation of the paleo-spreading rate (Cannat, 1996; Godard et al., 2000; Dick et al., 2003; Michael et al., 2003; Godard et al., 2008; Cannat et al., 2009; Till et al., 2012). Additionally, the composition of the constituent peridotites and associated melts can contribute to characterize the origin of an ophiolite. For instance, while harzburgite compositions may represent an uppermost oceanic mantle melt source and higher degrees of partial melting, lherzolite compositions evidence a deeper oceanic mantle, as they represent more fertile residues subject to lesser degrees of partial melting (Fig. 1.1) (Jackson and Thayer, 1972; Boudier and Nicolas, 1985; Dilek and Furnes, 2011). Thus, ophiolite segments around the globe provide windows into fossilized melt transport systems that once fed the oceanic or arc crust and upper mantle. The presence of a zone of intense dike emplacement that represents the melt-focusing part of the system is a common feature in these exposed sections of the mantle (Robinson et al., 2008). When present, these dike networks provide an insight to the magmatic origin and geochemical evolution of a particular ophiolite.

Our study presents new $^{40}Ar/^{39}Ar$ ages, major and trace element data, and radiogenic isotopes from melts that intruded the Santa Elena Ophiolite, located in the northwestern Pacific coast of Costa Rica. This ophiolite represents an emplaced fragment of 250 km^2 of upper mantle lithologies overthrusting an ancient accretionary complex (Tournon, 1994; Baumgartner and Denyer, 2006; Denyer et al., 2006; Gazel et al., 2006; Denyer and Gazel, 2009; Tournon and Bellon, 2009; Escuder-Viruete and Baumgartner, 2014) (Fig. 1.2a). Occurrences of diabase dikes around the peninsula are frequent, however the well-preserved diabase dike transport system is largely exposed in two different sections of this ophiolite: the northwestern swarm and the southeastern swarm (Fig. 1.2c). In both outcrops, the diabases intrude lherzolite peridotite (Gazel et al., 2006; Tournon and Bellon, 2009). The goal of this integrated structural, geochemical and petrological analysis of the diabase melt-focusing system is to elucidate the magmatic origin and evolution of the Santa Elena Ophiolite and the implications of its origin in the understanding of melt transport and the evolution of the lithospheric mantle.

2. Geotectonic Background of the Santa Elena Ophiolite

Costa Rica is currently situated near the triple junction of the Cocos, Caribbean and Nazca plates (DeMets, 2001). Across the Middle American Trench, the Cocos plate is being subducted underneath the Caribbean plate resulting in an active volcanic front (Saginor et al., 2011; Saginor et al., 2013) (Fig. 1.2b). A series of oceanic complexes have been accreted onto the Caribbean Plate along the Pacific side of Costa Rica including the Santa Elena Ophiolite (Tournon et al., 1995; Hauff et al., 2000; Hoernle et al., 2004; Denyer and Gazel, 2009; Herzberg and Gazel, 2009; Buchs et al., 2013). Several authors correlated the Santa Elena Ophiolite with other serpentinized peridotite locations along the Costa Rica-Nicaragua border suggesting that it represents an E-W

suture zone between different tectonic blocks (Tournon et al., 1995; Hauff et al., 2000; Baumgartner et al., 2008; Denyer and Gazel, 2009).

The Santa Elena Ophiolite, constitutes a preserved fragment of the upper mantle that includes evidence for at least two different magmatic intrusive events. The oldest event is constituted by decimetric to centimetric pegmatitic gabbroic veins that intrude the lherzolite without showing any sign of cooling margins, suggesting that they were emplaced when the peridotite was still at high temperatures and in a plastic state (Gazel et al., 2006). The second and younger event is the diabase dike melt-focusing system, which crops out along the peninsula (Figs. 1.2 and 1.3); generally presenting cooling margins in contact with the peridotite. The pillow basalts from Murcielago Islands (~110 Ma; Hauff et al., 2000) do not show a clear lithological relation to the rest of the Santa Elena Ophiolite. Even though they have been interpreted as the uppermost basaltic sequence in agreement with ophiolite architectural models, the contact between this unit and the peridotite cannot be observed in the field. These pillow lavas are probably related to other pillow basalts and mafic lithologies in the Nicoya peninsula included in the Nicoya Complex (Dengo, 1962). This complex is interpreted as segments of oceanic plateaus and the Caribbean Large Igneous Province (CLIP), with geochemical affinities that are unrelated to the Santa Elena Ophiolite (Sinton et al., 1997; Hoernle et al., 2004; Geldmacher et al., 2008).

The Santa Elena ophiolite is overlain by Campanian (Upper Cretaceous) rudists-bearing reef limestones (Fig. 1.1a) (Meschede and Frisch, 1994; Gazel et al., 2006; Baumgartner et al., 2008; Escuder-Viruete and Baumgartner, 2014) suggesting that it was emplaced during the Upper Cretaceous with the peridotitic complex at the hanging-wall and an igneous-sedimentary complex at the footwall, known as the Santa Rosa Accretionary Complex (Baumgartner and Denyer, 2006; Denyer and Gazel, 2009; Buchs et al., 2013). A unit of layered gabbros (see Fig. 1.2a) has also

been identified at the footwall (Tournon and Azéma, 1980; Hauff et al., 2000; Arias, 2002); this unit yielded an $^{40}Ar/^{39}Ar$ age of 124±4.1 Ma (Hauff et al., 2000). Previous work from Gazel et al. (2006) interpreted a suprasubduction zone origin for the Santa Elena ophiolite, considering the layered gabbros unit as a part of the ophiolite. Here, this interpretation is revised in light of the new modern analytical data and our detail geologic mapping, as the layered gabbros unit belongs to the footwall, in a highly deformed shear zone bellow the overthrusting ophiolite (see Fig. 1.2a).

Based on spatial relations between the lithological units that compose the Santa Elena Ophiolite at least two rotation events can be identified in its geologic record. The pillow basalts from Murcielago Islands display a near 80° tilt towards the north, while the northern Cretaceous (Campanian) to Paleogene sedimentary cover show a dipping angle of 50-40° towards the north (Fig. 1.2a). However, the Plio-Pleistocene ignimbrite veneer appears unaffected by the rotation (dipping angles of 5° E). These relative structural disposition suggests that the two tilting events (one pre-Campanian age and the second one roughly in the Upper Eocene) affected the entire sequence for a current net rotation of 80° towards the north (Denyer et al., 2006; Denyer and Gazel, 2009).

3. Materials and methods

3.1. Structural methods and peridotite/dike determinations

Diabase dikes are exposed along the coasts and riverbeds of the Santa Elena Ophiolite intruding the peridotite at a variable density of diabase vs peridotite between localities (Fig. 1.2a). A spatial analysis was performed along the northwestern and southern coasts of the peninsula in order to quantitatively determine the dike density, dike orientation, and structural relationships (Fig. 1.2a and c). We collected a continuous photographic record and structural measurements

(strike/dip angles) of all the diabase dike outcrops on the coast. The data were corrected using the program Win-TENSOR (Delvaux and Sperner, 2003) to account for a tectonic 80° tilt of the entire complex towards the north in order to obtain the original strike and dip angle of the diabase dikes. This tilt creates an apparent 80° increase in the dip angles of the dikes intruding the block. The continuous photographic record from the coastal outcrops was used to generate panoramic sections of the peninsula (Fig. 1.3). We carried out a 2D analysis, which included calculation of Cartesian areas in each of the panoramic images created. Considering the rock exposure areas of every outcrop as the total area (100%) we calculated the relative abundance of peridotite and diabase. We focused the analysis on the areas that display a continuous occurrence of peridotite and diabase (i.e., along the NW and SE coast of Santa Elena peninsula) (Fig. 1.2a, c).

3.2. Samples and analytical methods

Fresh diabase dikes were sampled from coastal exposures and riverbeds in the Santa Elena Ophiolite. We also sampled pegmatitic gabbroic veins to constrain the timing of the evolution of this ophiolite given the spatial relationship between the units.

Using a rock saw, fresh pieces of the samples were cut and later crushed into gravel, cleaned with deionized water and dry-sieved to get rock chips of 425-300 μm in diameter. To obtain the $^{40}Ar/^{39}Ar$ data, the groundmass and mineral separates were irradiated for 60 hours at the Oregon State University TRIGA-type reactor in the Cadmium-Lined In-Core Irradiation Tube. At the University of Wisconsin-Madison Rare Gas Geochronology Laboratory, incremental heating experiments were conducted using a 25 Watt CO_2 laser. Each step of the experiment included heating at a given laser power, followed by an additional 10 min for gas cleanup. The gas was

cleaned with two SAES C50 getters, one of which was operated at ~450 °C and the other at room temperature. Blanks were analyzed after every second laser heating step, and were less than 5 x 10^{-20} mol/V for ^{36}Ar and 2 x 10^{-17} mol/V for ^{40}Ar, respectively. Argon isotope analyses were performed using a MAP 215–50, and the isotope data was reduced using ArArCalc software version 2.5 (http://earthref.org/ArArCALC/). Ages were calculated from the blank-discrimination and decay-corrected Ar isotope data after correction for interfering isotopes produced from potassium and calcium in the nuclear reactor. Ages are reported with 2σ uncertainties (includes the J uncertainty) and are calculated relative to a Fish Canyon standard age of 28.201 ± 0.046 Ma (Kuiper et al., 2008) and a value for $\lambda^{40}K$ of 5.463 ± 0.107 x 10^{-10} yr^{-1} (Min et al., 2000).

For major and trace element analyses, alteration-free rock chips were selected under a stereoscope microscope and were powdered in an alumina mill. Major element (wt%) concentrations were measured by X-ray fluorescence (XRF; Siemens SR3000 spectrometer) at the University of Auckland following the methods described by Norrish and Hutton (1969). In general, precision for each major element is better than ±1% (1σ) of the reported value as described by Norrish and Hutton (1969). Trace elements were measured by laser-ablation inductively-coupled-plasma mass-spectrometry (LA-ICP-MS) at the Research School of Earth Sciences, Australian National University, using Excimer LPX120 laser (193 nm) and Agilent 7500 series mass spectrometer following the method of Eggins et al. (1998). Samples were run in batches of 15 using the NIST612 glass standard at the beginning and end of each run to calibrate. USGS glass standards BCR-2 and AGV-2 were also run to monitor analytical performance. Three replicate analyses of standard BCR-2 and two replicates for standard AGV-2 indicate precision of <4% (RSD) and accuracy better than 8% confidence level, with the exception of the elements Ni, Cu, Cr, La and Ta.

Basaltic glass samples collected from the Murcielago Island pillow basalts rims were selected under a stereoscope microscope, and arranged in a 1-inch round epoxy mount which was later polished for electron microprobe (EMP) analyses. These analyses were performed at the Electron Beam Laboratory at Virginia Tech with a Cameca SX50 Electron Microprobe using a 60 μm diameter electron beam at a 10 nA current a 15 kV acceleration voltage. Trace element contents were obtained at Virginia Tech LA-ICPMS lab facilities using an Agilent 7500ce ICPMS coupled with a Geolas laser ablation system. Three analyses were performed in each glass using a 90 μm diameter spot and at 10 Hz repetition rate. Standards were run at the start and end of the run to correct for drift. The data was reduced using the USGS standards BCR-2G, BHVO-2G and BIR-1. Replicates of these standards indicate a precision of <5% (RSD) and accuracy better than 10% for the elements analyzed, with the exception of the elements Ni, Cu, Cr, Zn, Sr, Ta, Pb and U that was better than 30%.

Radiogenic isotope analyses were conducted in the Geochronology and Isotope Geochemistry Laboratory at the University of North Carolina, Chapel Hill. 500 mg of the selected powdered samples were digested with a mixture of HF+HNO_3 in Teflon beakers. These solutions were placed on a hotplate for three days at a temperature of 165 °C. Each sample was dried and re-dissolved in HCl. After their dissolution three aliquots were separated for Sr, Nd and Pb, each one containing 5 mg of sample; these aliquots were dried and re-dissolved in the appropriate acid solution to undergo ion exchange chromatography columns (Gray et al., 2008). The separates were analyzed using a Micromass VG Sector 54 thermal ionization mass spectrometer (TIMS). Strontium measurements were normalized to $^{86}Sr/^{88}Sr = 0.1194$, and Nd isotopes to $^{146}Nd/^{144}Nd = 0.7219$. Standard replicate measurements yielded a mean $^{87}Sr/^{86}Sr = 0.710257 \pm 0.000022$ (2σ) for NBS 987, a mean $^{143}Nd/^{144}Nd = 0.512112 \pm 0.000011$ (2σ) for JNdi-1, and a mean $^{206}Pb/^{207}Pb =$

1.0940 ± 0.0003 (2σ) for NBS-981 with a mean fractionation correction of 0.098 ± 0.008% per amu (Coleman et al., 2004; Gray et al., 2008).

4. Results

4.1. Structural analysis of the diabase unit

After correcting for the 80° northward tilt of the ophiolite determined in the field the general strike orientation for the diabase dikes throughout the Santa Elena Ophiolite is NNE in a sub-parallel arrangement. The resulting dip angles reflect a predominance of angles higher than 60°, with a primary population of dikes dipping between 70° and 90°. Evidence of this disposition is largely visible at the NW coast of the peninsula (Fig. 1.2a).

The northwestern dike swarm (Fig. 1.2a) represents the higher density of diabase intruding the peridotite in the entire ophiolite with a dip between 70° and 80° (Fig. 1.2c). Our density analysis suggests that in this section there is a significant increase of diabase dikes from ~78% to ~92% (relative to the peridotite) towards the southwest in the direction of Punta Santa Elena (Fig. 1.2a), where the peridotites became boudins embedded in the net of diabase dikes.

The outcrops along the southern coast of the peninsula are predominantly composed of peridotite with scarcer occurrences of diabase dikes. In this area the presence of diabase versus peridotite is less than 20% (Fig. 1.2a). The preferential strike direction for the southeastern dike swarm is towards the NW, with a secondary population striking ENE-WSW. In this area, the arrangement of the intrusions is clearly not parallel; however, most of the dip angles remain in a range between 60° and 90° (Fig. 1.2c). Additionally, other diabase intrusions measured in the interior of the peninsula yielded a preferential strike of NNE-NNW with sub-vertical dip angles (Fig. 1.2a).

4.2. Geochronology and geochemistry data

The four new $^{40}Ar/^{39}Ar$ ages collected in this work yielded an average age of 121 Ma (considering the uncertainty within the measurements) for the diabase dike intrusion event. Diabase samples collected from the NW end of the Santa Elena Peninsula yielded 126.6 ± 2.1 Ma to 116 ± 5.1 Ma (Fig. 1.2a). A sample from the southern coast of the peninsula yielded an age of 118.7 ± 3.5 Ma. Also, a diabase sample from the inner part of the ophiolite was analyzed to achieve a good geographical distribution throughout the peninsula; this sample provided an age of 124.7 ± 3.0 Ma. One of the pegmatitic gabbroic veins sampled that intruded the peridotite when it was still hot and plastic (Gazel et al., 2006) yielded an age of 131 ± 3.8 Ma.

For this study we report 18 new major and trace element analyses for diabase dikes and 5 for Murcielago Islands basaltic glasses. The compositions of the diabase dikes are basaltic and belong to the tholeiitic magmatic series (Fig. 1.4a, b). Petrographically, they are aphyric and consist of a fine grained equigranular ensemble of semi-euhedral clinopyroxene and plagioclase and minor olivine, with a predominately ophitic texture characteristic of mafic hypabyssal intrusions. The rim glasses from Murcielago Islands are basaltic-andesite in composition and also belong to the tholeiitic series (Fig. 1.4a, b).

Along with the new analyses provided in this work from the diabase dikes, we also compiled geochemical data from previous studies (Kussmaul et al., 1982; Tournon, 1984; Wildberg, 1984; Meschede and Frisch, 1994; Tournon, 1994; Ragazzi, 1996; Beccaluva et al., 1999; Hauff et al., 2000; Arias, 2002; Tournon and Bellon, 2009), which are plotted as a shaded area in Fig. 1.4. Major element data were plotted against MgO (Fig. 1.5 and 1.6) to evaluate differentiation trends in the sample suite collected. Trace element data, normalized to a primitive mantle composition (McDonough and Sun, 1995) show a depleted composition in light rare earth

elements (LREE) and a flat pattern in the heavy rare earth elements (HREE), suggesting a garnet-free, shallow mantle source (e.g. Salters and Stracke, 2004) (Fig 1.7). Elevated concentrations in fluid-mobile large ion lithophile elements (LILE) such as Ba, K and Sr are indicative of seafloor alteration (Staudigel et al., 1981; Staudigel et al., 1996; Staudigel, 2003). Thus, to avoid the signature of ocean floor alteration, only fluid immobile ratios were used to generate the discrimination diagrams shown in Fig. 1.8. The Murcielago Islands pillow basalt glass rims show a more enriched incompatible-element signature compared to that of the Santa Elena diabase dikes (Fig 1.7e) which is almost identical to the basaltic glasses that belong to the Caribbean Large Igneous Province (CLIP) and other basaltic suites found in Nicoya Peninsula (Hauff et al., 1997; Sinton et al., 1997; Hauff et al., 2000; Hoernle et al., 2004).

The new Sr, Nd, and Pb radiogenic isotope analyses were carried out using the freshest samples of the diabase dikes, however Sr isotopes could still be affected by any low-grade ocean floor alteration, and thus explaining the spread in the data. The measured diabase dikes isotope values range from 0.70283 to 0.70396 in $^{87}Sr/^{86}Sr$; 0.51299 to 0.51341 in $^{143}Nd/^{144}Nd$; 18.149 to 18.536 in $^{206}Pb/^{204}Pb$; 15.500 to 15.595 in $^{207}Pb/^{204}Pb$; and 37.839 to 38.166 in $^{208}Pb/^{204}Pb$ (Fig. 1.9). These measured Sr-Nd-Pb ratios were then calculated to the initial (in) eruptive ratios using the parent/daughter ratios and an average age of 121 Ma. Age corrected ratios representative of the mantle source were then projected to 121 Ma using parent/daughter ratios obtained inverting the source composition from the most primitive diabase dike sample (A-28-7-05) to recreate the evolution of the source in 121 Ma and compared with recently erupted material. The model was done using aggregated fractional melting equations (Shaw, 1970) with a modal composition of 50% olivine, 25% orthopyroxene, 20% clinopyroxene and 5% spinel and the partition coefficients

compiled by Kelemen et al. (2003). These data were plotted in Fig. 1.9 and discussed in section 5.4.

5. Discussion

5.1. Architecture of the Santa Elena Ophiolite: diabase melt focusing zone analysis

The arrangement of dike intrusions in different tectonic environments provides important insight into the type of melt emplacement that occurred at a given location. For instance, radial arrangements of dikes typically indicate environments such as arc volcanoes or ocean islands (i.e. Ancochea et al., 2008; Acocella and Neri, 2009; Maccaferri et al., 2011). Whereas, in environments characterized by extension regimes, melts are likely to migrate perpendicularly to the direction of the minimum compressive stress (Macdonald, 1982; Gudmundsson, 1990a; Paquet et al., 2007; Gudmundsson, 2011), resulting in sub-parallel to parallel dike assemblages. This commonly occurs at mid-ocean ridges and back arc basins, where the intrusions normally show similar strike orientations perpendicular to extension as well as parallel sub-vertical arrangements.

Ophiolites, as preserved fragments of extension environments (e.g., mid-ocean ridges, back arc basins), usually display sheeted dike complexes composed by *dike-intruding-dike* structures of tholeiitic composition, that have been interpreted as the feeder channels between magma chamber/lenses and the overlying extrusive oceanic crust (Robinson et al., 2008 and references therein). At fast spreading ridges, such as in the exposed section at Hess Deep in the Pacific, the sheeted dike complex is a well-developed feature of the oceanic crust suggesting a high spreading rate and a steady magma supply (Stewart et al., 2005; Veloso et al., 2014). In contrast, at slow (<60 mm/yr full rate), and ultraslow spreading (<20 mm/yr full rate) ridges the magma generation is slow and tectonic extension and detachment faulting are the predominant trigger for melting,

resulting in the absence of a well-developed sheeted dike complex (Snow and Edmonds, 2007; Robinson et al., 2008; Lagabrielle et al., 2015). The Santa Elena Ophiolite preserves a relatively high density of diabase intrusions, however, in contrast to sheeted dike complexes, it lacks the typical *gabbro–sheeted dike–basalt* sequence and instead the dikes intrude the lithospheric mantle peridotite directly and there is not an overlying well-developed basaltic crust.

The absence of horizontal intrusions indicates that during melt migration no rheological or mechanical barrier was encountered that led to lateral migration. The dike swarms exhibit an almost vertical arrangement. Since dike emplacement tends to follow pre-existing paths, we suggest that this vertical to sub-vertical emplacement corresponds to the location of previous extension fractures, perpendicular to the direction of the minimum compressional stress. The results presented in this work indicate that the Santa Elena Ophiolite was formed in a tectonic environment subject to extension, with an expected dike arrangement of a mid-ocean ridge system (e.g. Gudmundsson, 1990b, 2011)

Mid-ocean ridge systems with slow and ultra-slow spreading rates can account for the emplacement of almost exclusively vertical intrusions due to limited melt productivity (Michael and Cornell, 1998; Dick et al., 2003; Gudmundsson, 2011). In these environments, dikes form at greater depths intruding directly in the lithospheric mantle. Even though it has been recognized that the rheological barrier of the crust-mantle boundary favors the formation of melt ponding (i.e., magma chambers or lenses) (Gudmundsson, 2011), there is no field evidence for such melt accumulations in the Santa Elena Ophiolite. Commonly, melt migration in slow and ultra-slow spreading mid-ocean ridges show little and generally deep melt ponding as a consequence of the low rates of melt productivity in this tectonic environment (Michael and Cornell, 1998). Melt forming in such conditions will travel along paths of minimum stress like the extensional fractures

and faults inherent to slow and ultra-slow spreading ridges which are essentially vertical as observed in the Santa Elena Ophiolite.

As melts are transported from the melt generation zone to the axis of extension, the frequency of intrusions decreases while their size and width increase (Kelemen et al., 1997; Kelemen et al., 2000). In the Santa Elena Ophiolite, we encountered a high spatial density of intrusions combined with distinct coalescent dikes as shown in Fig. 1.3. The presence of lherzolitic peridotite and the coalescing channels of diabase correlate with what would be expected at greater depths of the melt transport system in an extensional environment, characterized by a scarce magmatic supply at deeper levels in the lithospheric mantle (see Fig. 1.1). Moreover, this ophiolite lacks of an extrusive well-developed basaltic crust on top of the sequence which supports the interpretation that this ophiolite corresponds to a slow to ultra-slow spreading center (Dick et al., 2003; Cannat et al., 2009; Sauter et al., 2011). The absence of a well-developed gabbroic crust is also evident in this ophiolite. This is a noted characteristic in ultraslow spreading ridges, where the reduced melt production can lead to a small to nearly inexistent gabbroic crust (Jokat et al., 2003; Michael et al., 2003).

5.2. Geochronology data

The spatial relationships between the diabase and gabbroic intrusions of the Santa Elena Ophiolite become clearer in the light of the new $^{40}Ar/^{39}Ar$ data collected in this study. Both units post-date the formation of the peridotitic massif, but the pegmatitic gabbroic veins are the first magmatic event to occur (evidenced by cross-cutting relationships), at circa 131 ± 3.8 Ma. This event is particularly interesting since the field evidence suggests that there are no cooling margins between the pegmatitic gabbro veins and the host peridotite. This implies that during the emplacement the host rock and the intrusion were roughly at the same temperature. Most likely

the gabbroic melts infiltrated when the peridotite was still under plastic deformation conditions (Gazel et al., 2006).

On the other hand, the diabase dikes present clear cooling margins suggesting that by the time the diabase magmatic event occurred (roughly circa 121 Ma) the peridotite had already reached lithospheric temperatures. Consequently, the $^{40}Ar/^{39}Ar$ ages obtained in this study constrain the cooling of the ophiolite massif to sometime between 131 ± 3.8 Ma and the youngest of the diabase dikes, 116 ± 5.1 Ma, which coincides with a Barremian to Aptian age. This interpretation is in good agreement with the age constraints from other authors based in the rudist-bearing reef ages, that also places the tectonic emplacement no earlier than Campanian (Upper Cretaceous) (Meschede and Wolfgang, 1998; Gazel et al., 2006; Baumgartner et al., 2008; Escuder-Viruete and Baumgartner, 2014).

5.3. Fractional crystallization models and implications for crystallization pressures

The architecture of the Santa Elena Ophiolite along with the variable observed cooling textures suggests that the diabase dikes were emplaced at depths within the lithospheric mantle (Fig. 1.3). In order to better determine these depths, we used Petrolog3 (Danyushevsky and Plechov, 2011) to produce models that simulate the fractional crystallization processes at different pressures (results in Fig. 1.5 and 1.6). For these calculations, we used the olivine (ol), plagioclase (plag) and clinopyroxene (cpx) models of Danyushevsky (2001). The cotectic crystallization was modeled at a 100% fractionation of these minerals in equilibrium with a liquid (L+ol+plag+cpx). When more than one mineral phase crystallizes together, the software calculates a "pseudoliquidus" temperature (PST), which is the highest recorded temperature of crystallization of the two or three mineral phases. These PST's can be plotted as liquid lines of descent (LLD), where every discontinuity in the line indicates a new crystallizing mineral phase (Fig. 1.5 and 1.6).

The calculations were made using the QFM buffer of oxygen fugacity according to the model of Kress and Carmichael (1988). We created models from a pressure range of 0.001 GPa (1 atm) to 1.0 GPa, in 0.2 GPa increments, keeping the pressure constant during each run. The amount of melt extracted in each step was 0.01%; this small calculation step improves the accuracy of the model (Danyushevsky, 2001). The calculations stopped when the melt MgO content reached 3 wt%.

To evaluate our initial hypothesis of a mid-ocean ridge origin for the melts that formed the diabase dikes, we input a primary magma composition for MORB (East Pacific Rise, EPR) from Herzberg and O'Hara (2002), as well as a primary magma calculated from our most primitive diabase composition (Fig. 1.6). Albeit, the resulting LLDs of these models plotted in bivariate major element diagrams were able to reproduce experimental MORB glasses at the same range of pressures (see references in the figure caption), they failed to reproduce the crystallization trends and compositional changes that can be observed in the diabase dike suite. Because an EPR-MORB starting composition and our most primitive diabase sample did not describe the differentiation path of our samples, the input composition was empirically modified by an optimization method to include 0.5 wt% H_2O, 50.06 wt% SiO_2 and 2.83 wt% Na_2O to the initial EPR-MORB. This final composition successfully recreates and explains the compositional evolution of the diabase dikes. One important result from this modeling is that the diabase dike compositions cannot be reproduced by anhydrous MORB (Fig 1.6). The effect of small amounts of H_2O on MORB melt compositions results in a displacement of the cotectic points (the discontinuities in the LLD) due to the suppression of plagioclase crystallization relative to olivine and clinopyroxene (see Fig. 1.6a through e) (Danyushevsky, 2001). The estimated amount of H_2O (0.5 wt%) necessary to explain

our data is atypical for MORB, however, it still falls into the high end-member of hydrated MORB magmas (Hirth and Kohlstedt, 1996; Danyushevsky, 2001; Asimow and Langmuir, 2003).

The SiO_2 variation of the diabase dike suite is controlled by olivine partitioning as a function of temperature and pressure (Langmuir et al., 1992a). The crystallization of plagioclase and pyroxene is most likely responsible for the increase in SiO_2 contents at low pressures (<0.4 GPa). In the diabase dike samples, the cotectic crystallization of olivine and plagioclase is suggested by a positive correlation between MgO and Al_2O_3 (Fig. 1.5b). Using a MORB composition, this correlation tends to be positive because increasing levels of fractionation will lead to a decrease of MgO and Al_2O_3 in the melt due to the crystallization of olivine and plagioclase, respectively (Danyushevsky, 2001). As the pressure increases, the liquids in equilibrium with Ol+Plag+Cpx will increase their Al_2O_3 content and this can lead to a higher modal plagioclase content (Herzberg, 2004). FeO_t shows the expected enrichment during fractionation of tholeiitic magmas (Zimmer et al., 2010).

CaO vs. MgO systematics (Fig. 1.5c and 1.6) can be used to evaluate whether or not a melt has crystallized clinopyroxene because CaO contents increase during the L+Ol and L+Ol+Plag steps of crystallization and promptly decrease as soon as the liquid starts to crystallize Ol+Plag+Cpx. The sensitivity of CaO to pressure effects was evaluated by Langmuir et al. (1992) and Herzberg (2004). The Santa Elena diabase dikes plot within the LLDs modeled from 1 atm to 1 GPa (Fig. 1.5); however, a larger set of samples plot at pressures >0.4 GPa. We also plotted our data onto a projection of liquids for the equilibrium L+Ol+Plag+Cpx into the plane Anorthite-Diopside-Enstatite following the methods of Herzberg and O'Hara (1998) and Herzberg (2004) (Fig. 1.5e). In this projection the pressures of crystallization of most of the diabase dikes also yielded >0.4 GPa, further supporting a deep origin for the dikes. Although these values are model-

dependent and absolute pressures are not easy to obtain, our results are consistent with deep crystallization in the lithospheric mantle rather than at crustal levels, as it is obvious in the field exposures (Fig. 1.3).

The data from the Santa Elena Ophiolite were also compared to geochemical data from mid-ocean ridges globally, compiled by Gale et al. (2013). Fast spreading ridges group around the LLDs that belong to pressures from 1 atm to 0.4 GPa, which can be correlated with shallow depths of melt crystallization. Correlations between spreading rate and depth of crystallization have been noted by other authors (Grove et al., 1993; Michael and Cornell, 1998; Herzberg, 2004; Escartin et al., 2008); and in general, slower spreading rates are associated with deeper crystallization. In this respect, the Santa Elena Ophiolite diabase dikes show a range of pressures of crystallization that are consistent with deep crystallization environments. These pressures (>0.4 GPa) correspond to depths >15 km (assuming an average density of ~3.0 g/cm^3 for the oceanic lithosphere). The results are in good agreement with the estimated pressures of partial crystallization at the top of the melting regime in slow and ultra-slow spreading ridges (Herzberg, 2004), thus, providing supportive information for a slow to ultra-slow spreading rate for the extensional environment preserved in the Santa Elena Ophiolite.

5.4. Trace element signatures and tectonic implications

In order to further understand the tectonic environment in which the Santa Elena Ophiolite formed, the diabase dike trace element compositions were normalized to a Primitive Mantle composition (McDonough and Sun, 1995). Primitive-normalized data are depleted in the most incompatible elements, such as the LREE, consistent with the trace element composition of a depleted MORB-like source (Salters and Stracke, 2004) (Fig. 1.7a). When the trace element patterns of the Santa Elena Ophiolite are compared with other primitive-normalized trace element

compositions of other extensional tectonic environments, our results are similar to signatures that are found in slow to ultra-slow spreading ridges and back-arc spreading centers, but always at the depleted end of these environments consistent with a normal MORB signature (Fig. 1.6).

Because magmas record information about their original tectonic setting of formation in their trace-element signatures, a series of geochemical proxies have been identified that can be used to discriminate paleo-tectonic environments (e.g., Pearce, 2008 and references therein). In order to better determine the tectonic environment that formed the Santa Elena Ophiolite, we used fluid-immobile elements to distinguish between a mid-ocean ridge environment and a subduction influenced environment. For comparison, we compiled geochemical data from various ophiolites (Mayari-Baracoa Ophiolitic Belt, Oman, Newfoundland, Josephine, Mirdita, Macquarie Island, Ingalls, Tangihua, Shuanggou, Kizildag, Anatolia, Troodos, Duarte, Loma La Monja, La Desiderade) as well as trace element data from other extensional environments (Atlantis Massif, Atlantis Bank, San Souci volcanic formation, Atlantic oceanic crust of ca. 121 Ma, ultra-slow spreading centers, back-arc basins) and plotted along with the results from the Santa Elena Ophiolite and the Murcielago Islands pillow basalts in Fig. 1.8.

In these fluid-immobile element systems the mantle array is defined by where MORB-OIB data plots. Data that plots away from this array suggests the influence of subduction processes or crustal interaction, as for example, samples that belong to SSZ ophiolites such as Oman, Newfoundland, Ingalls, Anatolia, and Kizildag, plot away from the mantle array as indicated by the "subduction interaction" vector as shown in the plot of Zr/Nb vs. Ti/Th (Fig. 1.8a). Similarly, as shown in the Ce/Nb vs. Th/Nb diagram (Fig. 1.8b), the subduction influenced samples plot towards higher Ce and higher Th. Ce can be considered as a proxy for H_2O content, since both elements have a similar incompatible behavior during melting (Saunders et al., 1988). This

diagram provides an easy visualization of the effect of increasing subduction interaction, which is especially evident in SSZ ophiolite samples. Fig. 1.8c shows the Th/Yb vs. Nb/Yb diagram first developed by Pearce (2008). Th and Nb are well-known proxies for subduction input within a system, as Th is carried by subduction fluids (especially sediment recycling) and Nb is retained by a residual phase in the subducting slab (Wood et al., 1979; Pearce, 2008; Pearce, 2014). Thus, samples influenced by subduction fluids trend towards higher Th contents and lower Nb contents relative to the mantle array. This is why samples coming from back-arc basins plot parallel to and higher than the mantle array and SSZ ophiolites also show an upward trend.

Our results indicate that the Murcielago Islands pillow basalts plot well into the mantle array limits, trending towards the enriched endmember of MORB. Meanwhile, the Santa Elena Ophiolite diabase dikes plot on the limits between the data from back-arc basins and slow to ultra-slow spreading ridge MORB consistent with our previously discussed major element results. In comparison with the global compilation, our data also show similarities with the Atlantis Massif, Atlantic oceanic crust, and the Atlantis Bank (Fig. 1.8a, b and c). The location that shows the most consistency with the diabase dikes are the tholeiites from the Mirdita Ophiolite in Albania. This is a Jurassic ophiolite interpreted as a transition from a MORB to a SSZ environment (Dilek and Furnes, 2009). Santa Elena intrusions are also geochemically similar to the Continental Margin Ophiolite classification of Dilek and Furnes (2014) which plot on the NMORB field of the mantle arrange and towards the upper limit. Therefore, our diabase dike samples resemble a MORB-type magma that show only a "hint" of subduction interaction.

5.5. Mantle signatures from radiogenic isotopes

Radiogenic isotopes are a reliable way to evaluate the source of a given sample, since they do not fractionate during magmatic processes such as melting or crystal fractionation. In terms of

radiogenic isotopes, MORB was thought to be derived through melting of a homogeneous mantle reservoir (the upper mantle). However, more recent studies reveal the significant variations in the radiogenic isotope ratios indicating that it is more likely that they are generated from mantle sources that are heterogeneous (Salters and Stracke, 2004; Workman and Hart, 2005). Isotopic variability in MORB from fast spreading and slow spreading ridges may differ depending on the mixing mechanisms intervening in the systems. In this regard, small-scale convection contributes to mixing of different sources at slow spreading ridges, producing geochemically homogeneous reservoirs (Samuel and King, 2014).

The new age corrected (accounting for the source evolution in ~121 Ma) data from the Santa Elena Ophiolite mafic dikes are presented in Fig. 1.9. The diabase dikes share isotopic signatures that resemble those from back-arc basins and slow to ultra-slow spreading ridges and are separate from those of fast spreading ridges (Fig. 1.9). This is consistent with the results discussed above for major and trace element compositions. The diabase samples yield $^{87}Sr/^{86}Sr$ values between 0.70285 and 0.70357 (Fig. 1.8a), which are on the higher end for NMORB but not as high as the range of EMORB. Also, they overlap with the lower $^{87}Sr/^{86}Sr$ values for back-arc basins. The εNd values obtained for the diabase dikes range between +6 and +12, and when plotted against $^{87}Sr/^{86}Sr$ they overlap with data from slow and ultraslow spreading ridges, and with data from back arc basins to a lesser extent (Fig. 1.9a).

The data also show that the diabase dikes are more enriched in $^{206}Pb/^{204}Pb$, $^{207}Pb/^{204}Pb$ and $^{208}Pb/^{204}Pb$ than depleted DMM (Fig. 1.9b, c and d), following a linear array that suggests a mixture of a depleted component and an enriched component (EMII), most likely due to small-scale convection, a consistent characteristic in slow-spreading systems (Samuel and King, 2014). The EMII mantle reservoir is interpreted as deep mantle storage of metasomatized oceanic lithosphere

or sub-continental lithosphere (Workman et al., 2004). Detachment of sub-continental lithosphere may occur during continental break-up (Saunders et al., 1988). Therefore, this isotopic signature can be correlated with the remnants of lithospheric mantle components disseminated during the opening of the Atlantic and the proto-Caribbean ocean. Additionally, the presence and mixing of these likely subduction-modified remnants of the sub-continental lithosphere could account for the subtle subduction signature evident in our samples (see discussion in Gazel et al., 2012).

5.6. Paleotectonic setting for the Santa Elena Ophiolite formation

Data presented in this work shows that the Santa Elena Ophiolite preserves structural and geochemical evidences for an extension environment of formation. Whether it is a mid-ocean ridge or a back-arc basin environment is still a matter of further constraints, such as paleomagnetic surveys and detailed tectonic reconstructions. However, the similarities with data coming from back-arc basin tectonic settings like Lau Basin and Marianas (Fig. 1.8) suggest that Santa Elena Ophiolite might have originated from an analogous setting.

Moreover, the Santa Elena Ophiolite characteristics are comparable with the structure and geochemical affinities present in some oceanic core complexes (OCC). For instance, the Godzilla Megamullion located in the extinct Parece Vela Rift in the back-arc basin of the Marianas (Fig. 1.10) consists of an exposed lower crust to mantle sequence of plutonic rocks including peridotites (lherzolites and harzburgites), gabbroic and diabase intrusions and a varying presence of a basaltic crust (Ohara et al., 2001; Ohara et al., 2003; Loocke et al., 2013). Sanfilippo et al. (2013) also mention that the basalts retain their MORB affinity and their REE and isotope compositions appear enriched by a minor slab component. OCCs like the Kane Megamullion (Dick et al., 2008) and the Atlantis Massif (Blackman et al., 2002) in the Mid-Atlantic Ridge, or the Atlantis Bank in the

Indian Ridge (Baines et al., 2003) also show mantle sequences consisting in peridotites, diabase dikes and to a lesser extent gabbros.

The idea of OCCs being preserved as ophiolites has been suggested by several authors (i.e. Nicolas et al., 1999; Tremblay et al., 2009; Manatschal et al., 2011; Lagabrielle et al., 2015). If Santa Elena is an OCC preserved as an ophiolite, it would explain the lack of a basaltic crust since in many OCCs low magmatic supply is common and the basaltic crust gets variably displaced by the hanging-wall during detachment (Escartín et al., 2003; Dick et al., 2008).

An alternative model for the origin of Santa Elena would be that it represents a fragment of the Mesquito Composite Oceanic Terrane (Baumgartner et al., 2008), a series of accreted Pacific oceanic terranes conformed by mafic and ultramafic lithologies. This explanation is supported by findings of Pacific Radiolarian fauna in different Caribbean locations that pre-dates the opening of the Proto-Caribbean (Baumgartner and Denyer, 2006; Baumgartner et al., 2008; Bandini et al., 2011). This hypothesis however is not mutually exclusive to the OCC origin, since the preservation and emplacement of this fragment of the lithospheric mantle could have happened in the context of accretion of distinct Pacific terranes.

Finally, a Proto-Caribbean origin should also be explored in future studies. Proto-Caribbean remnants have been found along the Great and Lesser Antilles (Lapierre et al., 1999; Marchesi et al., 2006; Escuder-Viruete et al., 2009). For instance, samples from the San Souci Volcanic Group, in Trinidad y Tobago, which have been interpreted as preserved pieces of Proto-Caribbean oceanic crust (Neill et al., 2014) show similar fluid immobile element signatures as the diabase dikes explored in this study (Fig. 1.8).

6. Conclusions

Structural and geochemical evidence suggest an extensional environment for the formation of the Santa Elena Ophiolite. The ophiolite architecture shows clear characteristics of mid-ocean ridge origin that include sub-parallel and sub-vertical arrangement of the dikes, coalescing channels of melt, absence of horizontal intrusions, zones of higher density of dikes relative to peridotite. Additionally, the lack of overlaying sequences of developed oceanic crust, the predominant presence of lherzolite as opposed to harzburgite, and the absence of significant magma chamber or lenses suggest that the Santa Elena Ophiolite is a preserved deep section (in the lithospheric mantle) of a melt-focusing zone in a slow to ultra-slow spreading ridge.

Major and trace element data are also in good agreement with the assessment of the origin of the Santa Elena Ophiolite as a slow/ultra-slow spreading center, possibly with a limited subduction interaction. The calculated pressures of crystallization are more consistent of slow to ultra-slow spreading ridges, where partial crystallization can occur deeper in the mantle since there is a lower magma supply and thus less heat flow. However, as evidenced from our geochemical data, the tectonic environment of formation for Santa Elena Ophiolite, even though it corresponds with an oceanic extension environment, it was not purely a Mid-Ocean Ridge nor a Back-Arc Basin setting *sensu stricto*, but possibly a combination between both environments. A possible analogous tectonic scenario could be similar to what is found at an oceanic core complex that developed in a back-arc basin, where the proximity to transform faults reduces the velocity of the spreading rates and induces detachment which emplaces the lithospheric mantle and the melt-focusing zone of the system at the seafloor.

7. References

Acocella, V. and Neri, M., 2009. Dike propagation in volcanic edifices: Overview and possible developments. Tectonophysics, 471(1–2): 67-77.

Ancochea, E., Brändle, J.L., Huertas, M.J., Hernán, F. and Herrera, R., 2008. Dike-swarms, key to reconstruction of major volcanic edifices: The basic dikes of La Gomera (Canary Islands). Journal of Volcanology and Geothermal research, 173: 207-216.

Arias, M., 2002. Petrografía y geoquímica de las rocas del Complejo Ígneo Estratificado de Bahía Nancite y su relación con los filones basálticos, península de Santa Elena, Costa Rica, Universidad de Costa Rica, San José, Costa Rica, 90 pp.

Asimow, P.D. and Langmuir, C., 2003. The importance of water to oceanic mantle melting regimes. Nature, 421(6925): 815-820.

Baines, A.G., Cheadle, M.J., Dick, H.J.B., Scheirer, A.H., John, B.E., Kusznir, N.J. and Matsumoto, T., 2003. Mechanism for generating the anomalous uplift of oceanic core complexes: Atlantis Bank, southwest Indian Ridge. Geology, 31(12): 1105-1108.

Baker, D.R. and Eggler, D.H., 1987. Compositions of anhydrous and hydrous melts coexisting with plagioclase, augite, and olivine or low-Ca pyroxene from 1 atm to 8 kbar; application to the Aleutian volcanic center of Atka. American Mineralogist, 72(1-2): 12-28.

Bandini, A., Baumgartner, P., Flores, K., Dumitrica, P., Hochard, C., Stampfli, G. and Jackett, S.-J., 2011. Aalenian to Cenomanian Radiolaria of the Bermeja Complex (Puerto Rico) and Pacific origin of radiolarites on the Caribbean Plate. Swiss Journal of Geosciences, 104(3): 367-408.

Bartels, K.S., Kinzler, R.J. and Grove, T.L., 1991. High pressure phase relations of primitive high-alumina basalts from Medicine Lake volcano, northern California. Contributions to Mineralogy and Petrology, 108(3): 253-270.

Baumgartner, P. and Denyer, P., 2006. Evidende for middle Cretaceous accretion at Santa Elena Peninsula (Santa Rosa Accretionary Complex), Costa Rica. Geologica Acta, 4(1-2): 179-191.

Baumgartner, P., Flores, K., Bandini, A., Girault, F. and Cruz, D., 2008. Upper Triassic to Cretaceous radiolaria from Nicaragua and northern Costa Rica: The Mesquito composite oceanic terrane. Ofioliti, 33(1): 1-19.

Beccaluva, L., Chinchilla-Cháves, A.L., Coltorti, M., Giunta, G., Siena, F. and Vaccaro, C., 1999. Petrological and structural significance of the Santa Elena-Nicoya Ophiolitic Complex in Costa Rica and geodynamic implications. European Journal of Mineralogy, 11: 1091-1107.

Bender, J., Hodges, F. and Bence, A., 1978. Petrogenesis of basalts from the project FAMOUS area: experimental study from 0 to 15 kbars. Earth and Planetary Science Letters, 41(3): 277-302.

Blackman, D., Karson, J., Kelley, D., Cann, J., Früh-Green, G., Gee, J., Hurst, S., John, B., Morgan, J., Nooner, S., Ross, D.K., Schroeder, T. and Williams, E., 2002. Geology of the Atlantis Massif (Mid-Atlantic Ridge, 30° N): Implications for the evolution of an ultramafic oceanic core complex. Marine Geophysical Researches, 23(5-6): 443-469.

Boudier, F., Ceuleneer, G. and Nicolas, A., 1988. Shear zones, thrusts and related magmatism in the Oman ophiolite: initiation of thrusting on an oceanic ridge. Tectonophysics, 151: 275-296.

Boudier, F. and Nicolas, A., 1985. Harzburgite and lherzolite subtypes in ophiolitic and oceanic environments. Earth and Planetary Science Letters, 76: 84-92.

Bouilhol, P., Connolly, J.A.D. and Burg, J.-P., 2011. Geological evidence and modeling of melt migration by porosity waves in the sub-arc mantle of Kohistan (Pakistan). Geology, 39(12): 1091-1094.

Buchs, D.M., Pilet, S., Cosca, M., Flores, K.E., Bandini, A.N. and Baumgartner, P.O., 2013. Low-volume intraplate volcanism in the Early/Middle Jurassic Pacific basin documented by accreted sequences in Costa Rica. Geochemistry, Geophysics, Geosystems, 14(5): 1552-1568.

Cann, J.R., 1970. Rb, Sr, Y, Zr and Nb in some ocean floor basaltic rocks. Earth and Planetary Science Letters, 10(1): 7-11.

Cannat, M., 1996. How thick is the magmatic crust at slow spreading oceanic ridges? Journal of Geophysical Research, 101(B2): 2847-2857.

Cannat, M., Manatschal, G., Sauter, D. and Péron-Pinvidic, G., 2009. Assessing the conditions of continental breakup at magma-poor rifted margins: What can we learn from slow spreading mid-ocean ridges? Comptes Rendus Geoscience, 341(5): 406-427.

Cannat, M., Sauter, D., Mendel, V., Ruellan, E., Okino, K., Escartin, J., Combier, V. and Baala, M., 2006. Modes of seafloor generation at a melt-poor ultraslow-spreading ridge. Geology, 34(7): 605-608.

Coleman, D.S., Gray, W. and Glazner, A.F., 2004. Rethinking the emplacement and evolution of zoned plutons: Geochronologic evidence for incremental assembly of the Tuolumne Intrusive Suite, California. Geology, 32(5): 433-436.

Coleman, R.G., 1971. Plate tectonic emplacement of Upper Mantle Peridotites along continental edges. Journal of Geophysical Research, 76(5): 1212-1222.

Danyushevsky, L.V., 2001. The effect of small amounts of H2O on crystallisation of mid-ocean ridge and backarc basin magmas. Journal of Volcanology and Geothermal Research, 110(3–4): 265-280.

Danyushevsky, L.V. and Plechov, P., 2011. Petrolog3: Integrated software for modeling crystallization processes. Geochemistry, Geophysics, Geosystems, 12(7): Q07021.

Dasgupta, R. and Hirschmann, M.M., 2006. Melting in the Earth's deep upper mantle caused by carbon dioxide. Nature, 440(7084): 659-662.

Delvaux, D. and Sperner, B., 2003. New aspects of tectonic stress inversion with reference to the TENSOR program. Geological Society, London, Special Publications, 212(1): 75-100.

DeMets, C., 2001. A new estimate for present-day Cocos-Caribbean plate motion: Implications for slip along the Central American volcanic arc. Geophysical Research Letters, 28(21): 4043-4046.

Dengo, G., 1962. Tectonic-igenuos sequence in Costa Rica In: Engel, A. E. J., James, H. J., Leonard, B. F. (Eds.), A volume to honor A. F. Budington. Geological Society of America Special Volume: pp. 133-161.

Denyer, P., Baumgartner, P. and Gazel, E., 2006. Characterization and tectonic implications of Mesozoic-Cenozoic oceanic assemblages of Costa Rica and Western Panama. Geologica Acta, 4(1-2): 219-235.

Denyer, P. and Gazel, E., 2009. The Costa Rican Jurassic to Miocen oceanic complexes: Origin, tectonics and relations. Journal of South American Earth Sciences, 28: 429-442.

Dewey, J.F., 1976. Ophiolite obduction Tectonophysics, 31: 93-120.

Dewey, J.F. and Bird, J.M., 1971. Origin and emplacement of the Ophiolite Suite: Appalachian Ophiolites in Newfoundland. Journal of Geophysical Research, 76(14): 3179-3206.

Dewey, J.F. and Casey, J.F., 2011. The Origin of Obducted Large-Slab Ophiolite Complexes, Arc-Continent Collision. Frontiers in Earth Sciences. Springer Berlin Heidelberg, pp. 431-444.

Dick, H.J.B., Lin, J. and Schouten, H., 2003. An ultraslow-spreading class of ocean ridge. Nature, 426: 405-412.

Dick, H.J.B., Tivey, M.A. and Tucholke, B.E., 2008. Plutonic foundation of a slow-spreading ridge segment: Oceanic core complex at Kane Megamullion, 23°30′N, 45°20′W. Geochemistry, Geophysics, Geosystems, 9(5): Q05014.

Dilek, Y. and Furnes, H., 2009. Structure and geochemistry of Tethyan ophiolites and their petrogenesis in subduction rollback systems. Lithos, 113(1–2): 1-20.

Dilek, Y. and Furnes, H., 2011. Ophiolite genesis and global tectonics: Geochemical and tectonic fingerprinting of ancient oceanic lithosphere. Geological Society of America Bulletin, 123(3-4): 387-411.

Dilek, Y. and Furnes, H., 2014. Ophiolites and Their Origins. Elements, 10(2): 93-100.

Eggins, S.M., Rudnick, R.L. and McDonough, W.F., 1998. The composition of peridotites and their minerals: a laser-ablation ICP–MS study. Earth and Planetary Science Letters, 154(1–4): 53-71.

Escartín, J., Mével, C., MacLeod, C.J. and McCaig, A.M., 2003. Constraints on deformation conditions and the origin of oceanic detachments: The Mid-Atlantic Ridge core complex at 15°45′N. Geochemistry, Geophysics, Geosystems, 4(8): 1067.

Escartin, J., Smith, D.K., Cann, J., Schouten, H., Langmuir, C.H. and Escrig, S., 2008. Central role of detachment faults in accretion of slow-spreading oceanic lithosphere. Nature, 455(7214): 790-794.

Escuder-Viruete, J. and Baumgartner, P.O., 2014. Structural evolution and deformation kinematics of a subduction-related serpentinite-matrix mélange, Santa Elena Peninsula, northwest Costa Rica. Journal of Structural Geology 66, 356-381.

Escuder-Viruete, J., Pérez-Estaún, A. and Weis, D., 2009. Geochemical constraints on the origin of the late Jurassic proto-Caribbean oceanic crust in Hispaniola. International Journal of Earth Sciences, 98(2): 407-425.

Falloon, T. and Green, D., 1987. Anhydrous partial melting of MORB pyrolite and other peridotite compositions at 10 kbar: implications for the origin of primitive MORB glasses. Mineralogy and Petrology, 37(3-4): 181-219.

Falloon, T.J., Danyushevsky, L.V. and Green, D.H., 2001. Peridotite Melting at 1 GPa: Reversal Experiments on Partial Melt Compositions Produced by Peridotite–Basalt Sandwich Experiments. Journal of Petrology, 42(12): 2363-2390.

Falloon, T.J., Green, D.H., Danyushevsky, L.V. and McNeill, A.W., 2008. The Composition of Near-solidus Partial Melts of Fertile Peridotite at 1 and 1·5 GPa: Implications for the Petrogenesis of MORB. Journal of Petrology, 49(4): 591-613.

Faul, U.H., 2001. Melt retention and segregation beneath mid-ocean ridges. Nature, 410(6831): 920-923.

Floyd, P.A. and Winchester, J.A., 1975. Magma type and tectonic setting discrimination using immobile elements. Earth and Planetary Science Letters, 27(2): 211-218.

Gale, A., Dalton, C.A., Langmuir, C.H., Su, Y. and Schilling, J.-G., 2013. The mean composition of ocean ridge basalts. Geochemistry Geophysics Geosystems, 14(3): 489-518.

Gazel, E., Denyer, P. and Baumgartner, P., 2006. Magmatic and geotectonic significance of Santa Elena Peninsula, Costa Rica. Geologica Acta, 4(1-2): 193-202.

Gazel, E., Plank, T., Forsyth, D.W., Bendersky, C., Lee, C.-T.A. and Hauri, E.H., 2012. Lithosphere versus asthenosphere mantle sources at the Big Pine Volcanic Field, California. Geochemistry, Geophysics, Geosystems, 13(6): Q0AK06.

Geldmacher, J., Hoernle, K., van den Bogaard, P., Hauff, F. and Klügel, A., 2008. Age and Geochemistry of the Central American Forearc Basement (DSDP Leg 67 and 84): Insights into Mezosoic Arc Volcanism and Seamount Accretion on the Fringe of the Caribbean LIP. Journal of Petrology, 49(10): 1781-1815.

Godard, M., Jousselin, D. and Bodinier, J.-L., 2000. Relationships between geochemistry and structure beneath a palaeo-spreading centre: a study of the mantle section in the Oman ophiolite. Earth and Planetary Science Letters, 180(1–2): 133-148.

Godard, M., Lagabrielle, Y., Alard, O. and Harvey, J., 2008. Geochemistry of the highly depleted peridotites drilled at ODP Sites 1272 and 1274 (Fifteen-Twenty Fracture Zone, Mid-Atlantic Ridge): Implications for mantle dynamics beneath a slow spreading ridge. Earth and Planetary Science Letters, 267: 410-425.

Gray, W., Glazner, A.F., Coleman, D.S. and Bartley, J.M., 2008. Long-term geochemical variability of the Late Cretaceous Tuolumne Intrusive Suite, central Sierra Nevada, California. Geological Society, London, Special Publications, 304(1): 183-201.

Grove, T.L. and Bryan, W., 1983. Fractionation of pyroxene-phyric MORB at low pressure: an experimental study. Contributions to Mineralogy and Petrology, 84(4): 293-309.

Grove, T.L., Gerlach, D.C. and Sando, T.W., 1982. Origin of calc-alkaline series lavas at Medicine Lake volcano by fractionation, assimilation and mixing. Contributions to Mineralogy and Petrology, 80(2): 160-182.

Grove, T.L., Kinzler, R.J. and Bryan, W.B., 1993. Fractionation of mid-ocean ridge basalt (MORB). Mantle flow and melt generation at mid-ocean ridges: 281-310.

Gudmundsson, A., 1990a. Dyke emplacement at divergent plate boundaries. In: A.J. Parker, P.C. Rickwood and D.H. Tucker (Editors), Mafic Dykes and Emplacement Mechanisms, Balkema, Rotterdam, pp. 47-62.

Gudmundsson, A., 1990b. Emplacement of dikes, sills and crustal magma chambers at divergent plate boundaries. Tectonophysics, 176(3–4): 257-275.

Gudmundsson, A., 2011. Deflection of dykes into sills at discontinuities and magma-chamber formation. Tectonophysics, 500(1–4): 50-64.

Hauff, F., Hoernle, K., Schmincke, H.-U. and Werner, R., 1997. A Mid Cretaceous origin for the Galápagos hotspot: volcanological, petrologica and geochemical evidence from Costa Rican oceanic crustal segments. Geologische Rundschau, 86(1): 141-155.

Hauff, F., Hoernle, K., van den Bogaard, P., Alvarado, G. and Garbe-Schönberg, D., 2000. Age and geochemistry of basaltic complexes in western Costa Rica: Contributions to the geotectonic evolution of Central America. Geochemistry Geophysics Geosystems, 1.

Herzberg, C., 2004. Partial Crystallization of Mid-Ocean Ridge Basalts in the Crust and Mantle. Journal of Petrology, 45(12): 2389-2405.

Herzberg, C. and Gazel, E., 2009. Petrological evidence for secular cooling in mantle plumes. Nature, 458(7238): 619-622.

Herzberg, C. and O'Hara, M.J., 1998. Phase equilibrium constraints on the origin of basalts, picrites, and komatiites. Earth-Science Reviews, 44(1–2): 39-79.

Herzberg, C. and O'Hara, M.J., 2002. Plume-Associated Ultramafic Magmas of Phanerozoic Age. Journal of Petrology, 43(10): 1857-1883.

Hirth, G. and Kohlstedt, D.L., 1996. Water in the oceanic upper mantle: implications for rheology, melt extraction and the evolution of the lithosphere. Earth and Planetary Science Letters, 144(1–2): 93-108.

Hoernle, K., Hauff, F. and van den Bogaard, P., 2004. 70 m.y. history (136-69 Ma) for the Caribbean Large Igneous Province. Geological Society of America, 32(8): 697-700.

Irvine, T. and Baragar, W., 1971. A guide to the chemical classification of the common volcanic rocks. Canadian journal of earth sciences, 8(5): 523-548.

Ishiwatari, A., 1985. Alpine ophiolites: product of low-degree mantle melting in a Mesozoic transcurrent rift zone. Earth and Planetary Science Letters, 76: 93-108.

Jackson, E. and Thayer, T., 1972. Some criteria for distinguishing between stratiform, concentric and alpine peridotite-gabbro complexes. Proc. 24th Internat. Geol. Congr, 2: 289-296.

Jokat, W., Ritzmann, O., Schmidt-Aursch, M.C., Drachev, S., Gauger, S. and Snow, J., 2003. Geophysical evidence for reduced melt production on the Arctic ultraslow Gakkel mid-ocean ridge. Nature, 423(6943): 962-965.

Juster, T.C., Grove, T.L. and Perfit, M.R., 1989. Experimental constraints on the generation of FeTi basalts, andesites, and rhyodacites at the Galapagos Spreading Center, 85 W and 95 W. Journal of Geophysical Research: Solid Earth (1978–2012), 94(B7): 9251-9274.

Karato, S.-i. and Jung, H., 1998. Water, partial melting and the origin of the seismic low velocity and high attenuation zone in the upper mantle. Earth and Planetary Science Letters, 157(3–4): 193-207.

Karson, J.A., Früh-Green, G.L., Kelley, D.S., Williams, E.A., Yoerger, D.R. and Jakuba, M., 2006. Detachment shear zone of the Atlantis Massif core complex, Mid-Atlantic Ridge, 30°N. Geochemistry, Geophysics, Geosystems, 7(6): Q06016.

Kelemen, P.B., Braun, M. and Hirth, G., 2000. Spatial distribution of melt conduits in the mantle beneath oceanic spreading ridges: Observations from the Ingalls and Oman ophiolites. Geochemistry, Geophysics, Geosystems, 1(7): 1005.

Kelemen, P.B., Hirth, G., Shimizu, N., Spiegelman, M. and Dick, H.J., 1997. A review of melt migration processes in the adiabatically upwelling mantle beneath oceanic spreading ridges. Philosophical Transactions of the Royal Society of London. Series A: Mathematical, Physical and Engineering Sciences, 355(1723): 283-318.

Kelemen, P.B., Yogodzinski, G.M. and Scholl, D.W., 2003. Along-Strike Variation in the Aleutian Island Arc: Genesis of High Mg# Andesite and Implications for Continental Crust. Inside the subduction factory: 223-276.

Kinzler, R.J. and Grove, T.L., 1985. Crystallization and differentiation of Archean komatiite lavas from Northeast Ontario; phase equilibrium and kinetic studies. American Mineralogist, 70(1-2): 40-51.

Kress, V.C. and Carmichael, I.S.E., 1988. Stoichiometry of the iron oxidation reaction in silicate melts. American Mineralogist, 73: 1267-1274.

Kuiper, K.F., Deino, A., Hilgen, F.J., Krijgsman, W., Renne, P.R. and Wijbrans, J.R., 2008. Synchronizing Rock Clocks of Earth History. Science, 320(5875): 500-504.

Kussmaul, S., Paniagua, S. and Gainza, J., 1982. Recopilación, clasificación e interpretación petroquímica de las rocas ígneas de Costa Rica. Instituto Geográfico Nacional Informe Semestral julio–diciembre, 28: 17-79.

Lagabrielle, Y., Vitale Brovarone, A. and Ildefonse, B., 2015. Fossil oceanic core complexes recognized in the blueschist metaophiolites of Western Alps and Corsica. Earth-Science Reviews, 141(0): 1-26.

Langmuir, C.H., Klein, E.M. and Plank, T., 1992. Petrological systematics of mid-ocean ridge basalts: Constraints on melt generation beneath ocean ridges. Geophysical Monograph Series, 71: 183-280.

Lapierre, H., Dupuis, V., Lépinay, B.M.d., Bosch, D., Monié, P., Tardy, M., Maury, R.C., Hernandez, J., Polvé, M., Yeghicheyan, D. and Cotten, J., 1999. Late Jurassic Oceanic Crust and Upper Cretaceous Caribbean Plateau Picritic Basalts Exposed in the Duarte Igneous Complex, Hispaniola. The Journal of Geology, 107(2): 193-207.

Le Maitre, R.W., Bateman, P., Dudek, A., Keller, J., Lameyre, J., Le Bas, M., Sabine, P., Schmid, R., Sorensen, H. and Streckeisen, A., 1989. A classification of igneous rocks and glossary of terms: Recommendations of the International Union of Geological Sciences Subcommission on the Systematics of Igneous Rocks, 193. Blackwell Oxford.

Loocke, M., Snow, J.E. and Ohara, Y., 2013. Melt stagnation in peridotites from the Godzilla Megamullion Oceanic Core Complex, Parece Vela Basin, Philippine Sea. Lithos, 182–183(0): 1-10.

Maccaferri, F., Bonafede, M. and Rivalta, E., 2011. A quantitative study of the mechanisms governing dike propagation, dike arrest and sill formation. Journal of Volcanology and Geothermal Research, 208(1–2): 39-50.

Macdonald, K.C., 1982. Mid-ocean ridges: Fine scale tectonic, volcanic and hydrothermal processes within the plate boundary zone. Annual Review of Earth and Planetary Sciences, 10: 155.

Mahood, G.A. and Baker, D.R., 1986. Experimental constraints on depths of fractionation of mildly alkalic basalts and associated felsic rocks: Pantelleria, Strait of Sicily. Contributions to Mineralogy and Petrology, 93(2): 251-264.

Manatschal, G., Sauter, D., Karpoff, A.M., Masini, E., Mohn, G. and Lagabrielle, Y., 2011. The Chenaillet Ophiolite in the French/Italian Alps: An ancient analogue for an Oceanic Core Complex? Lithos, 124(3–4): 169-184.

Marchesi, C., Garrido, C., Godard, M., Proenza, J., Gervilla, F. and Blanco-Moreno, J., 2006. Petrogenesis of highly depleted peridotites and gabbroic rocks from the Mayarí-Baracoa Ophiolitic Belt (eastern Cuba). Contributions to Mineralogy and Petrology, 151(6): 717-736.

McDonough, W.F. and Sun, S.s., 1995. The composition of the Earth. Chemical Geology, 120(3–4): 223-253.

Meschede, M. and Frisch, W., 1994. Geochemical characteristics of basaltic rocks from the Central American ophiolites. Profil, 7: 71-85.

Meschede, M. and Wolfgang, F., 1998. A plate-tectonic model for the Mesozoic and Early Cenozoic history of the Caribbean plate. Tectonophysics, 296: 269-291.

Michael, P.J. and Cornell, W.C., 1998. Influence of spreading rate and magma supply on crystallization and assimilation beneath mid-ocean ridges: Evidence from chlorine and major element chemistry of mid-ocean ridge basalts. Journal of Geophysical Research: Solid Earth, 103(B8): 18325-18356.

Michael, P.J., Langmuir, C.H., Dick, H.J.B., Snow, J.E., Goldstein, S.L., Graham, D.W., Lehnert, K., Kurras, G., Jokat, W., Mühe, R. and Edmonds, H.N., 2003. Magmatic and amagmatic seafloor generation at the ultraslow-spreading Gakkel ridge, Artic Ocean. Nature, 423: 956-961.

Min, K., Mundil, R., Renne, P.R. and Ludwig, K.R., 2000. A test for systematic errors in 40Ar/39Ar geochronology through comparison with U/Pb analysis of a 1.1-Ga rhyolite. Geochimica et Cosmochimica Acta, 64(1): 73-98.

Neill, I., Kerr, A.C., Chamberlain, K.R., Schmitt, A.K., Urbani, F., Hastie, A.R., Pindell, J.L., Barry, T.L. and Millar, I.L., 2014. Vestiges of the proto-Caribbean seaway: Origin of the San Souci Volcanic Group, Trinidad. Tectonophysics, 626(0): 170-185.

Nicolas, A. and Boudier, F., 2003. Where ophiolites come from and what they tell us. In: Y. Dilek and S. Newcomb (Editors), Ophiolite concept and the evolution of geological thought. Geological Society of America Special Paper 373, Boulder, Colorado, pp. 137-152.

Nicolas, A., Boudier, F. and Meshi, A., 1999. Slow spreading accretion and mantle denudation in the Mirdita ophiolite (Albania). Journal of Geophysical Research: Solid Earth, 104(B7): 15155-15167.

Norrish, K. and Hutton, J.T., 1969. An accurate X-ray spectrographic method for the analysis of a wide range of geological samples. Geochimica et Cosmochimica Acta, 33(4): 431-453.

O'Hara, M.J., 1985. Importance of the `shape' of the melting regime during partial melting of the mantle. Nature, 314(6006): 58-62.

Ohara, Y., Fujioka, K., Ishii, T. and Yurimoto, H., 2003. Peridotites and gabbros from the Parece Vela backarc basin: Unique tectonic window in an extinct backarc spreading ridge. Geochemistry, Geophysics, Geosystems, 4(7): 8611.

Ohara, Y., Yoshida, T., Kato, Y. and Kasuga, S., 2001. Giant Megamullion in the Parece Vela Backarc Basin. Marine Geophysical Researches, 22(1): 47-61.

Paquet, F., Dauteuil, O., Hallot, E. and Moreau, F., 2007. Tectonics and magma dynamics coupling in a dyke swarm of Iceland. Journal of Structural Geology, 29: 1477-1493.

Pearce, J.A., 1975. Basalt geochemistry used to investigate past tectonic environments on Cyprus. Tectonophysics, 25(1–2): 41-67.

Pearce, J.A., 2008. Geochemical fingerprinting of oceanic basalts with applications to ophiolite classification and the search for Archean oceanic crust. Lithos, 100: 14-48.

Pearce, J.A., 2014. Immobile Element Fingerprinting of Ophiolites. Elements, 10(2): 101-108.

Pearce, J.A. and Cann, J.R., 1971. Ophiolite origin investigated by discriminant analysis using Ti, Zr and Y. Earth and Planetary Science Letters, 12(3): 339-349.

Ragazzi, C., 1996. Petrologia e geologia del Complesso Ofiolitico di Nicoya-St. Elena (Costa Rica). Università degli Studi di Ferrara, 115 pp.

Robinson, P.T., Malpas, J., Dilek, Y. and Zhou, M., 2008. The significance of sheeted dike complexes in ophiolites. GSA Today, 18(11): 4-10.

Saginor, I., Gazel, E., Carr, M.J., Swisher, C.C. and Turrin, B., 2011. New Pliocene–Pleistocene 40 Ar/39 Ar ages fill in temporal gaps in the Nicaraguan volcanic record. Journal of Volcanology and Geothermal Research, 202(1): 143-152.

Saginor, I., Gazel, E., Condie, C. and Carr, M.J., 2013. Evolution of geochemical variations along the Central American volcanic front. Geochemistry, Geophysics, Geosystems, 14(10): 4504-4522.

Salters, V.J.M. and Stracke, A., 2004. Composition of the depleted mantle. Geochemistry, Geophysics, Geosystems, 5(5): Q05B07.

Samuel, H. and King, S.D., 2014. Mixing at mid-ocean ridges controlled by small-scale convection and plate motion. Nature Geosci, 7(8): 602-605.

Sanfilippo, A., Dick, H.J.B. and Ohara, Y., 2013. Melt–Rock Reaction in the Mantle: Mantle Troctolites from the Parece Vela Ancient Back-Arc Spreading Center. Journal of Petrology, 54(5): 861-885.

Saunders, A.D., Norry, M.J. and Tarney, J., 1988. Origin of MORB and Chemically-Depleted Mantle Reservoirs: Trace Element Constraints. Journal of Petrology, Special_Volume(1): 415-445.

Sauter, D., Sloan, H., Cannat, M., Goff, J., Patriat, P., Schaming, M. and Roest, W.R., 2011. From slow to ultra-slow: How does spreading rate affect seafloor roughness and crustal thickness? Geology, 39(10): 911-914.

Shaw, D.M., 1970. Trace element fractionation during anatexis. Geochimica et Cosmochimica Acta, 34(2): 237-243.

Shervais, J.W., 1982. Ti-V plots and the petrogenesis of modern and ophiolitic lavas. Earth and Planetary Science Letters, 59(1): 101-118.

Sinton, C.W., Duncan, R.A. and Denyer, P., 1997. Nicoya Peninsula, Costa Rica: A single suite of Caribbean oceanic plateau magmas. Journal of Geophysical Research: Solid Earth, 102(B7): 15507-15520.

Snow, J.E. and Edmonds, H.N., 2007. Ultraslow-spreading ridges: rapid paradigm changes. OCEANOGRAPHY-WASHINGTON DC-OCEANOGRAPHY SOCIETY-, 20(1): 90.

Spiegelman, M., Kelemen, P.B. and Aharonov, E., 2001. Causes and consequences of flow organization during melt transport: The reaction infiltration instability in compactible media. Journal of Geophysical Research: Solid Earth (1978–2012), 106(B2): 2061-2077.

Staudigel, H., 2003. Hydrothermal alteration processes in the oceanic crust. Treatise on geochemistry, 3: 511-535.

Staudigel, H., Hart, S.R. and Richardson, S.H., 1981. Alteration of the oceanic crust: Processes and timing. Earth and Planetary Science Letters, 52(2): 311-327.

Staudigel, H., Plank, T., White, B. and Schmincke, H.U., 1996. Geochemical fluxes during seafloor alteration of the basaltic upper oceanic Crust: DSDP sites 417 and 418, Subduction Top to Bottom. Geophys. Monogr. Ser. AGU, Washington, DC, pp. 19-38.

Steinmann, G., Bernoulli, D. and Friedman, G.M., 2003. Die ophiolithischen Zonen in den mediterranen Kettengebirgen (The ophiolitic zones in the Mediterranean mountain chains). SPECIAL PAPERS-GEOLOGICAL SOCIETY OF AMERICA: 77-92.

Stewart, M.A., Karson, J.A. and Klein, E.M., 2005. Four-dimensional upper crustal construction at fast-spreading mid-ocean ridges: A perspective from an upper crustal cross-section at the Hess Deep Rift. Journal of Volcanology and Geothermal Research, 144(1–4): 287-309.

Sun, S.-s. and McDonough, W.F., 1989. Chemical and isotopic systematics of oceanic basalts: implications for mantle composition and processes. Geological Society, London, Special Publications, 42(1): 313-345.

Thy, P. and Lofgren, G., 1992. Experimental constraints on the low-pressure evolution of transitional and mildly alkalic basalts: multisaturated liquids and coexisting augites. Contributions to Mineralogy and Petrology, 112(2-3): 196-202.

Thy, P. and Lofgren, G., 1994. Experimental constraints on the low-pressure evolution of transitional and mildly alkalic basalts: the effect of Fe-Ti oxide minerals and the origin of basaltic andesites. Contributions to Mineralogy and Petrology, 116(3): 340-351.

Till, C.B., Grove, T.L. and Krawczynski, M.J., 2012. A melting model for variably depleted and enriched lherzolite in the plagioclase and spinel stability fields. Journal of Geophysical Research: Solid Earth (1978–2012), 117(B6).

Tormey, D., Grove, T. and Bryan, W., 1987. Experimental petrology of normal MORB near the Kane Fracture Zone: 22–25 N, mid-Atlantic ridge. Contributions to Mineralogy and Petrology, 96(2): 121-139.

Tournon, J., 1984. Magmatismes du mesozoique à l'actuel en Amerique Centrale: L'exemple de Costa Rica, des ophiolites aux andesites.

Tournon, J., 1994. The Santa Elena Peninsula: an ophiolitic nappe and a sedimentary volcanic relative autochthonus. Profil, 7(7): 87-96.

Tournon, J. and Azéma, J., 1980. Sobre la estructura y la petrología del macizo ultrabásico de Santa Elena (Provincia de Guanacaste, Costa Rica). Inst. Geogr. Nacional, Inf. Semestral, 26: 17-54.

Tournon, J. and Bellon, H., 2009. The southern Central America puzzle: cronology and structure a review. Revista Geológica de América Central, 40(40): 11-47.

Tournon, J., Seyler, M. and Astorga, A., 1995. Les périodotites du Rio San Juan (Nicaragua et Costa Rica): jalons possibles d'une suture ultrabasique EW en Amérique Centrale méridionale. Comptes rendus de l'Académie des sciences. Série 2. Sciences de la terre et des planètes, 320(8): 757-764.

Tremblay, A., Meshi, A. and Bédard, J.H., 2009. Oceanic core complexes and ancient oceanic lithosphere: Insights from Iapetan and Tethyan ophiolites (Canada and Albania). Tectonophysics, 473(1–2): 36-52.

Ussler III, W. and Glazner, A.F., 1989. Phase equilibria along a basalt-rhyolite mixing line: Implications for the origin of calc-alkaline intermediate magmas. Contributions to Mineralogy and Petrology, 101(2): 232-244.

Veloso, E.E., Hayman, N.W., Anma, R., Tominaga, M., González, R.T., Yamazaki, T. and Astudillo, N., 2014. Magma flow directions in the sheeted dike complex at superfast spreading mid-ocean ridges: Insights from IODP Hole 1256D, Eastern Pacific. Geochemistry, Geophysics, Geosystems, 15(4): 1283-1295.

Villiger, S., Ulmer, P. and Müntener, O., 2007. Equilibrium and Fractional Crystallization Experiments at 0·7 GPa; the Effect of Pressure on Phase Relations and Liquid Compositions of Tholeiitic Magmas. Journal of Petrology, 48(1): 159-184.

Villiger, S., Ulmer, P., Müntener, O. and Thompson, A.B., 2004. The Liquid Line of Descent of Anhydrous, Mantle-Derived, Tholeiitic Liquids by Fractional and Equilibrium Crystallization—an Experimental Study at 1·0 GPa. Journal of Petrology, 45(12): 2369-2388.

Walker, D., Shibata, T. and DeLong, S.E., 1979. Abyssal tholeiites from the Oceanographer fracture zone. Contributions to Mineralogy and Petrology, 70(2): 111-125.

Wildberg, H.G.H., 1984. Der Nicoya Komplex, Costa Rica, Zentralamerika: Magmatismus und genese eines polymagmatischen Ophiolith-Komplexes. Münster Forschngsschwerpunkte Geologisch Paläontologisches, 62: 1-123.

Wood, D.A., Joron, J.-L. and Treuil, M., 1979. A re-appraisal of the use of trace elements to classify and discriminate between magma series erupted in different tectonic settings. Earth and Planetary Science Letters, 45(2): 326-336.

Workman, R.K. and Hart, S.R., 2005. Major and trace element composition of the depleted MORB mantle (DMM). Earth and Planetary Science Letters, 231(1–2): 53-72.

Workman, R.K., Hart, S.R., Jackson, M., Regelous, M., Farley, K.A., Blusztajn, J., Kurz, M. and Staudigel, H., 2004. Recycled metasomatized lithosphere as the origin of the Enriched Mantle II (EM2) end-member: Evidence from the Samoan Volcanic Chain. Geochemistry, Geophysics, Geosystems, 5(4): Q04008.

Yang, H.-J., Kinzler, R.J. and Grove, T., 1996. Experiments and models of anhydrous, basaltic olivine-plagioclase-augite saturated melts from 0.001 to 10 kbar. Contributions to Mineralogy and Petrology, 124(1): 1-18.

Zimmer, M.M., Plank, T., Hauri, E.H., Yogodzinski, G.M., Stelling, P., Larsen, J., Singer, B., Jicha, B., Mandeville, C. and Nye, C.J., 2010. The Role of Water in Generating the Calc-alkaline Trend: New Volatile Data for Aleutian Magmas and a New Tholeiitic Index. Journal of Petrology, 51(12): 2411-2444.

8. Figures

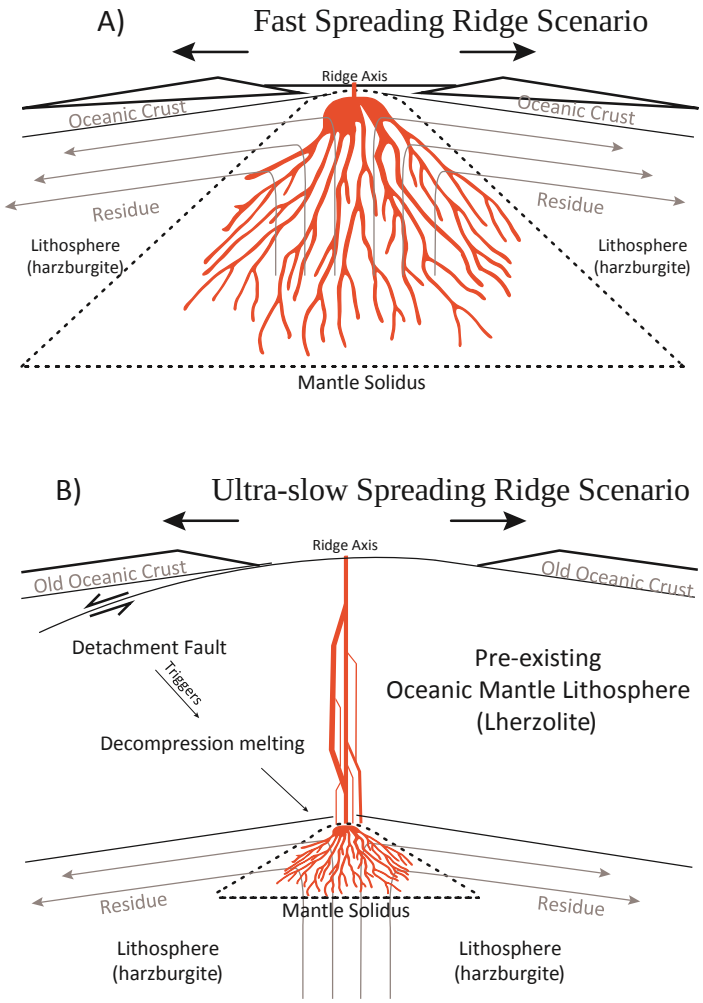

Figure 1.1. Two models of the architecture of the oceanic crust modified from Kelemen et al. (2000) and Cannat (1996). A) At a fast spreading ridge, magmatic supply is abundant and melting occurs at shallower levels in the lithosphere; these melts ascend and form coalescing channels (Kelemen, 2000). Melt fractions are higher than at slow spreading ridges, which allow the development of an oceanic crust on top (Cannat et al., 2006). B) At ultra-slow spreading centers, melts are triggered by detachment faulting which drives a much deeper melting regime. Slower magma generation and lower melt fraction are characteristic of this environment. In this model, melt travels along a pre-existing oceanic mantle lithosphere composed predominantly of lherzolite (Dick et al., 2003; Cannat et al., 2009).

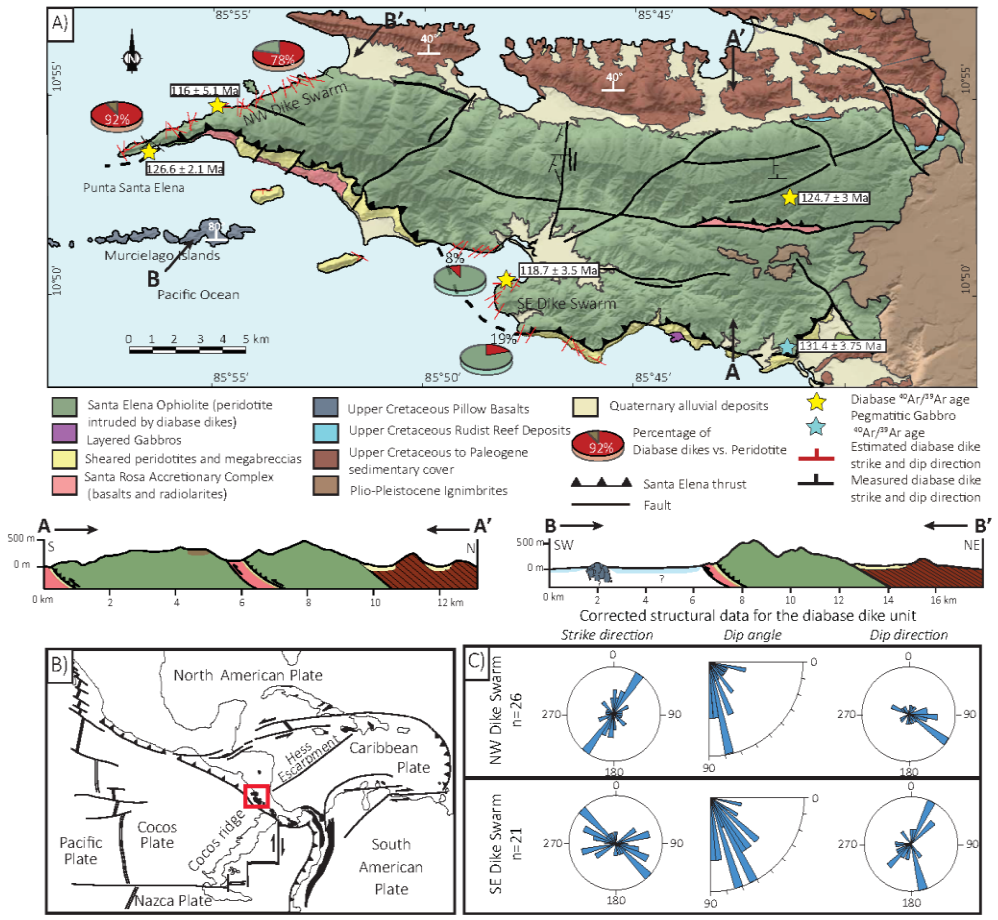

Figure 1.2. Overview map of the Santa Elena peninsula. A) Geologic map modified by our field observations from Tournon et al. (1994), Gazel et al. (2006) and Escuder-Viruete and Baumgartner (2014). B) Geotectonic setting of the Santa Elena Ophiolite after Denyer and Gazel (2009). C) Structural data for the diabase dikes from the NW dike swarm and SE dike swarm measured and corrected in this study.

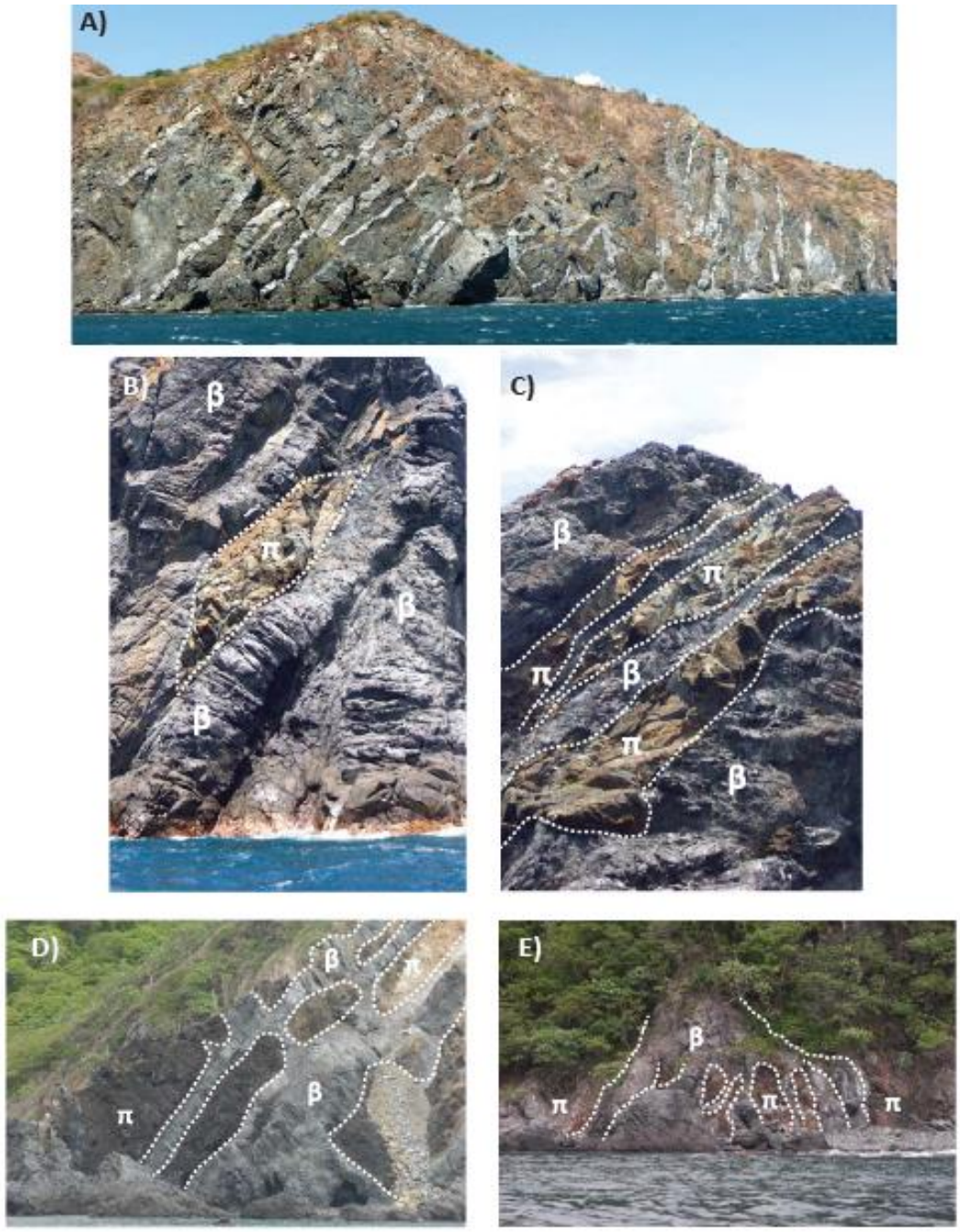

Figure 1.3. Photographs from the diabase dike swarms in the Santa Elena Ophiolite; β denotes diabase dikes and π peridotite. A) Southeastern diabase swarm; diabase dikes intrude the peridotite in a sub-parallel arrangement. B) Boudins of peridotite created by the intruding diabase. C) Boudins of peridotite northwestern diabase swarm. D) and E) Diabase dikes branching out in the shape of an "inverted bush" at a metric scale.

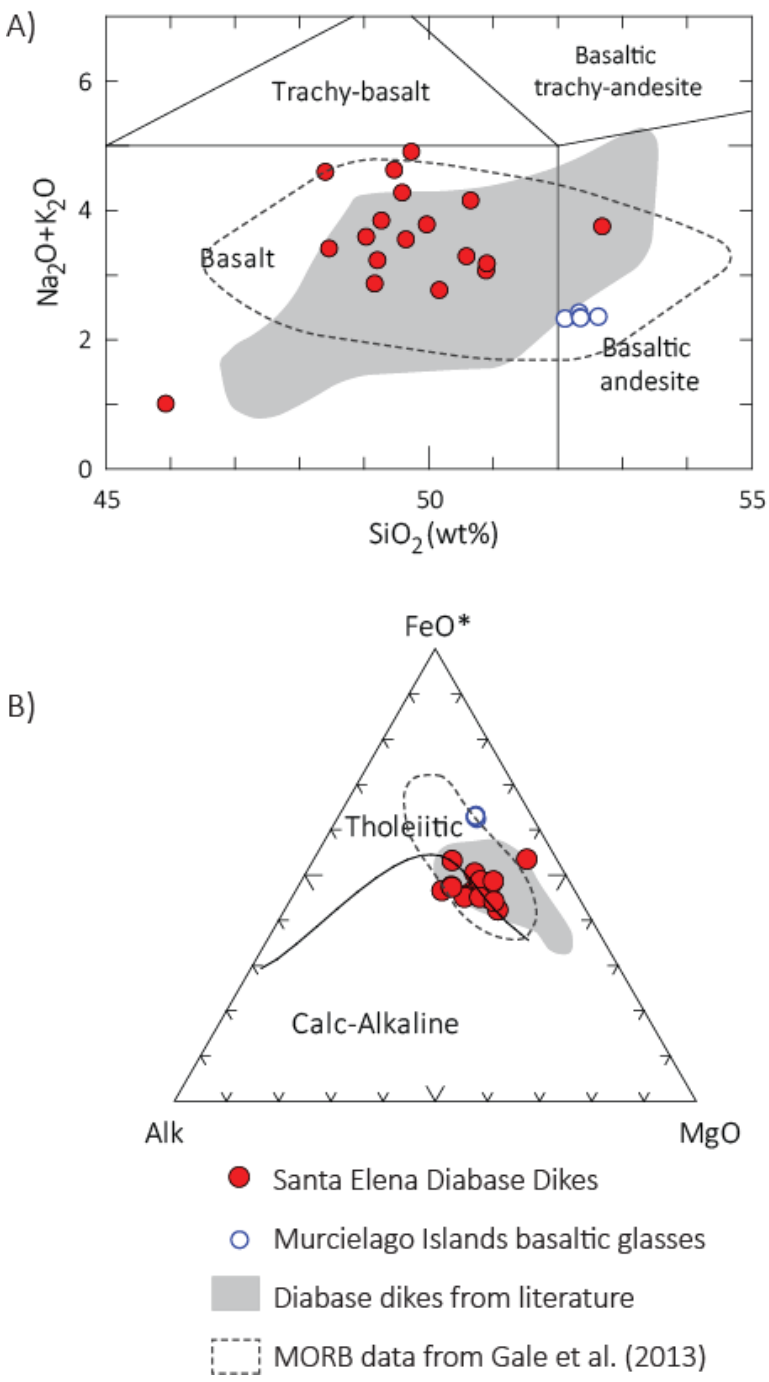

Figure 1.4. Geochemical classification of the diabase dikes of the Santa Elena Ophiolite. A) Total Alkalis-Silica (TAS) diagram (Le Maitre et al., 1989) where the samples from the Santa Elena Ophiolite display a dominant basaltic composition. B) AFM classification diagram (Irvine and Baragar, 1971) suggesting a predominant tholeiitic affinity for the diabase samples. Red symbols denote the new data presented in this paper and gray fields includes data compiled from literature. The dashed lines show the compositional range of MORB data (Gale et al., 2013).

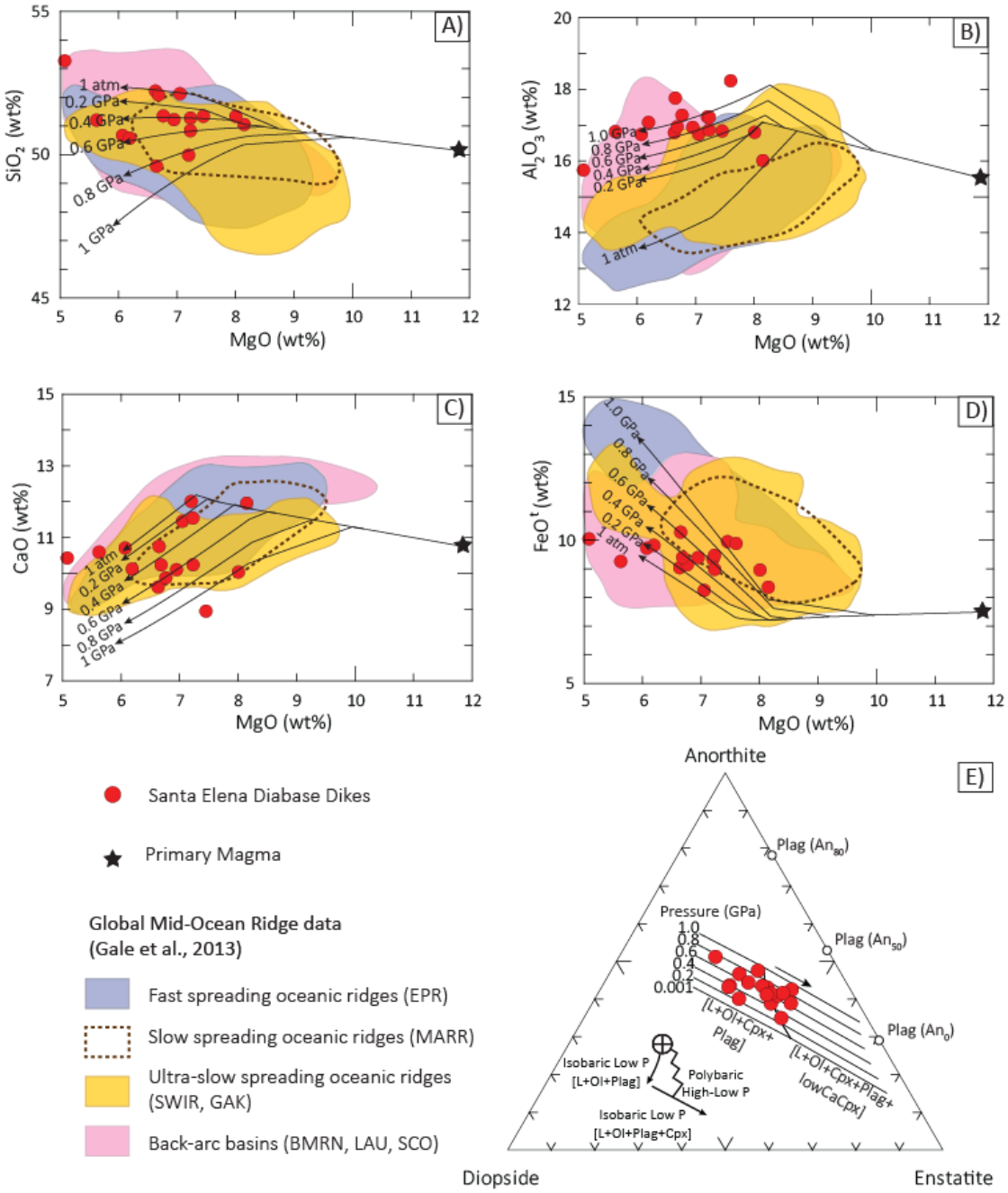

Figure 1.5. Major element variation diagrams for the diabase dikes of the Santa Elena ophiolite. Liquid Lines of Descent (LLD) were calculated using Petrolog3 (Danyushevsky and Plechov, 2011) at different pressures (1.0 atm to 1.0 GPa in increments of 0.2 GPa). The crystallization processes modeled start at a primary magma (PM) that has been modified from the EPR composition of Herzberg and O'hara (2002) in order to explain our data. For the fast spreading ridges, we used values from the East Pacific Rise (EPR); for slow spreading ridges we used values from slow segments of the Mid-Atlantic ridge (MARR) (<60 mm/yr); for ultra-slow spreading ridges we used values from the Southwestern Indian Ridge (SWIR) and Gakkel Ridge (GAK); for back arc basins we used values from Marianas (BMRN), Lau Basin (LAU) and Scotia Back Arc (SCO) (data compiled by Gale et al., 2013).

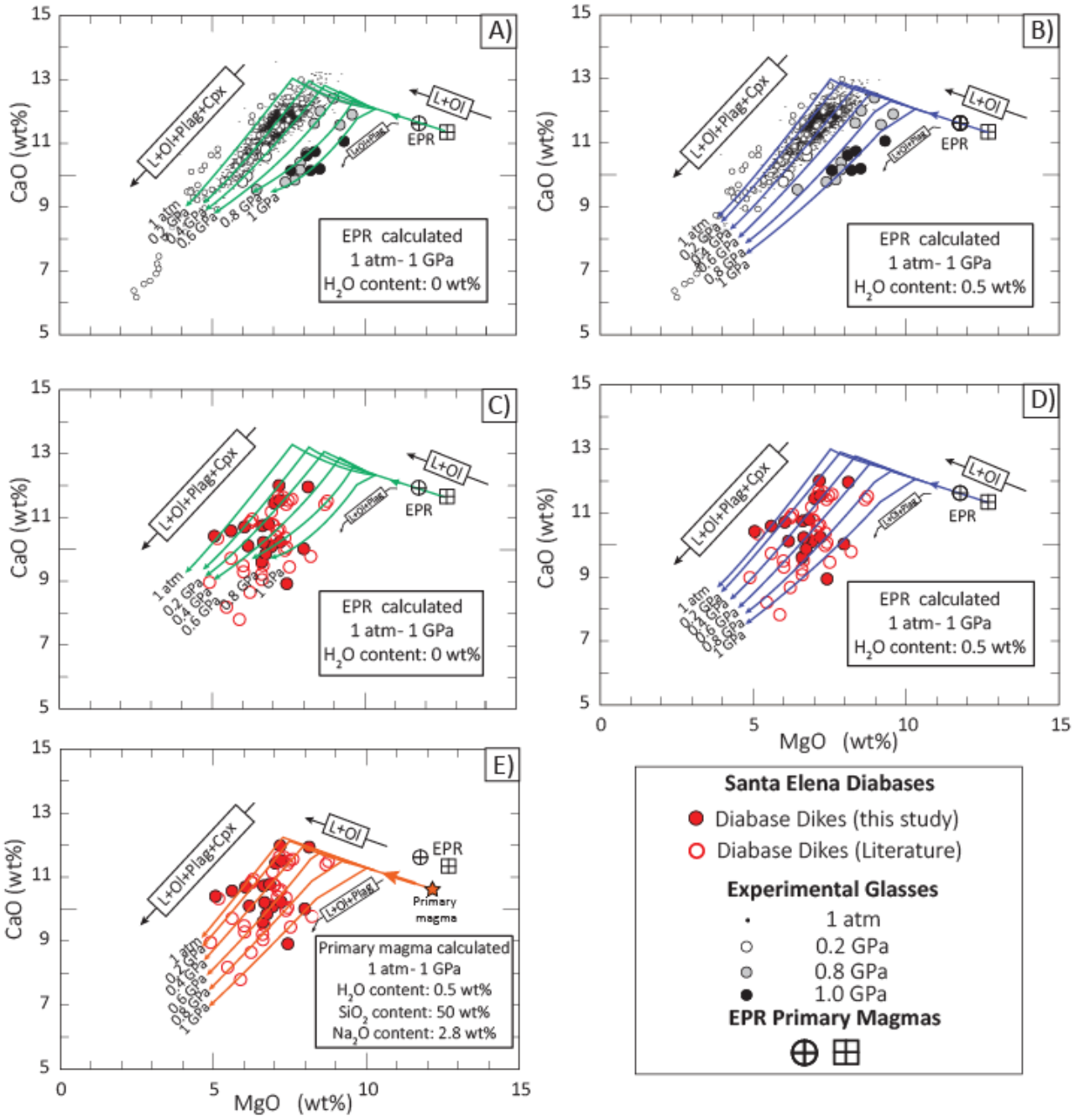

Figure 1.6. Variation diagrams for CaO and MgO at different initial compositions. LLDs were modeled for pressures from 0.001 GPa (1atm) to 1.0 GPa using Petrolog3 (Danyushevsky and Plechov, 2011). Panels A and B show experimental glass compositions for pressures at 1 atm, 0.2 GPa, 0.8 GPa and 1 GPa. The experimental glass data collected by different authors was compiled by Herzberg (2004) and includes data from: Bender et al. (1978); Walker et al. (1979), Grove et al. (1982); Grove and Bryan (1983); Kinzler and Grove (1985); Mahood and Baker (1986); Baker and Eggler (1987); Falloon and Green (1987); Tormey et al. (1987); Juster et al. (1989); Ussler III and Glazner (1989); Bartels et al. (1991); Thy and Lofgren (1992); Grove et al. (1993); Thy and Lofgren (1994); Yang et al. (1996). We also compiled data from Falloon et al.

(2001); Villiger et al. (2004); Villiger et al. (2007); and Falloon et al. (2008). The experimental data was plotted against the LLDs generated for a primary magma from the East Pacific Rise (EPR) calculated by Herzberg and O'Hara (2002) with 0 wt% H_2O added (A) and for the same primary EPR magma containing 0.5 wt% H_2O (B). Note how the experimental data consistently plots in the appropriate LLD for each value. Also, it should be note how adding H_2O in these two model causes an upward displacement in the cotectic points. Panels C and D show the data collected in this work using the same LLDs as in A and B, respectively. It should be noted that neither of the two models seem to appropriately describe the trends in the diabase dikes, however, the model with 0.5 wt% H_2O added has the best correlation of the two models. Panel E shows the diabase dike compositions with the LLDs generated based on the optimized crystallization model for our data. The model parameters used to generate the LLDs are shown in the inset. The resulting model shows a displacement towards lower CaO and lower MgO providing a better fit for the diabase samples, where the majority of our samples fall in the LLDs for pressures >0.4 GPa.

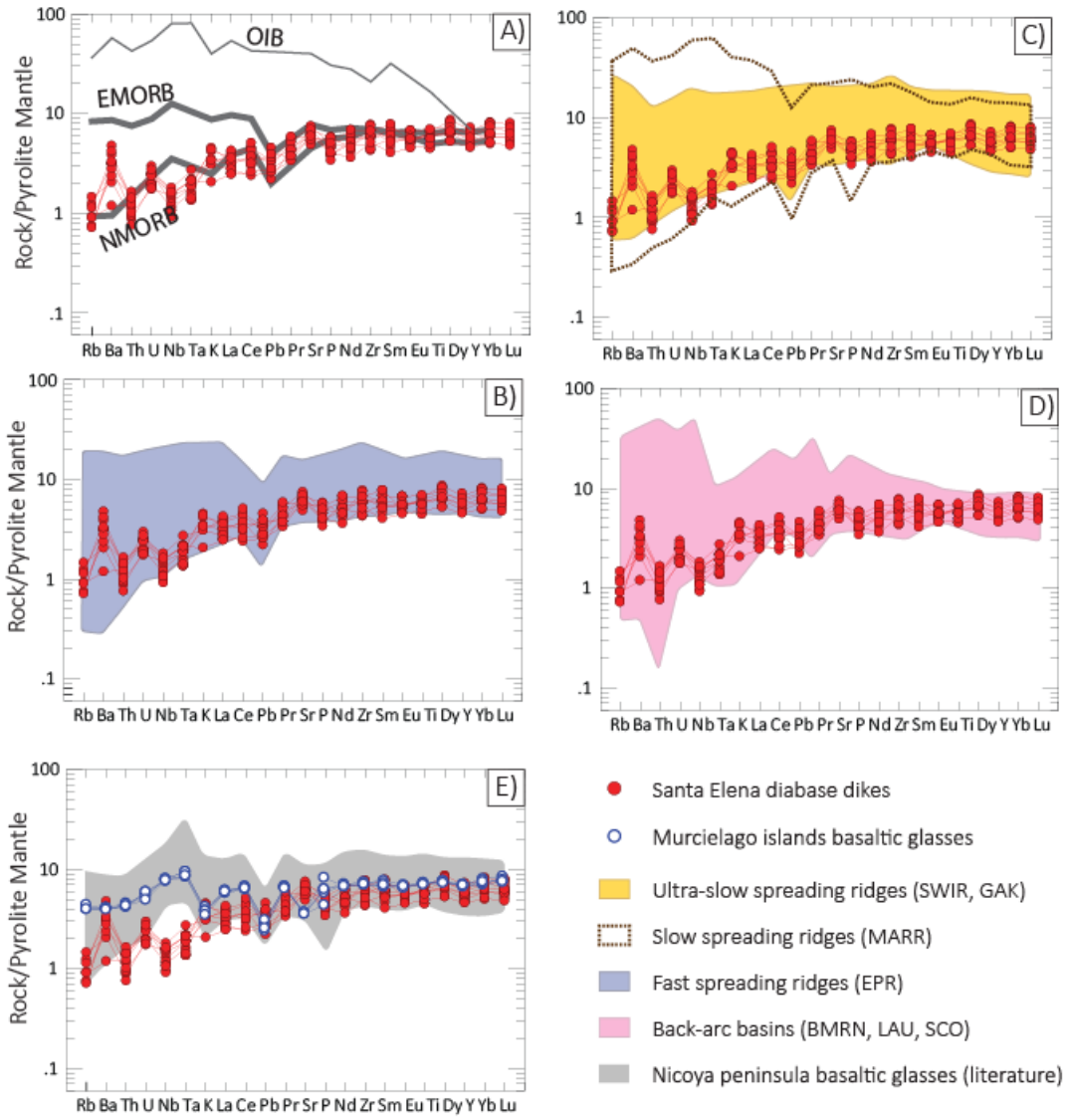

Figure 1.7. Multi-element diagram showing the incompatible element compositions for the Santa Elena Ophiolite diabase dikes normalized to primitive mantle (McDonough and Sun, 1995). Shaded fields represent the values compiled by Gale et al. (2013) from different types of spreading centers. A) Comparison of the Santa Elena diabases and standard values of NMORB, EMORB and OIB (Sun and McDonough, 1989). B) The blue shaded area represents values of fast spreading ridges from the East Pacific Rise (EPR). C) The yellow area represents values from ultra-slow spreading ridges form Gakkel ridge (GAK) and Southwestern Indian ridge (SWIR). Values for slow spreading segments of the Mid-Atlantic ridge (MARR) are represented as a dashed line. D) The pink shaded area are values from Marianas (BMRN), Lau (LAU) and Scotia (SCO) back-arc basins.

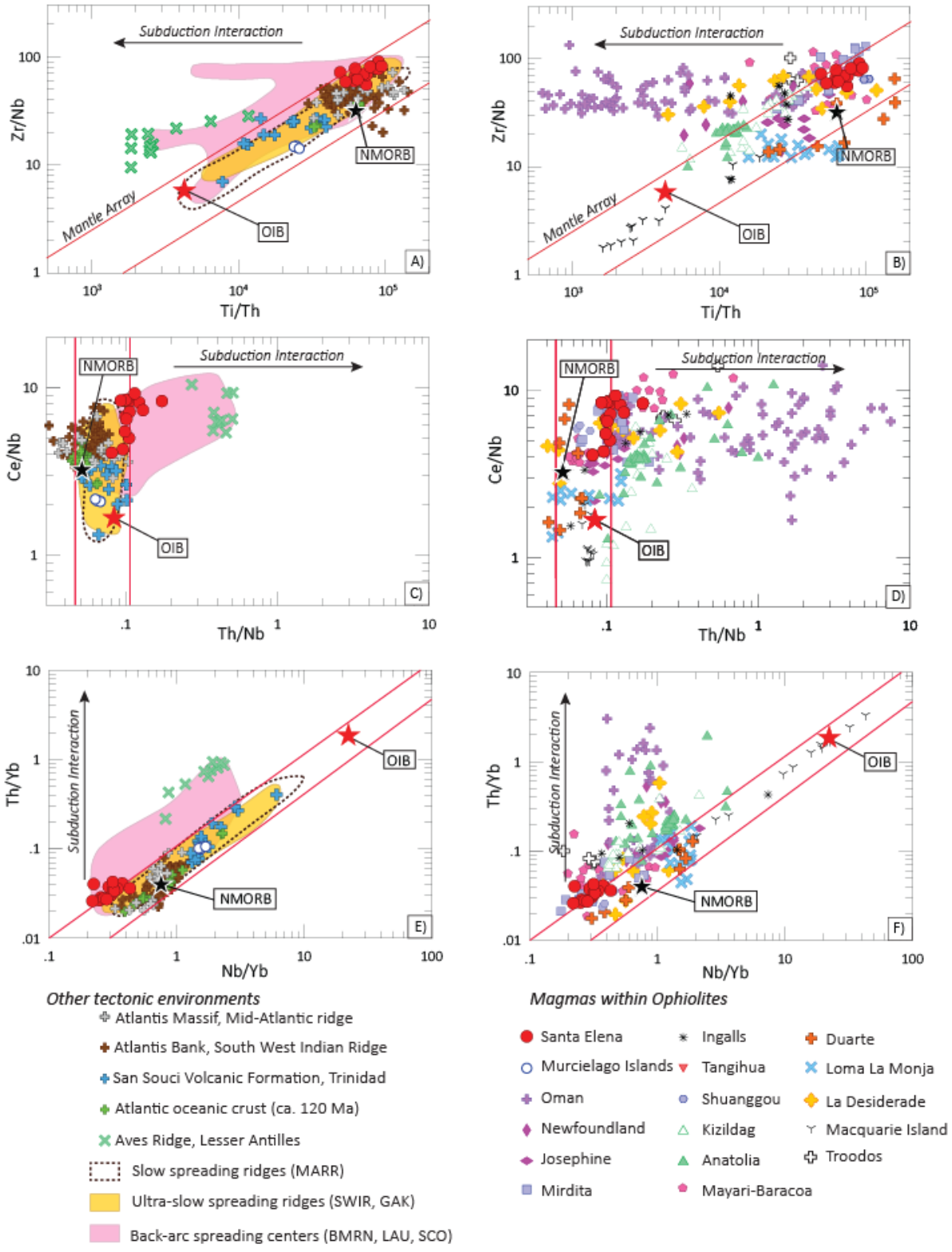

Figure 1.8. Tectonic environment discrimination diagrams of Santa Elena Ophiolite samples compared to other ophiolites or oceanic environments. A) and B) Zr/Nb vs. Ti/Th diagram. Lower Ti/Th and higher Zr/Nb indicate increasing subduction fluid interaction. C) and D) Ce/Nb vs. Th/Nb diagram. Subduction influenced samples plot towards higher Ce and higher Th. Ce can be considered as a proxy for H_2O content,

since both elements have a similar incompatible behavior during melting (Saunders et al., 1988). E) and F) Th/Yb vs. Nb/Yb diagram. Th/Nb is a well-known proxy for subduction input within a system as Th is mobile in fluids and Nb is retained by a residual phase in the subducting slab (Pearce, 2008). We compiled the most recent geochemical data for similar tholeiitic magmas related to ophiolites: Oman, Newfoundland, Josephine, Mirdita, Macquarie Island, Ingalls, Tangihua, Shuanggou, Kizildag, Anatolia and Troodos, Mayarí-Baracoa Ophiolitic Belt, Loma La Monja, La Desiderade. Information from other analog tectonic environments was also collected: Atlantis Massif in the Mid-Atlantic Ridge, Atlantis Bank in the South West Indian Ridge, the San Souci volcanic formation in Trinidad, contemporaneous Atlantic oceanic crust, Aves Ridge crust, slow (Mid-Atlantic Ridge, MARR) and ultra-slow spreading ridges (Gakkel, GAK and Southwest Indian Ridge, SWIR) and back-arc basins (Marianas, BMRN, Lau Basin, LAU, and Scotia Basin, SCO). Note that the diabase dike samples plot in the transition between a MORB environment and a SSZ environment.

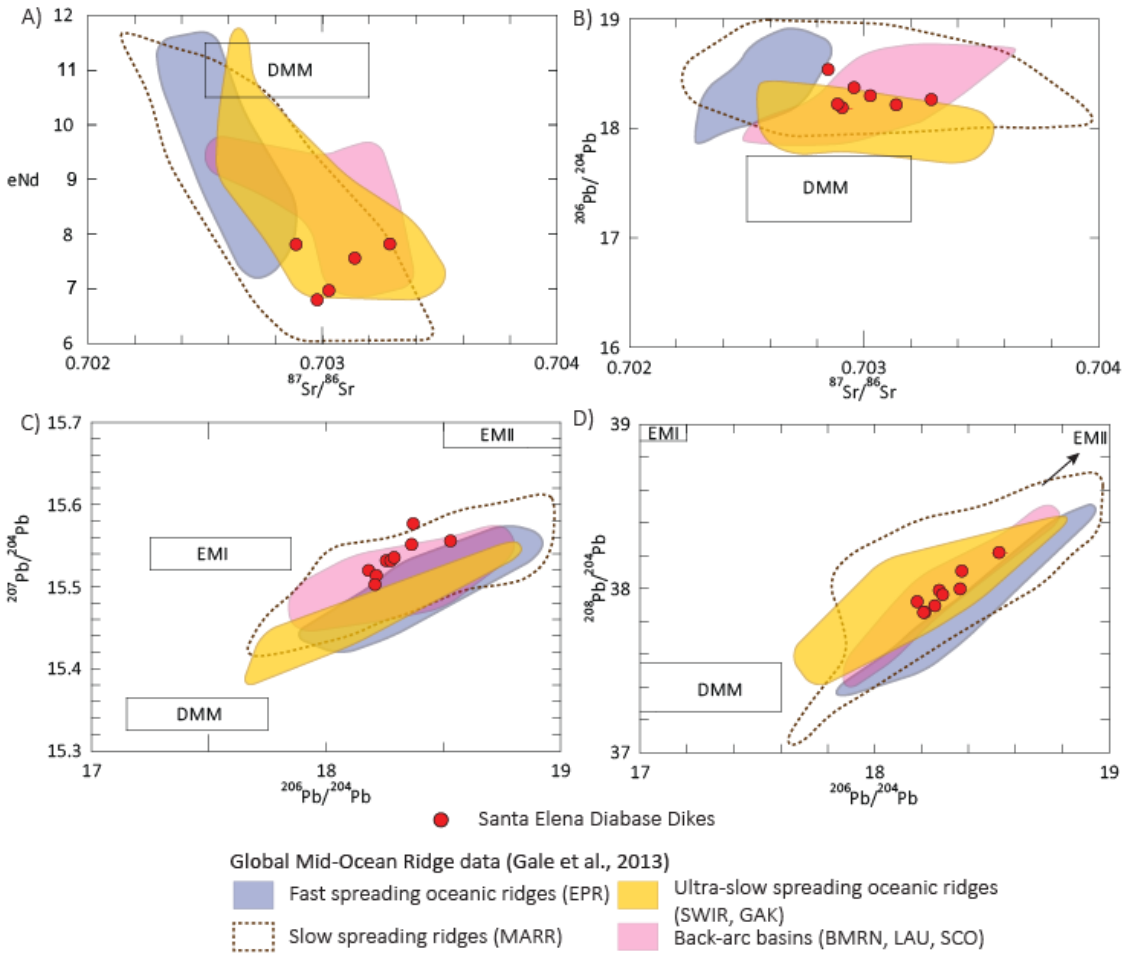

Figure 1.9. Results from the radiogenic isotope analyses. Values were corrected to the initial ratios and projected considering the evolution of the source at 121 Ma. A) εNd vs $^{87}Sr/^{86}Sr$. B) $^{206}Pb/^{204}Pb$ vs$^{87}Sr/^{86}Sr$. C) $^{207}Pb/^{204}Pb$ vs $^{206}Pb/^{204}Pb$. Santa Elena Diabase dikes data show a mixing trend between DMM and EMII. D) $^{208}Pb/^{204}Pb$ vs $^{206}Pb/^{204}Pb$. The linearity of the data points also denotes the mixing of DMM and EMII. Note that the isotope signatures of the Santa Elena diabases show similarities with data from slow spreading ridges (Mid-Atlantic ridge, MARR), ultra-slow spreading ridges (Gakkel, GAK and Southwest Indian Ridge, SWIR) and Back Arc Basins, and separates from fast spreading ridges (East Pacific Rise, EPR). Data from Gale et al. (2013). DMM: Depleted MORB Mantle; EMI: Enriched Mantle I; EMII: Enriched Mantle II.

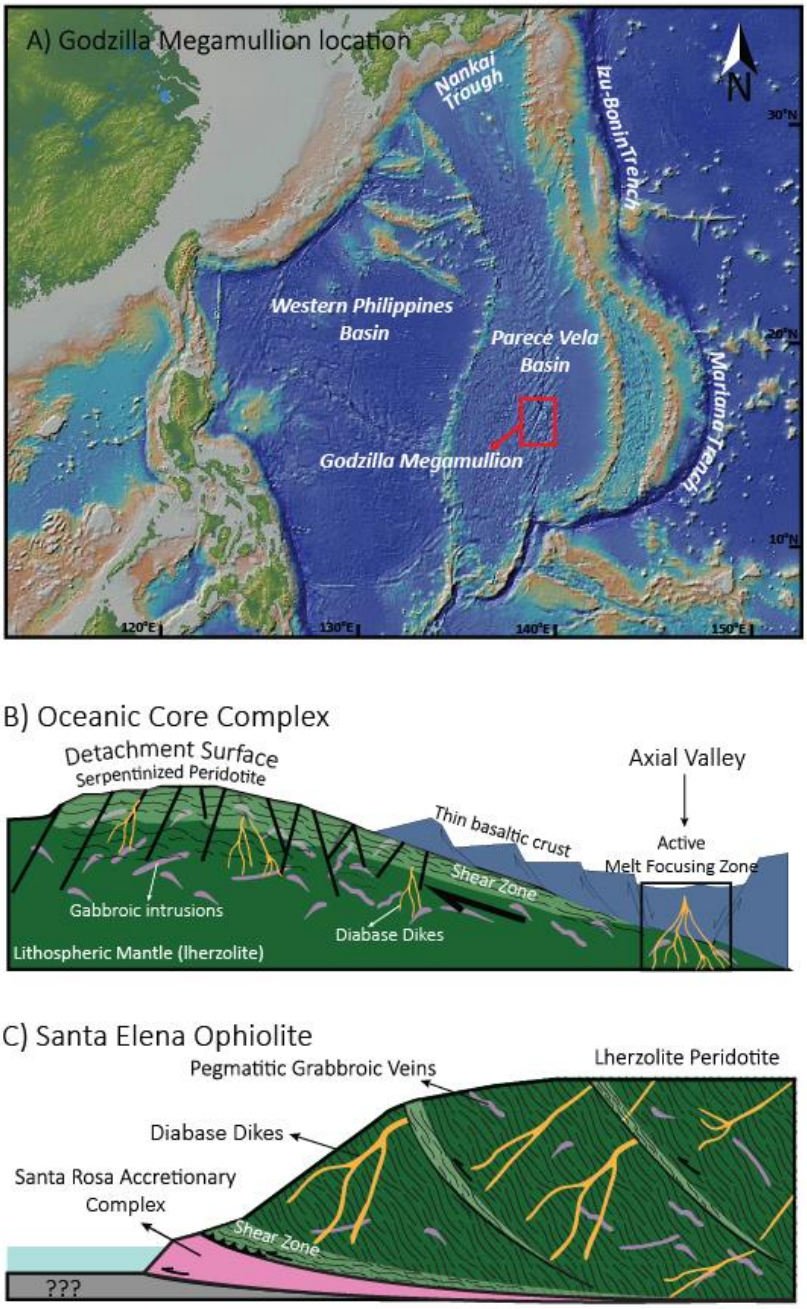

Figure 1.10. Similarities between oceanic core complexes and the Santa Elena Ophiolite. A) Location of the Godzilla Megamullion in the Parece Vela Basin, Marianas back-arc (Loocke et al., 2013). A similar geotectonic scenario is proposed for the formation of the Santa Elena Ophiolite. The architectural and geochemical affinities of oceanic core complexes are in good agreement with the evidences found for the Santa Elena Ophiolite. Map obtained from GeoMapApp (http://www.geomapapp.org). B) Schematic section of a OCC, modified from Karson et al. (2006). C) Schematic cross section of Santa Elena Ophiolite.

Chapter 2: Record of Massive Upwellings from the Pacific Large Low Shear Velocity Province

Abstract

Large igneous provinces and their mechanisms of formation play a key role in the evolution of the planet. As the surface expression of deep mantle processes, it is essential to understand the time frames and geodynamics that trigger these massive lava outpourings. While continental large igneous provinces are more readily accessible, oceanic plateaus have only been studied through drilling and sampling of fragments accreted to active margins, hence they are relatively less understood. The impact of oceanic large igneous provinces in the marine biota is conspicuously recorded in global occurrences of black shale deposits that evidence episodes of anoxia and mass extinctions shortly after their eruption. Here we analyze the record and timing of preserved fragments of the Pacific Ocean Large Igneous Provinces to reconstruct the history of mantle plume upwellings and their relation with a deep-rooted source like the Pacific Large Low Shear Velocity Province during the Mid-Jurassic to Upper Cretaceous. We propose that since the formation of the Pacific Plate circa 180-175 Ma, a series of deep upwellings that interacted with mid-ocean ridge systems in cycles separated by 10 to 20 Ma periodically formed oceanic large igneous provinces.

1. Introduction

Global tomography and numerical models suggest that mantle plume occurrences are closely linked to the margins of large low shear velocity provinces (LLSVPs) (Torsvik et al., 2014; French and Romanowicz, 2015). In these marginal zones the ascent of material from the core-mantle boundary connects deep mantle dynamics with surface processes through mantle plume activity, forming large igneous provinces (LIPs) and some of the modern hotspot volcanoes (Burke

et al., 2008; Steinberger and Torsvik, 2012). Petrological (Herzberg and Gazel, 2009) and geodynamic (Whittaker et al., 2015) evidence suggest a link between the formation of oceanic plateaus and the interactions of mantle plumes and mid-ocean ridges (MOR). Even though the causality relationship between both processes is still unclear (either rifting is initiated by plume impact or it pre-dates plume interaction) larger volumes of upwelling mantle material will preferentially reach the surface when impacting or captured by a MOR (Schilling, 1991; Whittaker et al., 2015). Consequently, it is possible to trace the potential interactions between MORs and mantle plume upwellings by referencing the tectonic and magmatic evolution of the Pacific Plate in time to the current location of the LLSVP, considering the long-lived (~500 Ma) existence of these thermochemical anomalies (Torsvik et al., 2014; Mulyukova et al., 2015; Whittaker et al., 2015). Here, we identified episodic upwellings of the Pacific LLSVP during the Mesozoic by reconstructing the kinematic evolution of the Pacific Plate in the last ~168 Ma using the record of LIP fragments, both accreted in tectonic margins and at the seafloor (Fig. 2.1a). To accurately reconstruct the paleo-Pacific Plate layout we included both the oceanic plateaus and ocean-basin flood basalts, however for the purpose of this paper hereafter we will refer to both groups as oceanic LIPs considering that the processes that formed both types of features are intrinsically related (Kerr, 2014) as both are generated by extensive adiabatic decompression of material hotter than ambient asthenospheric mantle (Kerr, 2014; Ernst, 2014).

2. Record of Pacific related LIPS accreted in Costa Rica

LIPs emplaced over oceanic plates become thickened, buoyant sections of the lithosphere, making them prone to collision and accretion instead of subduction, as they reach convergent margins by means of the normal spreading processes of the oceanic plates (Kerr et al., 2000). These accretionary processes preserved a series of LIP fragments along the Pacific coast of Costa Rica,

that range from near the formation of the Pacific Plate at ~170 Ma to the last Pacific LIP at ~90 Ma, representing one of the most complete records of Pacific Plate mantle upwelling events (Hauff et al., 2000; Hoernle et al., 2004) (Fig. 2.1 a and b). Chronologically these suites of lavas can be clustered into three groups: Nicoya I at ~140 Ma, Nicoya II at ~120 Ma, and Nicoya III at ~90 Ma (Hauff et al., 2000; Hoernle et al., 2004). The lavas preserve fresh pillow-rim glasses, which we used to generate new geochronological and geochemical data from these oceanic LIP accreted terranes. These data were incorporated in a global compilation of radiometric ($^{40}Ar/^{39}Ar$), biostratigraphic and magnetic anomaly ages from Pacific LIPs, and they reveal periods of enhanced magmatic activity associated with mantle plume upwellings, almost since the formation of the Pacific Plate (Fig 2.1 a and b).

These Nicoya terranes were originally thought to belong to the Caribbean LIP (Hoernle et al., 2004; Kerr and Tarney, 2005), however the ages of the Nicoya I and Nicoya II basalts are not consistent with a Caribbean LIP origin. Their geochemical signature and association with black shales that record global oceanic anoxic events (Fig. 2.1b) suggest that they represent fragments of older LIPs. Therefore, to better assess their provenance, we created a series of kinematic reconstructions to show the possible episodicity of the Pacific LLSVP upwellings as well as the possible location where Nicoya I and II formed.

2.1.Nicoya Complex geotectonic background

The Nicoya Complex in northwestern Pacific coast of Costa Rica (Fig. 2.2) includes a series of oceanic terranes of Pacific origin that range ~170 Ma to ~80 Ma (see summary in Fig. 2.1). Geological studies of the Nicoya Complex exist from the early 1900's; however, its formal definition was made in the 1960s by Dengo (1962). It groups a series of terranes of oceanic origin that comprise of basaltic rocks, gabbros and plagiogranites interlayered with deep sea sediments

(radiolarian cherts) of Pacific origin (Sinton et al., 1997; Baumgartner and Denyer, 2006; Denyer and Baumgartner, 2006; Baumgartner et al., 2008). For this study we focused on the suites of pillow basalts that are exposed along the coasts of the Nicoya Peninsula and in the Murcielago Islands (Fig. 2.2). At these outcrops, pillow basalt flows can be found in excellent state of preservation, including fresh glass rims and inter-pillow hyaloclastite (Fig. 2.3).

The origin of these oceanic accreted terranes has been related to an early Galapagos mantle plume initiation (Sinton et al., 1997; Hoernle et al., 2004; Denyer and Gazel, 2009), accretion of Pacific MORB crust (Galli-Olivier, 1979; Kuijpers, 1980), accretion of Galapagos hotspot tracks (Hauff et al., 1997; Hauff et al., 2000), uplift of Caribbean oceanic plateau crust (Duncan and Hargraves, 1984). However, the most accepted models for the Nicoya are the ones that involve a pacific origin as part of the Caribbean Large Igneous Province (CLIP) (Denyer and Baumgartner, 2006). In their model different magmatic pulses disrupted and detached from the Jurassic-Cretaceous oceanic basement along with the overlying sedimentary sequences as they erupted, resulting in the older oceanic crust and radiolarian cherts embedded within the Caribbean LIP as "xenoliths".

Geochemical data from the Nicoya igneous complex clearly indicates intraplate origin; however, many authors proposed an oceanic island arc affinity (Wildberg, 1984; Frisch et al., 1992; Meschede and Frisch, 1994) but those interpretations were based on whole rock data that was influenced by ocean floor alteration. More recent geochemical analyses linked these mafic igneous suites to the Caribbean LIP event as the samples are characterized by flat rare earth element (REE) patterns, moderate high field strength element (HFSE) enrichments and common radiogenic isotopic signatures (Hauff et al., 1997; Sinton et al., 1997; Hauff et al., 2000; Hoernle et al., 2004). In this study we present five new $^{40}Ar/^{39}Ar$ ages, 35 new geochemical analyses

including major and trace element data and 12 new radiogenic isotope measurements from these Nicoya accreted terranes.

Here we propose an alternative interpretation. We suggest that the older groups of basaltic flows at around 140 Ma and 120 Ma are fragments of older oceanic LIPs unrelated to the Galapagos Hotspot but closely linked to the Pacific LLSVP from which a series of mantle plumes (including Galapagos) have risen since the Late Cretaceous. This hypothesis reconciles the age difference and the geochemical similarities between the older basalts and the CLIP.

3. Methods

3.1.Geochronology and Geochemistry Methods

Fresh basaltic glasses from the hyaloclastite and pillow rims were collected from the Murcielago Islands and the Nicoya Peninsula. These samples were carefully selected and cleaned in order to get the fresher pieces of glass. Glass chips of 425-300 μm in diameter were obtained by dry-sieving.

To acquire the $^{40}Ar/^{39}Ar$ data, the groundmass and mineral separates were irradiated for 60 hours at the Oregon State University TRIGA-type reactor in the Cadmium-Lined In-Core Irradiation Tube. At the University of Wisconsin-Madison Rare Gas Geochronology Laboratory, incremental heating experiments were conducted using a 25 Watt CO_2 laser. Each step of the experiment included heating at a given laser power, followed by an additional 10 min for gas cleanup. The gas was cleaned with two SAES C50 getters, one of which was operated at ~450 °C and the other at room temperature. Blanks were analyzed after every second laser heating step, and were less than 5×10^{-20} mol/V for ^{36}Ar and 2×10^{-17} mol/V for ^{40}Ar, respectively. Argon isotope analyses were performed using a MAP 215–50, and the isotope data was reduced using ArArCalc

software version 2.5 (http://earthref.org/ArArCALC/). Ages were calculated from the blank-discrimination and decay-corrected Ar isotope data after correction for interfering isotopes produced from potassium and calcium in the nuclear reactor. Ages are reported with 2σ uncertainties (includes the J uncertainty) and are calculated relative to a Fish Canyon standard age of 28.201 ± 0.046 Ma (Kuiper et al., 2008) and a value for $\lambda^{40}K$ of 5.463 ± 0.107 x 10^{-10} yr^{-1} (Min et al., 2000).

Basaltic glass samples collected from the Murcielago Islands and Nicoya Peninsula pillow basalts rims were selected under a stereoscope microscope, and arranged in a 1-inch round epoxy mount which was later polished for electron microprobe (EMP) analyses. Major element data were collected at the Electron Beam Laboratory at Virginia Tech with a Cameca SX50 Electron Microprobe using a 60 µm diameter electron beam at a 10 nA current a 15 kV acceleration voltage. Trace elements were obtained at Virginia Tech LA-ICPMS lab facilities using an Agilent 7500ce ICPMS coupled with a Geolas laser ablation system. Three analyses were performed in each glass using a 90 µm diameter spot and at 10 Hz repetition rate. Standards were run at the start and end of the run to correct for drift. The data was reduced using the USGS standards BCR-2G, BHVO-2G and BIR-1G. Replicates of these standards indicate a precision of <5% (RSD) and accuracy better than 10% for most of the elements analyzed. Analysis of Sr, Nd, and Pb radiogenic isotope ratios were carried out at the Center for Elemental Mass Spectrometry, University of South Carolina following established techniques for this lab (e.g. Bizimis et al., 2013; Khanna et al., 2014).

3.2.Kinematic plate tectonic reconstruction parameters

Our new kinematic plate tectonic model is based on data derived from different geological, geodynamic and kinematic constraints. Besides our own geological investigations in Central

America, the distribution, composition, age and evolution of the continental blocks, magmatic provinces, suture zones, sedimentary basin and accreted complexes in Middle America region have been systematically compiled in a geo-referenced data base (Flores, 2009, 2015). Our model differs from earlier models because we integrated dynamic plate boundaries, plate buoyancy factors, oceanic spreading rates, subsidence patterns, stratigraphy and paleobiogeographic data, as well as the major tectonic and magmatic events. Our new plate tectonic models also combine the classically used Atlantic Ocean constraints (Pangea breakup) with the geodynamic history of the Americas active margins in order to place and reconstruct the Pacific Ocean plates. This new approach represents a distinct departure from classical continental drift models, which only consider displacement of continents, terranes and blocks on a sphere and do not take into account plate boundaries and oceanic crust geometry.

The new plate tectonic results presented here (see Fig. 2.4) were created using a geological-geodynamic approach first explained and applied by Stampfli and Borel (2002). The reconstructions were performed using an ArcGis® base, which enabled us to apply and quantify rotational motions and spreading/subduction rates to the numerous plates and tectonic blocks involved in the evolution of the study area. Boundary conditions are provided by the relative motions of the different plates with respect to a fixed Europe (Baltica). Plate tectonic concepts are applied all along the process and plate boundaries are built and transformed in space and time. Plate velocities can be calculated at any time and are never in excess of 20 cm/yr. The reconstructions were created from the past to the present, although an iterative approach is always necessary. The size of the ancient oceanic domains was created using geometric constraints done by geometry of Pacific and Atlantic oceans magnetic isochrones (see Fig. 2.5; Müller et al., 1997; Müller et al., 2008) and by the ages of collision events recorded in the Middle American region

(Flores et al., 2013; Flores et al., 2015 and references therein). The lithospheric plates were constructed through time by adding/removing oceanic crust to the major continents and terranes. Plates were created systematically using tight fits in order not to underestimate crustal extension. Each plate was moved step by step, as single rigid entities. The only evolving elements are the plate boundaries, which are preserved and follow a consistent geodynamic evolution through time. This methodology offers us a good control on plate kinematics and geometries, which provide new constraints for plate tectonic scenarios and their relationship with the geological record.

Data and methodology applied here are part of a larger global geodynamic database created in order to support plate tectonic reconstruction extending from the Late Neoproterozoic to the Cenozoic. Examples of this new approach can be found in Hochard (2008; whole globe), Bagheri and Stampfli (2008; Iran), Moix et al. (2008; Turkey),Ferrari et al. (2008; Southeast Asia) , von Raumer and Stampfli (2008; Rheic Ocean), Flores (2009; Central America), Stampfli and Hochard (2009; Alpine realm), Vérard et al. (2012a; South America-Antarctica), Wilhem et al. (2012; Altaids), Vérard et al. (2012b; Global Euler poles distribution) Vérard and Stampfli (2013a; 2013b; Australides) and Stampfli et al. (2013; Pangea).

4. Results

4.1.Fresh pillow lavas glass rims vs. whole rock analyses

Immediately after basaltic lavas erupt in deep oceanic environments, the thermal differences between seawater and lava creates a quenching glass rim around the pillow basalt (Fig. 2.3). Numerous authors have described the physical and chemical dynamic of such interaction, which usually results in an exchange of dissolved cations between seawater and the newly formed oceanic

crust (Fig. 2.6) (Bach et al., 2001; Stroncik and Schmincke, 2001; Foustoukos and Seyfried, 2007; Seyfried et al., 2013).

During the quenching process, a decrease of volume occurs, allowing the development of several sets of radial cracks surrounding the pillow basalts. These cooling cracks enable the seawater to percolate inside the hotter interior of the pillow where it reacts with the pillow cores (Scott and Hajash, 1976). These interactions result in different geochemical signatures for the inner pillow basalt and their glass rims (Scott and Hajash, 1976; Seyfried et al., 1998; Polat et al., 2003; Staudigel, 2003).

Large Ion Litophile Elements (LILE) behave similarly during hydrothermal alteration and during melting processes, i.e., they partition strongly into the fluid phase. Hence, alkali elements like Rb, Sr, K, Mg, Ca, Na, and Ba show variations in content from rims to cores in pillow basalts displaying a mobile behavior. High field strength elements (HFSE) such as Al, Ti, Th, Zr, Nb, and Ta and to some extent heavy rare earth elements (HREE) are less mobile in fluid phases during hydrothermal alteration, which results in their contents remaining unchanged from rims to cores in the pillow basalts (Polat et al., 2003).

Consequently, pillow glass rims are usually enriched in elements like Fe, Mg, Mn, and Rb while showing depletions in Si, Ca, Na, K, Sr and Pb. The latter elements tend to percolate inside the pillow basalt and enrich the core of the pillow basalts (Polat et al., 2003). These patterns in element behavior motivated us to comparatively analyze the core and the glass rims of the pillow basalts from the Nicoya accreted oceanic terranes (Fig. 2.6). Peaks in elements like Rb, Ba, K, Pb and Sr show an enriched signature in the pillow cores when performing analyses in bulk rock pillow core and/or rim. However, when the analyses were made in situ in the fresh basaltic glasses of the rims an opposite trace element pattern is evident (Fig. 2.6). Hence, by analyzing the glass

rims instead of the bulk core sample we can avoid the effect of seawater interaction and obtain a clearer signature of the original lava composition. This is of most importance given that the pillow core enriched signature can be interpreted as an arc signature when actually it is an artifact of seawater-lava interaction, which can result in misled interpretations of their origin.

4.2.Geochronology synthesis of accreted LIP terranes in the Nicoya Peninsula

In order to guarantee an acceptable quality in the data, we chose only the samples that yielded an $^{40}Ar/^{39}Ar$ plateau age (with ^{39}Ar% higher than 50%) or samples that generated inverse isochrones ages for our study. Also, we used only data obtained by step-heating techniques in order to avoid anomalous sub-systems within the measurements due to Ar loss or inherited Ar.

Previous studies have published K-Ar ages for the Nicoya Complex oceanic rocks; however, these ages are not included in our compilation because the low potassium contents of the basalt suites and the varying degrees of secondary seafloor alteration introduce uncertainty to the measurements. Altered samples can be subject of partial loss of radiogenic ^{40}Ar derived from in situ decay of ^{40}K which can lead to an under/over estimation of the crystallization ages.

Our work includes the $^{40}Ar/^{39}Ar$ geochronological analyses from the Nicoya Complex reported in previous works by Sinton et al. (1997), Hauff et al. (2000) and Hoernle et al. (2004). In this work we present five new ages from El Coco (137.09 ± 2.48 Ma), Murcielago Islands (113.43 ± 3.48 Ma), inner Nicoya (89.3 ± 4.3 Ma), Junquillal (79.9 ± 0.7 Ma), and Marbella (77.2 ± 2.7 Ma). The ages from El Coco and Murcielago Islands were measured in fresh pillow basalt glasses and they belong to the Nicoya I and II LIP pulses. Samples from Junquillal, Marbella and inner Nicoya are from diabases and belong to intrusive events related to the main and subsequent pulses of the Caribbean LIP.

4.3.Summary of Pacific LIP geochronology and geochemical signatures

Considering the same criteria, we used to filter the radiometric ages from Nicoya Complex, we compiled the available geochronological data for Pacific LIPs. Most of the ages compiled for the Pacific LIPs belong to drill core samples from DSDP, ODP, IODP and GEOMAR expeditions and drilling projects.

For our study we needed to compile only ages from the igneous basement of these Pacific LIPs, however this was not possible in some drilling sites like in the Mid-Pacific Mountains and Hess Rise. In these cases, we used the available biostratigraphic and estimated magnetic anomaly ages as an approximation of the minimum age of the basement. Further constraints on the ages of these LIPs are interpreted from the paleotectonic reconstructions.

The available geochemistry data for the Pacific oceanic LIPs come from extracted cores from deep seafloor drilling surveys and on-land accreted fragments. We filtered the data to include only analyses made on tholeiitic basalt samples from the LIPs. Alkaline basalts drilled or dredged from seamounts and guyots on top of the LIP base were excluded because these are likely a product of later stages of tectonic disruption as the LIPs separated and drifted apart by means of normal oceanic spreading processes (Kerr et al., 2000).

4.4.Kinematic evolution of the Pacific Plate and LIPs formation

Many models have been created to describe the Pacific Plate tectonic evolution since its formation during the Early to Middle Jurassic (Bartolini and Larson, 2001). Most of them are based on (a) matching magnetic lineations in places where both sides of the spreading ridge are preserved, (b) reconstructing older magnetic lineations in areas where they no longer exist, (c) using fixing Atlantic and Pacific hotspot as framework to calculate relative plate motions, and/or (d) interpreting the onshore geology such subduction complexes, accretionary terranes, ophiolites

and larger-scale crustal deformation (Seton et al., 2012 and references therein). Our kinematic model combines all the above mentioned approaches and also allows us to geometrically test the previously proposed models. A similar approach as (a) was used to match isochrones 5o and 6o on the Pacific, Antarctica, Nazca and Cocos plates (Fig. 2.5). The latter clearly evidence the asymmetry on the Pacific Ocean spreading centers. Asymmetric counterpart isochrones for 13y, 18o, 21o, 25y, 31y and 34y were constructed on the Farallon Plate seafloor from the Oligocene to the Campanian (e.g., Fig 2.4 i-k). A combination (b) and (d) approaches were used to reconstruct isochrones during the Cretaceous Normal Superchron (Fig. 2.4 f-h), as well as to reconstruct counterpart isochrones for M0, M10, M16, M25, and M42 (Fig. 2.4a-e). Finally, isochrones M21 and M4 were used as kinematic constrainers for the geometric evolution of the Pacific Plate during the Late Jurassic to Early Cretaceous.

The origin of the Pacific Plate is thought to start at ~170 Ma at a triple junction of the Izanagi-Farallon-Phoenix plates in what was the Panthalassa Ocean (Seton et al., 2012). In contrast to almost all existent models, we suggest that the onset of the Pacific Plate triangular shape (Fig. 2.4a) occurred in an intraoceanic supra-subduction tectonic setting (Gerya et al., 2015). In this tectonic scenario the Pacific Plate started due to extension, rifting and subsequent spreading of a series of continental and oceanic island arcs that lately collided along the continental margin of northeastern Asia, and North and Middle America (Baumgartner et al., 2008; van der Meer et al., 2012; and references therein). We did not use any of the current Cretaceous-Jurassic absolute plate motion models for the Pacific plate (e.g. Wessel and Kroenke, 2008; Chandler et al., 2012). None of these models provide us a suitable geometry for the island arcs that diachronously collided along the Middle America region. The timing for those collisions was estimated based on the ages of the exhumation of subduction related complexes (Flores et al., 2013, Flores et al., 2015 and

reference therein). Nonetheless, our kinematic reconstructions do not significantly differ from those on Müller et al. (2016, see Fig. 2.7), which integrated the above mentioned absolute plate motion models. In our reconstructions, the Triangle of Pacific plate display four different rotational paths inside the LLSVP edges (Fig. 2.8a), initially a clear south migration is observed from ~168 Ma to ~132 Ma (Fig. 2.8b). A small step backwards is followed by a steady SW rotation occur from ~120 Ma to ~103 Ma (Fig. 2.8c). A ~10 Ma reversal period of rotation towards the NE is observed (Fig. 2.8d) before its final NW migration recorded from ~68 Ma to the present (Fig. 2.8e). These rotational paths can be correlated to the growth, migration, and collision of the various island arcs that surrounded the Pacific plate since ~168 Ma to ~84 as well as the establishment of a continued eastward subduction zone along the Americas after the formation of the modern Caribbean plate around 68 Ma. The latter, detached the Pacific plate from the island arcs, and triggered its current rotational path towards the NE modern convergent boundaries.

At our M42 reconstruction (~168 Ma) the oldest sections of the Pigafetta Basin were already emplaced and our reconstructions suggest a correspondence between a MOR and the limit of LLSVP in the northern area of the Pacific triangle; in agreement with radiometric ages from Koppers et al. (2003). During the ~154 Ma reconstruction (Fig. 2.4b), the Pacific Plate rotates south triggering the migration of the triple point. Interactions between the MORs and the northern margin of the LSSVP are geometrically plausible; however, no upwelling of the LIPs has been recognized at this time.

As spreading progresses, the Pacific Plate expands and continues migrating towards the south. At ~142 Ma Shatsky Rise eruption marks an upwelling of the LLSVP (Fig. 2.4c). At this time, in our reconstructions the Mid-Pacific Mountains basement, the Magellan Rise and the Nicoya I terrane were being formed at the location where the MOR and the LLSVP coincided.

This interaction is plausible until the ~132 Ma reconstructions (Fig. 2.4d), suggesting that the LIPs formed during a period of at least 10 Ma.

According to several authors (Müller et al., 2008; Seton et al., 2012) circa Early and mid-Cretaceous an increase in the seafloor spreading velocities occurred. A slightly northeast rotation can be suggested based on the orientation of M4 and M0 isochrones. Moreover, a ridge jump of the northeastern and southern MORs are proposed. These ridge jumps into the older crust of the Pacific Plate satisfactory explained the geometry change and truncated nature of the M4 and M0 isochrones (Fig. 2.4e). The latter coincides with the beginning of the Cretaceous Normal Superchron (Olson and Amit, 2015) and with the time of onset of the southern LIPs: Ontong-Java, Manihiki, Hikurangi plateaus, along with the Nauru Basin and East Mariana Basin (Castillo et al., 1991; Castillo et al., 1994; Taylor, 2006; Chandler et al., 2012; Seton et al., 2012). However, according to our reconstructions, certain sections of the northern MORs were also active forming the Nicoya II terrane and possibly the elongate basement section of Mid-Pacific Mountains as well as oldest basement of the Hess Rise that has not yet been reached by drilling expeditions. Our work suggests that this time constitutes possibly the largest upwellings of the Pacific LLSVP recognized so far in the history of our planet.

Due to the lack of magnetic lineations during the Cretaceous Normal Superchron, we create three kinematic plate tectonic reconstructions at 112, 103, and 95 Ma (Fig. 2.4 f-h) using reconstructed isochrones at symmetries and spreading rates that would provide a seafloor geometry to satisfactory explain collisions and other major geological and tectonic events recorded on the Middle America active margin. At the 112 Ma (Fig. 2.4f), we propose a new ridge triple point formation in the southern Pacific Plate MOR, which connected the Pacific Plate with a new southeastern oriented ridge that opened perpendicular to Phoenix Plate seafloor. This triple point

will allow the separation of the Manihiki and Hikurangi LIPs from the Ontong-Java Plateau. Interactions between this triple point and the southern margin of the LLSVP probably are responsible for the youngest sections of the Hikurangi Plateau (Davy et al., 2008).

At 103 Ma (Fig. 2.4 g) the plate reorganization is still ongoing, a ridge jump in the southeastern Pacific Plate MOR takes back the Manihiki Plateau into the Pacific Plate. While the Hikurangi Plateau moves south within the Phoenix Plate. There is no identified LIP pulse recorded in the Pacific seafloor at this time; however, in our model a potential interaction between the MOR and the LLSVP margin at the northern section of the Pacific Plate may suggest the possible formation of LIPs at this time. The undated Alaskan Yakutat Oceanic Plateau (Christeson et al., 2010; Worthington et al., 2012) may represent a potential LIP that forms at this time along the Pacific-Farallon MOR.

In our 95 Ma (Fig. 2.4 h) reconstruction, the Pacific Plate change its rotation path and starts to migrate towards the northeast. Simultaneously, the Hikurangi Plateau gets closer to future New Zealand margin. A potential interaction between the LLSVP eastern margin and the Farallon Plate southern-eastern MOR are proposed as the responsible to generate the beginning of the Caribbean Plateau plume upwelling. It is likely that the plume that ascended from the limits of the LLSVP was captured by the curved MOR, which explains the shape and orientation of the Caribbean LIP. As the Farallon Plate moves towards the northeast, the Caribbean LIPs collided with the South America margin as well as with the inter-America island arc circa 84 Ma (Fig. 2.4 i). The latter will produce subduction inversion and subsequent migration of the Caribbean Plateau into the Americas. At the same time the Hikurangi Plateau collided with the future New Zealand margin, the Phoenix Plate continues to subduct into the Antarctica margin, and the Pacific Plate reverses the sense of it migration and started to move towards the north.

During our ~68 Ma and ~56 Ma reconstruction (Fig. 2.4 j-k) the Caribbean LIP is positioned in between the Americas and as the plate kept moving towards the east, subduction initiation occurs in its western boundary, forming the early Central America Trench. In the northern Pacific Ocean, the Kula Plate MOR underwent some instability producing a ridge jump that captures older seafloor from the Pacific and Farallon plates, including the potential LIPs formed at 103 Ma such the proposed Yakutat Oceanic Plateau. The latter will be accreted to the North American margin during the Eocene (Plafker et al., 1994).

5. Discussions

5.1. Reconstruction of the Pacific Plate and Implications for Upwelling Cycles of the LLSVP

By superimposing the limits of the current Pacific LLSVP (Becker and Boschi, 2002) on the surface of our kinematic plate tectonic reconstructions we can assess the potential interactions between the location of MORs and potential upwellings of the LLSVP in time (Fig 2.1a). Many of the existent Pacific tectonic reconstructions used only the position of hotspots as a fixed reference frame; however, this can introduce inconsistencies due to hotspot movement in large time scales since plumes could be affected by mantle "wind" or could be captured by a MOR (Jellinek et al., 2003; O'Neill et al., 2005). Therefore, in order to create a more accurate reconstruction, in our kinematic model we used an integral combination of paleomagnetic anomalies (reported (Müller et al., 1997) and reconstructed) with seafloor geometry (MORs, magnetic anomalies and relative locations of hotspot), and the geological and kinematic evolution of the circum-Americas active margins.

Our model evidences a close relationship between the formation of Pacific LIPs, the paleo locations of MORs, and the margins of the Pacific LLSVP at specific times. At ~168 Ma our

reconstruction shows the birth of the modern Pacific Plate and on its north-western border, close to the LLSVP margin, the emplacement of the Pigafetta Basin (Fig. 2.4a). This basin contains the oldest oceanic crust of the Pacific Plate (~170-160 Ma (Pringle, 1992; Fisk and Kelley, 2002)) and can be associated with a potential deep upwelling at the northwest edge of the LLSVP boundary. Even though the Pigafetta Basin is considered an ocean-basin floor basalt type of oceanic LIP, its formation could be related to the interaction of the mantle plume derived from the Pacific LLSVP and a MOR. This interpretation is in good agreement with the high resolution $^{40}Ar/^{39}Ar$ data collected by Koppers et al. (2003) and with previous reconstruction models.

Chronologically the next series of Pacific LIPs include the Nicoya I, Shatsky Rise, and Magellan Rise at ~140 Ma along with the plateau basement that contains the Mid-Pacific Mountains (Fig 2.4c). In the ~140 Ma reconstruction, the LIPs fit along a northern MOR that coincides with the LLSVP margin at that time, except from Magellan Rise, which forms at a MOR further to the southeast. The Mid-Pacific Mountains seat over an abnormally elevated seafloor area that have been interpreted as a mid-Cretaceous Superswell. The seamounts and guyots that constitute the Mid-Pacific Mountains, some of which have been drilled by DSDP and ODP cruises, display $^{40}Ar/^{39}Ar$ ages between 123-128 Ma (Winterer et al., 1993); however, the main bathymetric height that constitute their basement has not been successfully reached by drilling and its age is thought to be as old as Upper Jurassic-Lower Cretaceous (Winterer et al., 1993). The isotopic and geochemical enrichments of the alkali basalts recovered from these seamounts and guyots are in agreement with a volcanism controlled by shallow mantle processes and the tectonic stresses within the original plateau (Janney and Castillo, 1999). Hence, here we hypothesize that the Mid-Pacific Mountains represent a rejuvenated stage of a much older oceanic LIP that had its main volcanic constructing pulse circa 140 Ma (Winterer et al., 1993). This oceanic LIP appears in our

~140 Ma reconstruction notably alongside the oldest suites of the Nicoya I terrane (Fig. 2.1b) accreted in Costa Rica. We propose that the Nicoya I oceanic terrane constitute a drifted piece of that LIP which was subsequently accreted to the coast of Costa Rica (Fig. 2.4b).

In the ~120 Ma reconstruction a major episode of upwelling from the Pacific LLSVP generated the largest oceanic LIPs recorded in Earth's history: Ontong-Java, Manihiki and Hikurangi LIPs (Fig 2.4e) which are thought to have erupted synchronously as a single plateau that was later rifted apart (Kerr and Mahoney, 2007; Hoernle et al., 2010; Timm et al., 2011; Chandler et al., 2012). The East Mariana Basin and Nauru Basin oceanic LIPs also formed at this stage. These LIPs are possibly related to the formation of the Ontong-Java, Manihiki and Hikurangi Plateau event (Hoernle et al., 2010) which could have extended laterally, creating a thinner structure than the main plateau event. Younger seamounts from rejuvenated stages on top of these LIPs record intra-plateau deformation and low degree of partial melting of shallow heterogeneities (Hoernle et al., 2010), and thus are not representative of deep mantle upwellings as considered in other studies (van Keken et al., 2002). In our model, these LIPs formed along an east-west oriented MOR near the southern LLSVP margin. Likewise, at the northern edge of the LLSVP a potential upwelling reached a MOR at this stage. This upwelling triggered the eruption of the ca. 120 Ma basaltic suites that were accreted in the Nicoya Peninsula (Nicoya II, Fig. 2.1). We propose that the Nicoya II terrane formed alongside the younger section of the Mid-Pacific Mountains basement, but on the northwestern side of the MOR, causing the Nicoya II terrane to migrate towards the western margins of the Pacific Plate (Fig. 2.4e).

Our model is also in good agreement with chronologic and geometrical data, which suggest that there is a section of the Hikurangi Plateau that is slightly younger than Ontong-Java and Manihiki (Timm et al., 2011) (Fig. 2.4f). At the ~112 Ma reconstruction the interactions between

the southern margin of the LLSVP and a MOR triple point separated the Hikurangi LIP from the other plateaus; this upwelling is likely responsible for forming the younger sections of the Hikurangi Plateau (Fig. 2.1b and 2.4f). In the case of the Hess Rise, at the DSPD site 464 (Shipboard Scientific Party, 1981), sediments of Albian (~113-100 Ma) age have been drilled, suggesting that the basement below could be older than the radiogenic ages of the recovered material. Our model shows that this basement was possibly formed at the northern limits of the LLSVP margin between 120-112 Ma (Fig. 2.4e and f). Ages from the Nicoya II terrane circa 110 Ma also suggest that active upwelling was taking place at the northern LLSVP edge at this time (Fig. 2.4f).

Interestingly, there is no record for Pacific Ocean related LIP formation at ~103 Ma; however, our model suggests an interaction between a MOR and the northern edges of the LLSVP, potentially triggering the formation of an LIP at this time (Fig. 2.4g). A plausible candidate could be the undated Yakutat oceanic terrane (Worthington et al., 2012), which initially collided with the North American margin, then translated along the margin and became emplaced at the southern Alaska margin (Worthington et al., 2012). Furthermore, this raises the possibility of the existence of upwelling pulses of the LLSVP that have not yet been identified in the geologic record.

The youngest Pacific LLSVP upwelling pulses at ~90 Ma, include the Caribbean LIP and the younger parts of the Hess Rise. Recovered fragments of the Hess Rise of ~90 Ma show clear geochemical signature consistent with a LIP (Pringle and Dalrymple, 1993). At the ~95 Ma reconstruction (Fig. 2.4h) the Caribbean Plateau is forming by a plume connected to the easternmost part of the LLSVP in a near equatorial location. Although the interaction between the LLSVP upwelling and the mid-ocean ridge is only evident in the southern region, we suggest that the plume was captured by the mid-ocean ridge (Jellinek et al., 2003), hence the northward

configuration of the LIP, and probably still interacting until ~67 Ma; a similar model has been proposed to explain the massive volume and configuration of the Ontong Java, Manihiki and Hikurangi event (Chandler et al., 2012). Fragments of the Caribbean LIP have been identified in the Nicoya Peninsula as suites of massive basalts, diabase and gabbro intrusions. Radiometric $^{40}Ar/^{39}Ar$ ages group these suites of oceanic rocks between 92.5 and 83.2 Ma (Fig. 2.1b), consistent with the ages reported for the Caribbean Plateau in the region (Caribbean, Colombia, Ecuador; Fig. 2.1b)

5.2.Geochemical and petrological evidence for plume-ridge interaction in oceanic LIP formation

We applied geochemical constraints to further evaluate the provenance of the Nicoya terranes and their possible relation with other Pacific LIP events. Our samples display flat REE patterns (La/Yb= 1.0-1.6) (Fig. 2.9a), which have been interpreted as the result of the high melt fractions (20-30%) characteristic of the head stage of mantle plumes (Herzberg and Gazel, 2009). Although large melt fractions produced by the upwelling of a hot plume head will result in a homogenization of the melts, the trace element and isotopic compositions of oceanic LIP basalts can also suggest mixing between enriched components ascending within the mantle plume and entrained depleted material. As an example in La/Yb vs. Th/Yb space (Fig. 2.9a), all the data from oceanic LIP basalts (including our new data from the Nicoya terranes) can be explained by mixing between depleted and enriched MORB/OIB end-members (Kerr et al., 1995).

Along the same line, the radiogenic isotope data from the Pacific LIPs require a mixing relationship between a depleted MORB mantle (DMM) and a HIMU-like mantle reservoir (Kerr et al., 1995; White, 2010). Enriched mantle components like HIMU have been attributed to recycling of ancient subducted oceanic lithosphere and carbonated sediments (Castillo, 2015) that

persist for billions of years as heterogeneities ponded at the core-mantle boundary (Burke et al., 2008) at the location of the LLSVP (Fig. 2.4a). Once these heterogeneities destabilize and buoyantly ascend they entrain and mix with the surrounding ambient depleted mantle. Lavas from the Pacific LIPs show enrichments towards a HIMU component, when plotted in $^{208}Pb/^{204}Pb$ vs. $^{206}Pb/^{204}Pb$ space (Fig. 2.9c). The Nicoya I and II terranes seem to share this same isotopic signature. It should also be noted that the samples from the Pacific LIPs erupted at the northeastern edges (i.e., Shatsky, Nicoya I and II, Caribbean) of the LLSVP show a steeper isotopic trend than the values from the southern LIPs (i.e., Ontong Java, Manihiki, Hikurangi) denoting a slight difference in their source compositions (Fig. 2.9c). This is also evident in the high-field strength elements (e.g., Nb/Yb Fig. 2.9b) systematics as well as in $^{143}Nd/^{144}Nd$ vs. $^{206}Pb/^{204}Pb$ space (Fig. 2.9d) where Nicoya I and II terranes plot similarly to Shatsky and Caribbean LIPs. Samples from the Manihiki Plateau require another isotopic reservoir (lower in both Nd and Pb isotopes) not evident in the rest of the LIPs. But overall, the trace element and isotopic compositions found in these LIPs are remarkably similar, suggesting that perhaps mantle plumes ascending from the LLSVP are tapping a common deep source (Jackson and Carlson, 2011; Jackson et al., 2014) (Fig. 2.10a).

Our tectonic reconstructions as well as the geochemical signature of these lavas suggest that in order to produce the Pacific LIPs there was an interaction between upwellings at the edges of the LLSVP and MORs at the surface. Therefore, the major element composition of the primary magmas should be consistent with a deep melt source that also was able to reach relatively shallow levels through a MOR (Herzberg and Gazel, 2009). To test this hypothesis, we updated the work of Herzberg and Gazel (2009) with new modeled primary magmas using PRIMELT3 (Herzberg and Asimow, 2015). Conceptually, the initial melting pressures represent the pressure at which the

mantle adiabat crosses the peridotite solidus, and the final melting pressures possibly represent a rheological boundary like the lithosphere-asthenosphere boundary, or in extreme cases the exhaustion of a fusible mineral phases (Herzberg and Asimow, 2015) (Fig 2.10 b-d).

Using the FeO and MgO contents from the calculated primary magmas we determined the initial and final pressures at which melting occurred (Herzberg and Gazel, 2009; Sakamaki et al., 2013) (Fig. 2.11). Of particular importance are the average final melting pressure results for LIPs which are between 2.5 and 1.5 GPa, overlapping with modern MORB data; we interpret these results as the interaction between deep mantle upwellings and mid-ocean ridges during the formation of oceanic plateaus. In contrast, in recent OIB locations the average final melting pressures are >2.0 GPa consistent with the upwelling of thermal anomalies beneath thick lithosphere. The two exceptions are Iceland being formed near a ridge (Dalton et al., 2014) and Pitcairn that formed on top of young oceanic crust (Woodhead and Devey, 1993). The positive correlation between SiO_2 (and thus silica activity) of primary magmas and the final melting pressures (Fig. 2.11a) confirms the fact that LIP melting reached shallow levels (Langmuir et al., 1992b). On the other hand, the length of the melting column (as defined by $P_{initial}$-P_{final}) is significantly higher for most LIPs compared to modern MORB and OIB data, consistent with high melt productivity that characterize LIPs (Fig 2.11b) due to the excess temperature in their mantle source (Herzberg and Gazel, 2009; Coogan et al., 2014). We also found a negative correlation between average Na_2O contents and melt fraction (Fig. 2.11c) in agreement with similar correlations previously shown in global MORB systematics (Klein and Langmuir, 1987; Langmuir et al., 1992b). Finally, we plotted TiO_2 (a routinely analyzed incompatible element) with melt fraction, resulting in two evident trends, one for OIB and LIPs suggesting a more enriched mantle source than MORB (Fig. 2.11d), and a second depleted trend that includes MORB along with

Galapagos, Pigafetta, and partially overlapping with Iceland, that evidence a more depleted mantle component for these primary magmas, consistent with a current interaction with a MOR in these locations (Detrick et al., 2002; Fisk and Kelley, 2002).

6. Conclusions: Global impact of upwellings from LLVPs and LIP formation

Our kinematic plate tectonic reconstructions from ~168 Ma to ~95 Ma consistently show potential upwellings from the edges of the Pacific LLSVP coincided in the surface with a mid-ocean ridge during the formation of the known Pacific LIPs. These events are separated by time periods of 10 to 20 Ma and followed by periods of major oceanic chemistry change and anoxia that cause the disruption of the oceanic biodiversity (Kerr, 1998; Jenkyns, 2010). These changes in the ocean are evidenced by major disturbances to the planet's carbon cycle associated with a rise in temperatures and in organic productivity that remain recorded as global oceanic anoxic events (characterized by the widespread formation of black shales). These global oceanic anoxic events are associated with most of the Cretaceous LIPs (Erba et al., 2015), and in some cases they can be related with more than one LIP active at the same time (Fig. 2.1b); this scenario would exacerbate the conditions in the oceans triggering extensive oceanic biota extinctions.

The fact that the bulk emplacement of LIPs (~120-80 Ma) in the Pacific also coincide with the timing of the Cretaceous Normal Superchron (Fig. 2.1b), which can be related to fluctuations of mantle-core heat fluxes (Olson and Amit, 2015), further supports the hypothesis of deep mantle origin for LIPs. Thus, if LIP-producing plumes were rooted in a boundary layer at the base of the mantle (LLSVP) it is possible that instabilities of the buoyant perovskite-bearing peridotite equivalent progressively entrained recycled components (Mulyukova et al., 2015; Trela et al., 2015) making them less buoyant with time and thus explaining the potential cyclicity observed during the Cretaceous. Alternatively, the potential cyclicity of LIP emplacement could also be

related to core heat fluctuations interacting with the lower mantle, pulses of material crossing the transition zone (either upwelling hot material or downgoing dense slabs), or a combination of both processes. Even though these hypotheses require further evaluation, recognizing patterns and possible cycles is crucial to the link between deep processes and life. The Pacific Plate preserves the evidence for deep mantle upwellings in the Cretaceous but just as the accreted fragments found in Costa Rica, many other unrecognized LIP events could be preserved accreted along the margins of the Pacific Ocean. Tying these events to cyclical upwellings of long-lived anomalies such as the Pacific LLSVP can help us understand the Earth's interior processes that happened in the past and the potential for future catastrophic LIP activity.

7. References

Bach, W., Alt, J.C., Niu, Y., Humphris, S.E., Erzinger, J. and Dick, H.J.B., 2001. The geochemical consequences of late-stage low-grade alteration of lower ocean crust at the SW Indian Ridge: Results from ODP Hole 735B (Leg 176). Geochimica et Cosmochimica Acta, 65(19): 3267-3287.

Bagheri, S. and Stampfli, G.M., 2008. The Anarak, Jandaq and Posht-e-Badam metamorphic complexes in central Iran: New geological data, relationships and tectonic implications. Tectonophysics, 451(1–4): 123-155.

Bartolini, A. and Larson, R.L., 2001. Pacific microplate and the Pangea supercontinent in the Early to Middle Jurassic. Geology, 29(8): 735-738.

Baumgartner, P. and Denyer, P., 2006. Evidende for middle Cretaceous accretion at Santa Elena Peninsula (Santa Rosa Accretionary Complex), Costa Rica. Geologica Acta, 4(1-2): 179-191.

Baumgartner, P., Flores, K., Bandini, A., Girault, F. and Cruz, D., 2008. Upper Triassic to Cretaceous radiolaria from Nicaragua and northern Costa Rica: The Mesquito composite oceanic terrane. Ofioliti, 33(1): 1-19.

Becker, T. W. & Boschi, L. A comparison of tomographic and geodynamic mantle models. *Geochemistry, Geophysics, Geosystems* **3**, doi:10.1029/2001GC000168 (2002).

Becker, T.W. and Boschi, L., 2002. A comparison of tomographic and geodynamic mantle models. Geochemistry, Geophysics, Geosystems, 3(1).

Bizimis, M., Salters, V.J.M., Garcia, M.O. and Norman, M.D., 2013. The composition and distribution of the rejuvenated component across the Hawaiian plume: Hf-Nd-Sr-Pb isotope systematics of Kaula lavas and pyroxenite xenoliths. Geochemistry, Geophysics, Geosystems: n/a-n/a.

Burke, K., Steinberger, B., Torsvik, T. H. & Smethurst, M. A. Plume Generation Zones at the margins of Large Low Shear Velocity Provinces on the core–mantle boundary. *Earth and Planetary Science Letters* **265**, 49-60, doi:http://dx.doi.org/10.1016/j.epsl.2007.09.042 (2008).

Burke, K., Steinberger, B., Torsvik, T.H. and Smethurst, M.A., 2008. Plume Generation Zones at the margins of Large Low Shear Velocity Provinces on the core–mantle boundary. Earth and Planetary Science Letters, 265(1–2): 49-60.

Castillo, P. R. The recycling of marine carbonates and sources of HIMU and FOZO ocean island basalts. *Lithos* **216–217**, 254-263, doi:http://dx.doi.org/10.1016/j.lithos.2014.12.005 (2015).

Castillo, P.R., 2015. The recycling of marine carbonates and sources of HIMU and FOZO ocean island basalts. Lithos, 216–217(0): 254-263.

Castillo, P.R., Carlson, R.W. and Batiza, R., 1991. Origin of Nauru Basin igneous complex: Sr, Nd and Pb isotope and REE constraints. Earth and Planetary Science Letters, 103(1–4): 200-213.

Castillo, P.R., Pringle, M.S. and Carlson, R.W., 1994. East Mariana Basin tholeiites: Cretaceous intraplate basalts or rift basalts related to the Ontong Java plume? Earth and Planetary Science Letters, 123(1–3): 139-154.

Chandler, M. T. *et al.* Reconstructing Ontong Java Nui: Implications for Pacific absolute plate motion, hotspot drift and true polar wander. *Earth and Planetary Science Letters* **331–332**, 140-151, doi:http://dx.doi.org/10.1016/j.epsl.2012.03.017 (2012).

Chandler, M.T., Wessel, P., Taylor, B., Seton, M., Kim, S.-S. and Hyeong, K., 2012. Reconstructing Ontong Java Nui: Implications for Pacific absolute plate motion, hotspot drift and true polar wander. Earth and Planetary Science Letters, 331–332(0): 140-151.

Christeson, G.L., Gulick, S.P.S., van Avendonk, H.J.A., Worthington, L.L., Reece, R.S. and Pavlis, T.L., 2010. The Yakutat terrane: Dramatic change in crustal thickness across the Transition fault, Alaska. Geology, 38(10): 895-898.

Coogan, L. A., Saunders, A. D. & Wilson, R. N. Aluminum-in-olivine thermometry of primitive basalts: Evidence of an anomalously hot mantle source for large igneous provinces. *Chemical Geology* **368**, 1-10, doi:http://dx.doi.org/10.1016/j.chemgeo.2014.01.004 (2014).

Coogan, L.A., Saunders, A.D. and Wilson, R.N., 2014. Aluminum-in-olivine thermometry of primitive basalts: Evidence of an anomalously hot mantle source for large igneous provinces. Chemical Geology, 368: 1-10.

Dalton, C. A., Langmuir, C. H. & Gale, A. Geophysical and Geochemical Evidence for Deep Temperature Variations Beneath Mid-Ocean Ridges. *Science* **344**, 80-83, doi:10.1126/science.1249466 (2014).

Dalton, C.A., Langmuir, C.H. and Gale, A., 2014. Geophysical and Geochemical Evidence for Deep Temperature Variations Beneath Mid-Ocean Ridges. Science, 344(6179): 80-83.

Davy, B., Hoernle, K. and Werner, R., 2008. Hikurangi Plateau: Crustal structure, rifted formation, and Gondwana subduction history. Geochemistry, Geophysics, Geosystems, 9(7): 1-31.

Dengo, G., 1962. Tectonic igneous sequence in Costa Rica. In: Engel, A. E. J., James, H. J., Leonard, B. F. (Eds.), A volume to honor A. F. Budington. Geological Society of America Special Volume: pp. 133-161.

Denyer and Gazel, E., 2009. The Costa Rican Jurassic to Miocene oceanic complexes: Origin, tectonics and relations. Journal of South American Earth Sciences, 28: 429-442.

Denyer, P. and Baumgartner, P.O., 2006. Emplacement of Jurassic-Lower Cretaceous radiolarites of the Nicoya Complex (Costa Rica). Geologica acta, 4(1-2): 203.

Denyer, P., Aguilar, T. and Montero, W., 2014. Cartografia geologica de la peninsula de Nicoya, Costa Rica: estratigrafia y tectonica. Editorial UCR, San Jose, Costa Rica.

Detrick, R. *et al.* Correlated geophysical, geochemical, and volcanological manifestations of plume-ridge interaction along the Galápagos Spreading Center. *Geochemistry, Geophysics, Geosystems* **3**, 1-14 (2002).

Detrick, R., Sinton, J., Ito, G., Canales, J., Behn, M., Blacic, T., Cushman, B., Dixon, J., Graham, D.W. and Mahoney, J., 2002. Correlated geophysical, geochemical, and volcanological manifestations of plume-ridge interaction along the Galápagos Spreading Center. Geochemistry, Geophysics, Geosystems, 3(10): 1-14.

Duncan, R.A. and Hargraves, R.B., 1984. Plate tectonic evolution of the Caribbean region in the mantle reference frame. Geological Society of America Memoirs, 162: 81-94.

Erba, E. *et al.* Environmental consequences of Ontong Java Plateau and Kerguelen Plateau volcanism. *Geological Society of America Special Papers* **511**, SPE511-515 (2015).

Erba, E., Duncan, R.A., Bottini, C., Tiraboschi, D., Weissert, H., Jenkyns, H.C. and Malinverno, A., 2015. Environmental consequences of Ontong Java Plateau and Kerguelen Plateau volcanism. Geological Society of America Special Papers, 511: SPE511-15.

Ernst, R. E. *Large Igneous Provinces*. (Cambridge University Press, 2014).

Ernst, R.E., 2014. Large Igneous Provinces. Cambridge University Press.

Ferrari, O., Hochard, C. and Stampfli, G., 2008. An alternative plate tectonic model for the Palaeozoic–Early Mesozoic Palaeotethyan evolution of southeast Asia (Northern Thailand–Burma). Tectonophysics, 451(1): 346-365.

Fisk, M. & Kelley, K. A. Probing the Pacific's oldest MORB glass: mantle chemistry and melting conditions during the birth of the Pacific Plate. *Earth and Planetary Science Letters* **202**, 741-752, doi:http://dx.doi.org/10.1016/S0012-821X(02)00760-4 (2002).

Fisk, M. and Kelley, K.A., 2002. Probing the Pacific's oldest MORB glass: mantle chemistry and melting conditions during the birth of the Pacific Plate. Earth and Planetary Science Letters, 202(3–4): 741-752.

Flores, K.E., 2009. Mesozoic oceanic terranes of the southern Central America-Geology, geochemistry and geodynamics, University of Laussane, Laussane, 317 pp pp.

Flores, K.E., 2015. The formation of the Middle America and the Pacific ocean, GSA Abstracts and Programs vol 47, No 7, p 44.

Flores, K.E., Martens, U.C., Harlow, G.E., Brueckner, H.K. and Pearson, N.J., 2013. Jadeitite formed during subduction: In situ zircon geochronology constraints from two different tectonic events within the Guatemala Suture Zone. Earth and Planetary Science Letters, 371–372(0): 67-81.

Flores, K.E., Skora, S., Martin, C., Harlow, G.E., Rodríguez, D. and Baumgartner, P.O., 2015. Metamorphic history of riebeckite- and aegirine-augite-bearing high-pressure–low-temperature blocks within the Siuna Serpentinite Mélange, northeastern Nicaragua. International Geology Review, 57(5-8): 943-977.

Foustoukos, D.I. and Seyfried, W.E., 2007. Fluid phase separation processes in submarine hydrothermal systems. Reviews in Mineralogy and Geochemistry, 65(1): 213-239.

French, S. W. & Romanowicz, B. Broad plumes rooted at the base of the Earth's mantle beneath major hotspots. *Nature* **525**, 95-99, doi:10.1038/nature14876 http://www.nature.com/nature/journal/v525/n7567/abs/nature14876.html#supplementary-information (2015).

French, S.W. and Romanowicz, B., 2015. Broad plumes rooted at the base of the Earth's mantle beneath major hotspots. Nature, 525(7567): 95-99.

Frisch, W., Meschede, M. and Sick, M., 1992. Origin of the Central American ophiolites: Evidence from paleomagnetic results. Geological Society of America Bulletin, 104(10): 1301-1314.

Gale, A., Dalton, C. A., Langmuir, C. H., Su, Y. & Schilling, J.-G. The mean composition of ocean ridge basalts. *Geochemistry Geophysics Geosystems* **14**, 489-518 (2013).

Gale, A., Dalton, C.A., Langmuir, C.H., Su, Y. and Schilling, J.-G., 2013. The mean composition of ocean ridge basalts. Geochemistry Geophysics Geosystems, 14(3): 489-518.

Galli-Olivier, C., 1979. Ophiolite and island-arc volcanism in Costa Rica. Geological Society of America Bulletin, 90(5): 444-452.

Gerya, T.V., Stern, R.J., Baes, M., Sobolev, S.V. and Whattam, S.A., 2015. Plate tectonics on the Earth triggered by plume-induced subduction initiation. Nature, 527(7577): 221-225.

Hauff, F., Hoernle, K., Schmincke, H.-U. and Werner, R., 1997. A Mid Cretaceous origin for the Galápagos hotspot: volcanological, petrologica and geochemical evidence from Costa Rican oceanic crustal segments. Geologische Rundschau, 86(1): 141-155.

Hauff, F., Hoernle, K., van den Bogaard, P., Alvarado, G. & Garbe-Schönberg, D. Age and geochemistry of basaltic complexes in western Costa Rica: Contributions to the geotectonic evolution of Central America. *Geochemistry Geophysics Geosystems* **1** (2000).

Hauff, F., Hoernle, K., van den Bogaard, P., Alvarado, G. and Garbe-Schönberg, D., 2000. Age and geochemistry of basaltic complexes in western Costa Rica: Contributions to the geotectonic evolution of Central America. Geochemistry Geophysics Geosystems, 1.

Herzberg, C. & Asimow, P. D. PRIMELT3 MEGA.XLSM software for primary magma calculation: Peridotite primary magma MgO contents from the liquidus to the solidus. *Geochemistry, Geophysics, Geosystems* **16**, 563-578, doi:10.1002/2014GC005631 (2015).

Herzberg, C. & Gazel, E. Petrological evidence for secular cooling in mantle plumes. *Nature* **458**, 619-622 (2009).

Herzberg, C. and Asimow, P.D., 2015. PRIMELT3 MEGA.XLSM software for primary magma calculation: Peridotite primary magma MgO contents from the liquidus to the solidus. Geochemistry, Geophysics, Geosystems, 16(2): 563-578.

Herzberg, C. and Gazel, E., 2009. Petrological evidence for secular cooling in mantle plumes. Nature, 458(7238): 619-622.

Hochard, C., 2008. GIS and geodatabases application to global scale plate tectonics modelling. Unpublished PhD Thesis, Université de Lausanne, Lausanne.

Hoernle, K. *et al.* Age and geochemistry of volcanic rocks from the Hikurangi and Manihiki oceanic Plateaus. *Geochimica et Cosmochimica Acta* **74**, 7196-7219, doi:10.1016/j.gca.2010.09.030 (2010).

Hoernle, K., Hauff, F. & van den Bogaard, P. 70 m.y. history (136-69 Ma) for the Caribbean Large Igneous Province. *Geological Society of America* **32**, 697-700 (2004).

Hoernle, K., Hauff, F. and van den Bogaard, P., 2004. 70 m.y. history (136-69 Ma) for the Caribbean Large Igneous Province. Geological Society of America, 32(8): 697-700.

Hoernle, K., Hauff, F., van den Bogaard, P., Werner, R., Mortimer, N., Geldmacher, J., Garbe-Schönberg, D. and Davy, B., 2010. Age and geochemistry of volcanic rocks from the Hikurangi and Manihiki oceanic Plateaus. Geochimica et Cosmochimica Acta, 74(74): 7196-7219.

Jackson, M. G. & Carlson, R. W. An ancient recipe for flood-basalt genesis. *Nature* **476**, 316-319 (2011).

Jackson, M. G. *et al.* Helium and lead isotopes reveal the geochemical geometry of the Samoan plume. *Nature* **514**, 355-358, doi:10.1038/nature13794

http://www.nature.com/nature/journal/v514/n7522/abs/nature13794.html#supplementary-information (2014).

Jackson, M.G. and Carlson, R.W., 2011. An ancient recipe for flood-basalt genesis. Nature, 476(7360): 316-319.

Jackson, M.G., Hart, S.R., Konter, J.G., Kurz, M.D., Blusztajn, J. and Farley, K.A., 2014. Helium and lead isotopes reveal the geochemical geometry of the Samoan plume. Nature, 514(7522): 355-358.

Janney, P. E. & Castillo, P. R. Isotope geochemistry of the Darwin Rise seamounts and the nature of long-term mantle dynamics beneath the south central Pacific. *Journal of Geophysical Research: Solid Earth* **104**, 10571-10589, doi:10.1029/1998JB900061 (1999).

Janney, P.E. and Castillo, P.R., 1999. Isotope geochemistry of the Darwin Rise seamounts and the nature of long-term mantle dynamics beneath the south central Pacific. Journal of Geophysical Research: Solid Earth, 104(B5): 10571-10589.

Jellinek, A. M., Gonnermann, H. M. & Richards, M. A. Plume capture by divergent plate motions: implications for the distribution of hotspots, geochemistry of mid-ocean ridge basalts, and estimates of the heat flux at the core–mantle boundary. *Earth and Planetary Science Letters* **205**, 361-378, doi:http://dx.doi.org/10.1016/S0012-821X(02)01070-1 (2003).

Jellinek, A.M., Gonnermann, H.M. and Richards, M.A., 2003. Plume capture by divergent plate motions: implications for the distribution of hotspots, geochemistry of mid-ocean ridge basalts, and estimates of the heat flux at the core–mantle boundary. Earth and Planetary Science Letters, 205(3–4): 361-378.

Jenkyns, H. C. Geochemistry of oceanic anoxic events. *Geochemistry, Geophysics, Geosystems* **11** (2010).

Jenkyns, H.C., 2010. Geochemistry of oceanic anoxic events. Geochemistry, Geophysics, Geosystems, 11(3).

Kerr, A. C. & Mahoney, J. J. Oceanic plateaus: Problematic plumes, potential paradigms. *Chemical Geology* **241**, 332-353, doi:http://dx.doi.org/10.1016/j.chemgeo.2007.01.019 (2007).

Kerr, A. C. & Tarney, J. Tectonic evolution of the Caribbean and northwestern South America: The case for accretion of two Late Cretaceous oceanic plateaus. *Geology* **33**, 269-272, doi:10.1130/g21109.1 (2005).

Kerr, A. C. Oceanic plateau formation: a cause of mass extinction and black shale deposition around the Cenomanian–Turonian boundary? *Journal of the Geological Society* **155**, 619-626, doi:10.1144/gsjgs.155.4.0619 (1998).

Kerr, A. C. Oceanic Plateaus *Treatise on Geochemistry (Second Edition)*, 631-667, doi:http://dx.doi.org/10.1016/B978-0-08-095975-7.00320-X (2014).

Kerr, A. C., Saunders, A. D., Tarney, J., Berry, N. H. & Hards, V. L. Depleted mantle-plume geochemical signatures: No paradox for plume theories. *Geology* **23**, 843-846, doi:10.1130/0091-7613(1995)023<0843:dmpgsn>2.3.co;2 (1995).

Kerr, A. C., White, R. V. & Saunders, A. D. LIP Reading: Recognizing Oceanic Plateaux in the Geological Record. *Journal of Petrology* **41**, 1041-1056, doi:10.1093/petrology/41.7.1041 (2000).

Kerr, A.C. and Mahoney, J.J., 2007. Oceanic plateaus: Problematic plumes, potential paradigms. Chemical Geology, 241(3–4): 332-353.

Kerr, A.C. and Tarney, J., 2005. Tectonic evolution of the Caribbean and northwestern South America: The case for accretion of two Late Cretaceous oceanic plateaus. Geology, 33(4): 269-272.

Kerr, A.C., 1998. Oceanic plateau formation: a cause of mass extinction and black shale deposition around the Cenomanian–Turonian boundary? Journal of the Geological Society, 155(4): 619-626.

Kerr, A.C., 2014. Oceanic Plateaus Treatise on Geochemistry (Second Edition): 631-667.

Kerr, A.C., Saunders, A.D., Tarney, J., Berry, N.H. and Hards, V.L., 1995. Depleted mantle-plume geochemical signatures: No paradox for plume theories. Geology, 23(9): 843-846.

Kerr, A.C., White, R.V. and Saunders, A.D., 2000. LIP Reading: Recognizing Oceanic Plateaux in the Geological Record. Journal of Petrology, 41(7): 1041-1056.

Khanna, T.C., Bizimis, M., Yogodzinski, G.M. and Mallick, S., 2014. Hafnium–neodymium isotope systematics of the 2.7 Ga Gadwal greenstone terrane, Eastern Dharwar craton, India: implications for the evolution of the Archean depleted mantle. Geochimica et Cosmochimica Acta, 127: 10-24.

Klein, E. M. & Langmuir, C. H. Global correlations of ocean ridge basalt chemistry with axial depth and crustal thickness. *Journal of Geophysical Research: Solid Earth* **92**, 8089-8115, doi:10.1029/JB092iB08p08089 (1987).

Klein, E.M. and Langmuir, C.H., 1987. Global correlations of ocean ridge basalt chemistry with axial depth and crustal thickness. Journal of Geophysical Research: Solid Earth, 92(B8): 8089-8115.

Koppers, A. A. P., Staudigel, H. & Duncan, R. A. High-resolution 40Ar/39Ar dating of the oldest oceanic basement basalts in the western Pacific basin. *Geochemistry, Geophysics, Geosystems* **4**, doi:10.1029/2003GC000574 (2003).

Koppers, A.A.P., Staudigel, H. and Duncan, R.A., 2003. High-resolution 40Ar/39Ar dating of the oldest oceanic basement basalts in the western Pacific basin. Geochemistry, Geophysics, Geosystems, 4(11).

Kuijpers, E.P., 1980. The geologic history of the Nicoya Ophiolite Complex, Costa Rica, and its geotectonic significance. Tectonophysics, 68(3–4): 233-255.

Kuiper, K.F., Deino, A., Hilgen, F.J., Krijgsman, W., Renne, P.R. and Wijbrans, J.R., 2008. Synchronizing Rock Clocks of Earth History. Science, 320(5875): 500-504.

Langmuir, C. H., Klein, E. M. & Plank, T. Petrological systematics of mid-ocean ridge basalts: Constraints on melt generation beneath ocean ridges. *Mantle flow and melt generation at mid-ocean ridges*, 183-280 (1992).

Langmuir, C.H., Klein, E.M. and Plank, T., 1992. Petrological systematics of mid-ocean ridge basalts: Constraints on melt generation beneath ocean ridges. Mantle flow and melt generation at mid-ocean ridges: 183-280.

Larson, R.L., 1991. Latest pulse of Earth: Evidence for a mid-Cretaceous superplume. Geology, 19(6): 547-550.

McDonough, W. F. & Sun, S. s. The composition of the Earth. *Chemical Geology* **120**, 223-253, doi:http://dx.doi.org/10.1016/0009-2541(94)00140-4 (1995).

McDonough, W.F. and Sun, S.s., 1995. The composition of the Earth. Chemical Geology, 120(3–4): 223-253.

Meschede, M. and Frisch, W., 1994. Geochemical characteristics of basaltic rocks from the Central American ophiolites. Profil, 7: 71-85.

Min, K., Mundil, R., Renne, P.R. and Ludwig, K.R., 2000. A test for systematic errors in 40Ar/39Ar geochronology through comparison with U/Pb analysis of a 1.1-Ga rhyolite. Geochimica et Cosmochimica Acta, 64(1): 73-98.

Moix, P., Beccaletto, L., Kozur, H.W., Hochard, C., Rosselet, F. and Stampfli, G.M., 2008. A new classification of the Turkish terranes and sutures and its implication for the paleotectonic history of the region. Tectonophysics, 451(1–4): 7-39.

Müller, R. D., Roest, W. R., Royer, J.-Y., Gahagan, L. M. & Sclater, J. G. Digital isochrons of the world's ocean floor. *Journal of Geophysical Research: Solid Earth* **102**, 3211-3214, doi:10.1029/96JB01781 (1997).

Müller, R.D., Roest, W.R., Royer, J.-Y., Gahagan, L.M. and Sclater, J.G., 1997. Digital isochrons of the world's ocean floor. Journal of Geophysical Research: Solid Earth, 102(B2): 3211-3214.

Müller, R.D., Sdrolias, M., Gaina, C. and Roest, W.R., 2008. Age, spreading rates, and spreading asymmetry of the world's ocean crust. Geochemistry, Geophysics, Geosystems, 9(4): Q04006.

Müller, R.D., Seton, M., Zahirovic, S., Williams, S.E., Matthews, K.J., Wright, N.M., Shephard, G.E., Maloney, K., Barnett-Moore, N., Hosseinpour, M., Bower, D.J. and Cannon, J., 2016. Ocean Basin Evolution and Global-Scale Plate Reorganization Events Since Pangea Breakup. Annual Review of Earth and Planetary Sciences, 44(1): null.

Mulyukova, E., Steinberger, B., Dabrowski, M. & Sobolev, S. V. Survival of LLSVPs for billions of years in a vigorously convecting mantle: Replenishment and destruction of chemical anomaly. *Journal of Geophysical Research: Solid Earth* **120**, 3824-3847, doi:10.1002/2014JB011688 (2015).

Mulyukova, E., Steinberger, B., Dabrowski, M. and Sobolev, S.V., 2015. Survival of LLSVPs for billions of years in a vigorously convecting mantle: Replenishment and destruction of chemical anomaly. Journal of Geophysical Research: Solid Earth, 120(5): 3824-3847.

Olson, P. & Amit, H. Mantle superplumes induce geomagnetic superchrons. *Frontiers in Earth Science* **3**, doi:10.3389/feart.2015.00038 (2015).

Olson, P. and Amit, H., 2015. Mantle superplumes induce geomagnetic superchrons. Frontiers in Earth Science, 3.

O'Neill, C., Müller, D. & Steinberger, B. On the uncertainties in hot spot reconstructions and the significance of moving hot spot reference frames. *Geochemistry, Geophysics, Geosystems* **6**, n/a-n/a, doi:10.1029/2004GC000784 (2005).

O'Neill, C., Müller, D. and Steinberger, B., 2005. On the uncertainties in hot spot reconstructions and the significance of moving hot spot reference frames. Geochemistry, Geophysics, Geosystems, 6(4): n/a-n/a.

Plafker, G., Moore, J.C. and Winkler, G.R., 1994 Geology of the southern Alaska margin In: G. Plafker and H.C. Berg (Editors), The Geology of Alaska. Geological Society of America, Boulder, Colorado, pp. p. 389-448.

Polat, A., Hofmann, A.W., Münker, C., Regelous, M. and Appel, P.W.U., 2003. Contrasting geochemical patterns in the 3.7–3.8 Ga pillow basalt cores and rims, Isua greenstone belt, Southwest Greenland: implications for postmagmatic alteration processes. Geochimica et Cosmochimica Acta, 67(3): 441-457.

Pringle, M. Radiometric ages of basaltic basement recovered at Sites 800, 801, and 802, Leg 129, western Pacific Ocean. *Proc. Ocean Drill. Program Sci. Results* **129**, 389-399 (1992).

Pringle, M. S. & Dalrymple, G. B. in *The Mesozoic Pacific: Geology, Tectonics, and Volcanism* 263-277 (American Geophysical Union, 1993).

Pringle, M., 1992. Radiometric ages of basaltic basement recovered at Sites 800, 801, and 802, Leg 129, western Pacific Ocean. Proc. Ocean Drill. Program Sci. Results, 129: 389-399.

Pringle, M.S. and Dalrymple, G.B., 1993. Geochronological Constraints on a Possible Hot Spot Origin for Hess Rise and the Wentworth Seamount Chain, The Mesozoic Pacific: Geology, Tectonics, and Volcanism. American Geophysical Union, pp. 263-277.

Sakamaki, T. *et al.* Ponded melt at the boundary between the lithosphere and asthenosphere. *Nature Geosci* **6**, 1041-1044, doi:10.1038/ngeo1982 http://www.nature.com/ngeo/journal/v6/n12/abs/ngeo1982.html#supplementary-information (2013).

Sakamaki, T., Suzuki, A., Ohtani, E., Terasaki, H., Urakawa, S., Katayama, Y., Funakoshi, K.-i., Wang, Y., Hernlund, J.W. and Ballmer, M.D., 2013. Ponded melt at the boundary between the lithosphere and asthenosphere. Nature Geosci, 6(12): 1041-1044.

Schilling, J.-G. Fluxes and excess temperatures of mantle plumes inferred from their interaction with migrating mid-ocean ridges. *Nature* **352**, 397-403 (1991).

Schilling, J.-G., 1991. Fluxes and excess temperatures of mantle plumes inferred from their interaction with migrating mid-ocean ridges. Nature, 352(6334): 397-403.

Scott, R.B. and Hajash, A., 1976. Initial submarine alteration of basaltic pillow lavas; a microprobe study. American Journal of Science, 276(4): 480-501.

Seton, M., Müller, R.D., Zahirovic, S., Gaina, C., Torsvik, T., Shephard, G., Talsma, A., Gurnis, M., Turner, M., Maus, S. and Chandler, M., 2012. Global continental and ocean basin reconstructions since 200 Ma. Earth-Science Reviews, 113(3–4): 212-270.

Seyfried, W.E., Chen, X. and Chan, L.-H., 1998. Trace Element Mobility and Lithium Isotope Exchange During Hydrothermal Alteration of Seafloor Weathered Basalt: An Experimental Study at 350°C, 500 Bars. Geochimica et Cosmochimica Acta, 62(6): 949-960.

Seyfried, W.E., Pester, N. and Fu, Q., 2013. Phase Equilibria Controls on the Chemistry of Vent Fluids from Hydrothermal Systems On Slow Spreading Ridges: Reactivity Of Plagioclase and Olivine Solid Solutions And The Ph-Silica Connection, Diversity Of Hydrothermal Systems On Slow Spreading Ocean Ridges. American Geophysical Union, pp. 297-320.

Shipboard Scientific Party, S. 464: Northern Hess Rise. *Init. Rep. DSDP* **62**, 157-197 (1981).

Shipboard Scientific Party, S., 1981. 464: Northern Hess Rise. Init. Rep. DSDP, 62: 157-197.

Sinton, C.W., Duncan, R.A. and Denyer, P., 1997. Nicoya Peninsula, Costa Rica: A single suite of Caribbean oceanic plateau magmas. Journal of Geophysical Research: Solid Earth, 102(B7): 15507-15520.

Stampfli, G. and Borel, G., 2002. A plate tectonic model for the Paleozoic and Mesozoic constrained by dynamic plate boundaries and restored synthetic oceanic isochrons. Earth and Planetary Science Letters, 196(1): 17-33.

Stampfli, G.M. and Hochard, C., 2009. Plate tectonics of the Alpine realm. Geological Society, London, Special Publications, 327(1): 89-111.

Stampfli, G.M., Hochard, C., Vérard, C., Wilhem, C. and vonRaumer, J., 2013. The formation of Pangea. Tectonophysics, 593: 1-19.

Staudigel, H., 2003. Hydrothermal alteration processes in the oceanic crust. Treatise on geochemistry, 3: 511-535.

Steinberger, B. & Torsvik, T. H. A geodynamic model of plumes from the margins of Large Low Shear Velocity Provinces. *Geochemistry, Geophysics, Geosystems* **13**, n/a-n/a, doi:10.1029/2011GC003808 (2012).

Steinberger, B. and Torsvik, T.H., 2012. A geodynamic model of plumes from the margins of Large Low Shear Velocity Provinces. Geochemistry, Geophysics, Geosystems, 13(1): n/a-n/a.

Stroncik, N.A. and Schmincke, H.-U., 2001. Evolution of palagonite: Crystallization, chemical changes, and element budget. Geochemistry, Geophysics, Geosystems, 2(7): 1017.

Taylor, B., 2006. The single largest oceanic plateau: Ontong Java–Manihiki–Hikurangi. Earth and Planetary Science Letters, 241(3): 372-380.

Timm, C. *et al.* Age and geochemistry of the oceanic Manihiki Plateau, SW Pacific: New evidence for a plume origin. *Earth and Planetary Science Letters* **304**, 135-146 (2011).

Timm, C., Hoernle, K., Werner, R., Hauff, F., van den Bogaard, P., Michael, P., Coffin, M.F. and Koppers, A., 2011. Age and geochemistry of the oceanic Manihiki Plateau, SW Pacific: New evidence for a plume origin. Earth and Planetary Science Letters, 304(1): 135-146.

Torsvik, T. H. *et al.* Deep mantle structure as a reference frame for movements in and on the Earth. *Proceedings of the National Academy of Sciences* **111**, 8735-8740, doi:10.1073/pnas.1318135111 (2014).

Torsvik, T.H., van der Voo, R., Doubrovine, P.V., Burke, K., Steinberger, B., Ashwal, L.D., Trønnes, R.G., Webb, S.J. and Bull, A.L., 2014. Deep mantle structure as a reference frame for movements in and on the Earth. Proceedings of the National Academy of Sciences, 111(24): 8735-8740.

Trela, J. *et al.* Recycled crust in the Galápagos Plume source at 70 Ma: Implications for plume evolution. *Earth and Planetary Science Letters* **425**, 268-277, doi:http://dx.doi.org/10.1016/j.epsl.2015.05.036 (2015).

Trela, J., Vidito, C., Gazel, E., Herzberg, C., Class, C., Whalen, W., Jicha, B., Bizimis, M. and Alvarado, G.E., 2015. Recycled crust in the Galápagos Plume source at 70 Ma: Implications for plume evolution. Earth and Planetary Science Letters, 425: 268-277.

van der Meer, D.G., Torsvik, T.H., Spakman, W., van Hinsbergen, D.J.J. and Amaru, M.L., 2012. Intra-Panthalassa Ocean subduction zones revealed by fossil arcs and mantle structure. Nature Geosci, 5(3): 215-219.

van Keken, P. E., Hauri, E. H. & Ballentine, C. J. Mantle mixing: the generation, preservation, and destruction of chemical heterogeneity. *Annual Review of Earth and Planetary Sciences* **30**, 493-525 (2002).

van Keken, P.E., Hauri, E.H. and Ballentine, C.J., 2002. Mantle mixing: the generation, preservation, and destruction of chemical heterogeneity. Annual Review of Earth and Planetary Sciences, 30(1): 493-525.

Vérard, C. and Stampfli, G.M., 2013a. Geodynamic reconstructions of the Australides—1: Palaeozoic. Geosciences, 3(2): 311-330.

Vérard, C. and Stampfli, G.M., 2013b. Geodynamic Reconstructions of the Australides—2: Mesozoic–Cainozoic. Geosciences, 3(2): 331-353.

Vérard, C., Flores, K. and Stampfli, G., 2012a. Geodynamic reconstructions of the South America–Antarctica plate system. Journal of Geodynamics, 53: 43-60.

Vérard, C., Hochard, C. and Stampfli, G., 2012b. Non-random distribution of euler poles: is plate tectonics subject to rotational effects? Terra Nova, 24(6): 467-476.

von Raumer, J.F. and Stampfli, G.M., 2008. The birth of the Rheic Ocean — Early Palaeozoic subsidence patterns and subsequent tectonic plate scenarios. Tectonophysics, 461(1–4): 9-20.

Wessel, P. and Kroenke, L.W., 2008. Pacific absolute plate motion since 145 Ma: An assessment of the fixed hot spot hypothesis. Journal of Geophysical Research: Solid Earth (1978–2012), 113(B6).

White, W. M. Oceanic island basalts and mantle plumes: the geochemical perspective. *Annual Review of Earth and Planetary Sciences* **38**, 133-160 (2010).

White, W.M., 2010. Oceanic island basalts and mantle plumes: the geochemical perspective. Annual Review of Earth and Planetary Sciences, 38: 133-160.

Whittaker, J. *et al.* Long-term interaction between mid-ocean ridges and mantle plumes. *Nature Geoscience* **8**, 479-483 (2015).

Whittaker, J., Afonso, J., Masterton, S., Müller, R., Wessel, P., Williams, S. and Seton, M., 2015. Long-term interaction between mid-ocean ridges and mantle plumes. Nature Geoscience, 8(6): 479-483.

Wildberg, H.G.H., 1984. Der Nicoya Komplex, Costa Rica, Zentralamerika: Magmatismus und genese eines polymagmatischen Ophiolith-Komplexes. Münster Forschngsschwerpunkte Geologisch Paläontologisches, 62: 1-123.

Wilhem, C., Windley, B.F. and Stampfli, G.M., 2012. The Altaids of Central Asia: a tectonic and evolutionary innovative review. Earth-Science Reviews, 113(3): 303-341.

Winterer, E. L. *et al.* Cretaceous guyots in the northwest Pacific: An overview of their geology and geophysics. *The Mesozoic Pacific: Geology, Tectonics, and Volcanism*, 307-334 (1993).

Winterer, E.L., Natland, J.H., Van Waasbergen, R.J., Duncan, R.A., McNutt, M.K., Wolfe, C.J., Silva, I.P., Sager, W.W. and Sliter, W.V., 1993. Cretaceous guyots in the northwest Pacific: An overview of their geology and geophysics. The Mesozoic Pacific: Geology, Tectonics, and Volcanism: 307-334.

Woodhead, J. D. & Devey, C. W. Geochemistry of the Pitcairn seamounts, I: source character and temporal trends. *Earth and Planetary Science Letters* **116**, 81-99 (1993).

Woodhead, J.D. and Devey, C.W., 1993. Geochemistry of the Pitcairn seamounts, I: source character and temporal trends. Earth and Planetary Science Letters, 116(1): 81-99.

Worthington, L. L., Van Avendonk, H. J. A., Gulick, S. P. S., Christeson, G. L. & Pavlis, T. L. Crustal structure of the Yakutat terrane and the evolution of subduction and collision in southern Alaska. *Journal of Geophysical Research: Solid Earth* **117**, doi:10.1029/2011JB008493 (2012).

Worthington, L.L., Van Avendonk, H.J.A., Gulick, S.P.S., Christeson, G.L. and Pavlis, T.L., 2012. Crustal structure of the Yakutat terrane and the evolution of subduction and collision in southern Alaska. Journal of Geophysical Research: Solid Earth, 117(B1).

8. Figures

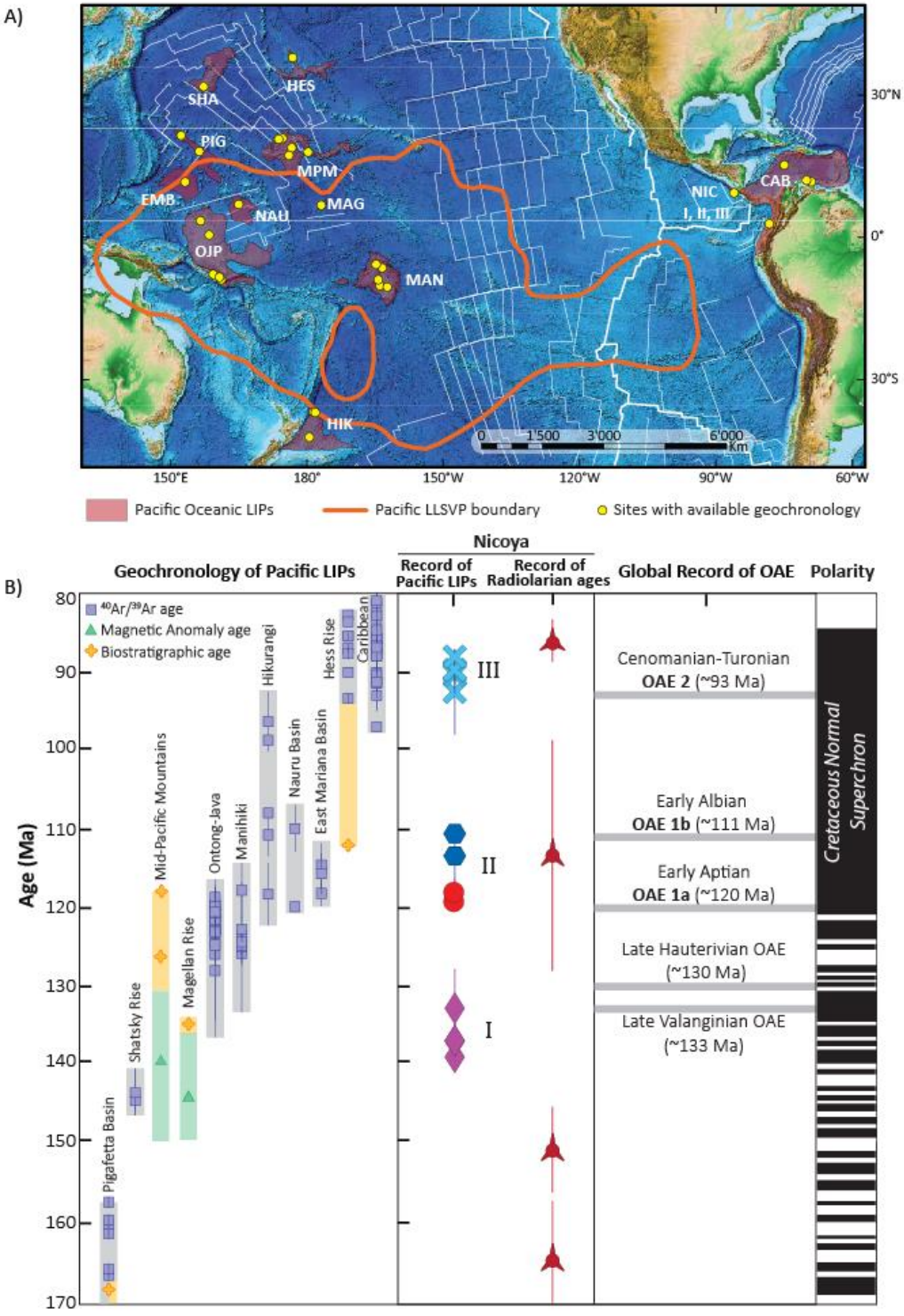

Figure 2.1. Location and geochronology of Pacific LIPs. (a) Present configuration of the central circum-Pacific Plate; highlighted purple areas correspond to fragments of oceanic plateaus and ocean basin flood basalts preserved at the seafloor and plate margins, yellow dots are sampled locations with geochronology and/or geochemistry, and the white lines represent magnetic anomalies of the Pacific seafloor after Muller

et al. (1997). The boundaries of the Pacific LLSVP (Becker et al., 2002) at 2500 km are projected to the surface. (b) Geochronological correlation of Pacific LIPs with the oceanic accreted terranes in Costa Rica, global oceanic anoxic events (Jenkyns, 2010) and geomagnetic polarity reversals48. PIG: Pigafetta Basin, SHA: Shatsky Rise, MPM: Mid-Pacific Mountains, NIC I: Nicoya I, MAG: Magellan Rise, EMB: East Mariana Basin, NAU: Nauru Basin, OJP: Ontong-Java, MAN: Manihiki, HIK: Hikurangi, HES: Hess Rise, NIC II: Nicoya II and CAB: Caribbean.

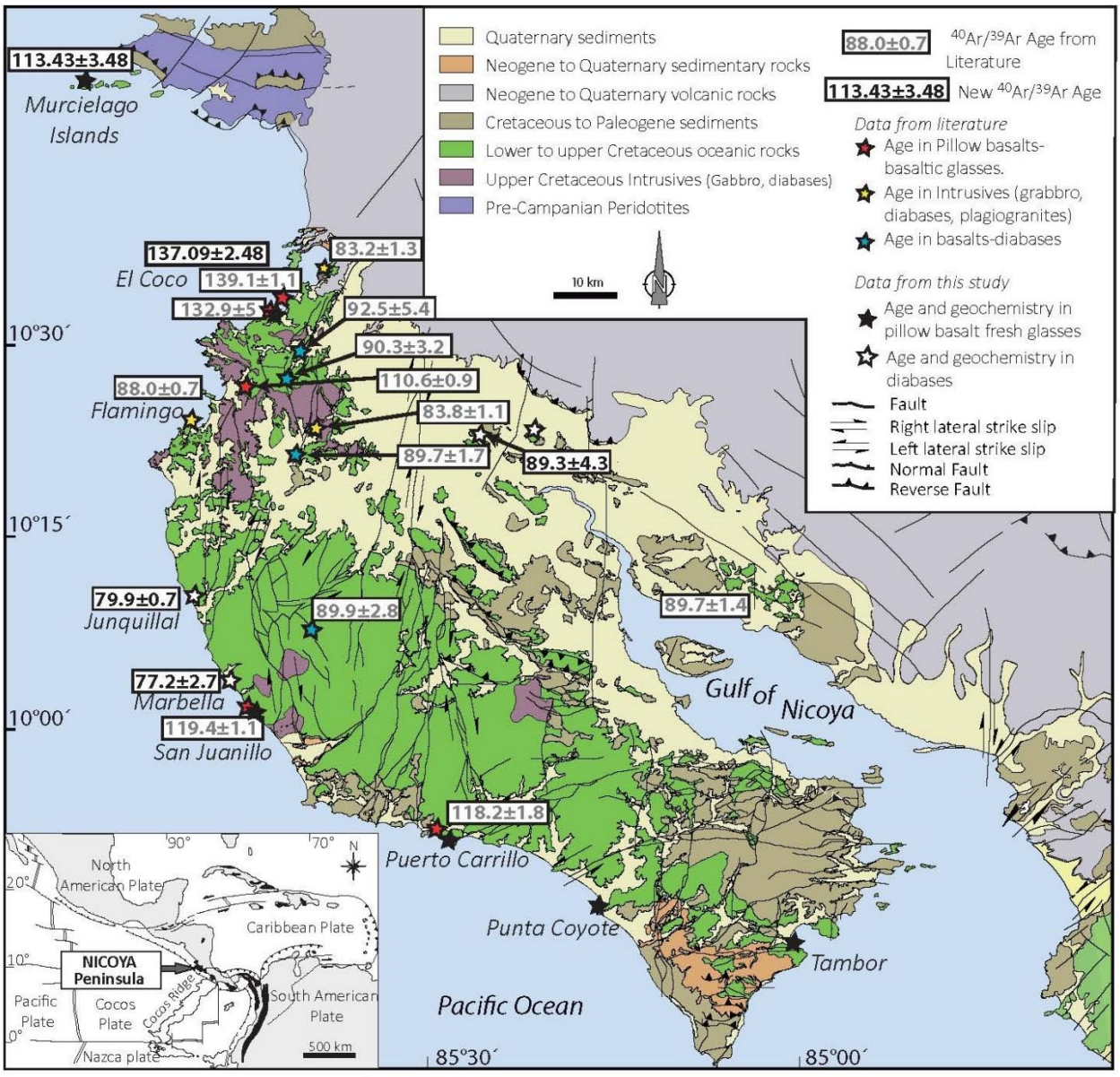

Figure 2.2: Geologic map of the Nicoya Peninsula Costa Rica, modified after Denyer et al. (2014). Samples collected and analyzed for this study are shown in black star symbols for pillow basalt fresh glasses and in white star symbols corresponding to diabases. Samples from the literature use the following symbols: red stars for pillow basalt and basaltic glass samples, yellow stars for ages in intrusive samples (gabbro, diabase or plagiogranites) and blue for samples described in the literature as coarse-to-fine grained basalt and that can correspond to massive flows or diabases. $^{40}Ar/^{39}Ar$ ages from the literature are shown in white boxes with gray font and our new $^{40}Ar/^{39}Ar$ analyses are in black fonts. Inset on the left shows the location of the Nicoya Peninsula within the geotectonic frame of the region. All ages are in millions of years (Ma).

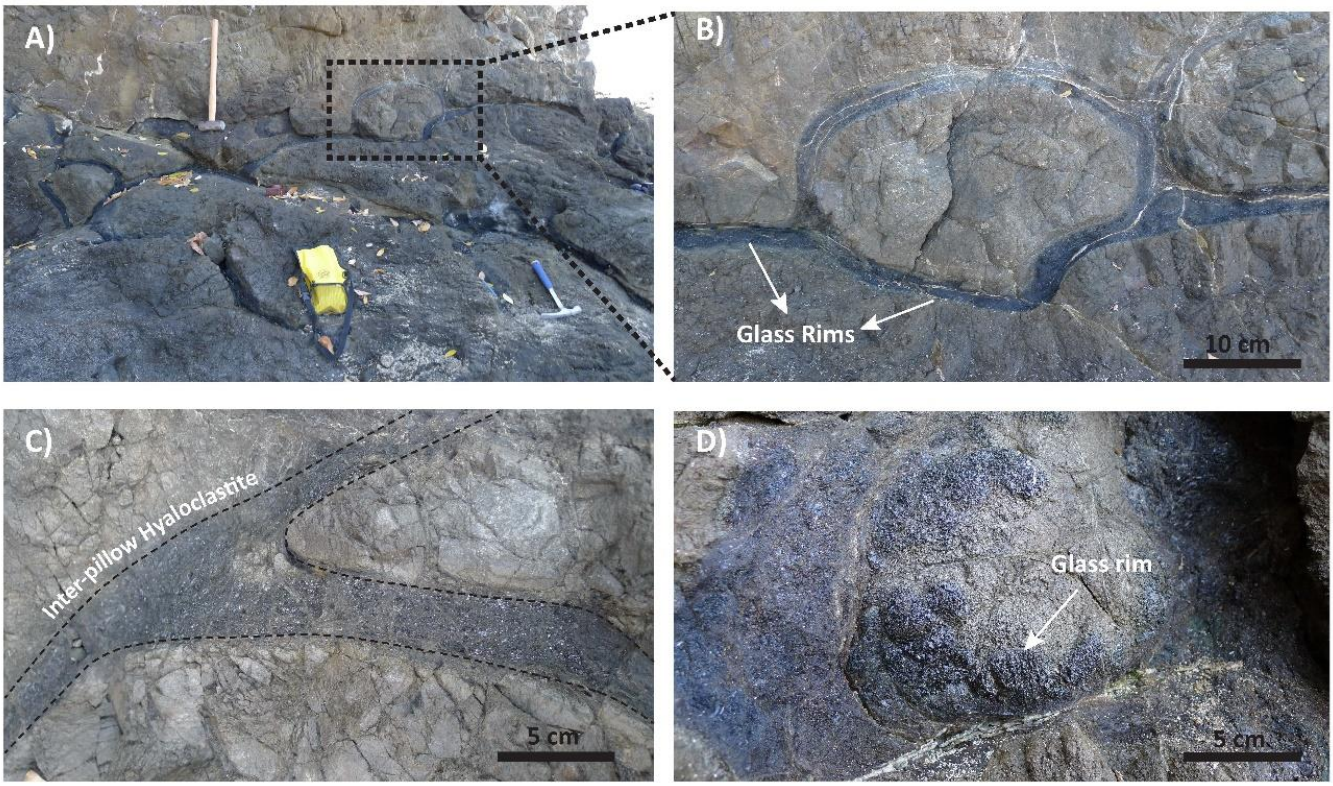

Figure 2.3. Field photographs of the pillow basalt outcrops at Nicoya Peninsula, Costa Rica. A) Pillow basalt flows at San Juanillo beach (lat/long: 10.03020/-85.7394) with quenched glass rims surrounding the pillow basalts. B) Closer look at an individual pillow basalt; the rims preserved glasses with little to no alteration. C) The hyaloclastite between pillow basalts also contains fragments of fresh glasses. D) Close up of the fresh glass rim surrounding the pillow basalt.

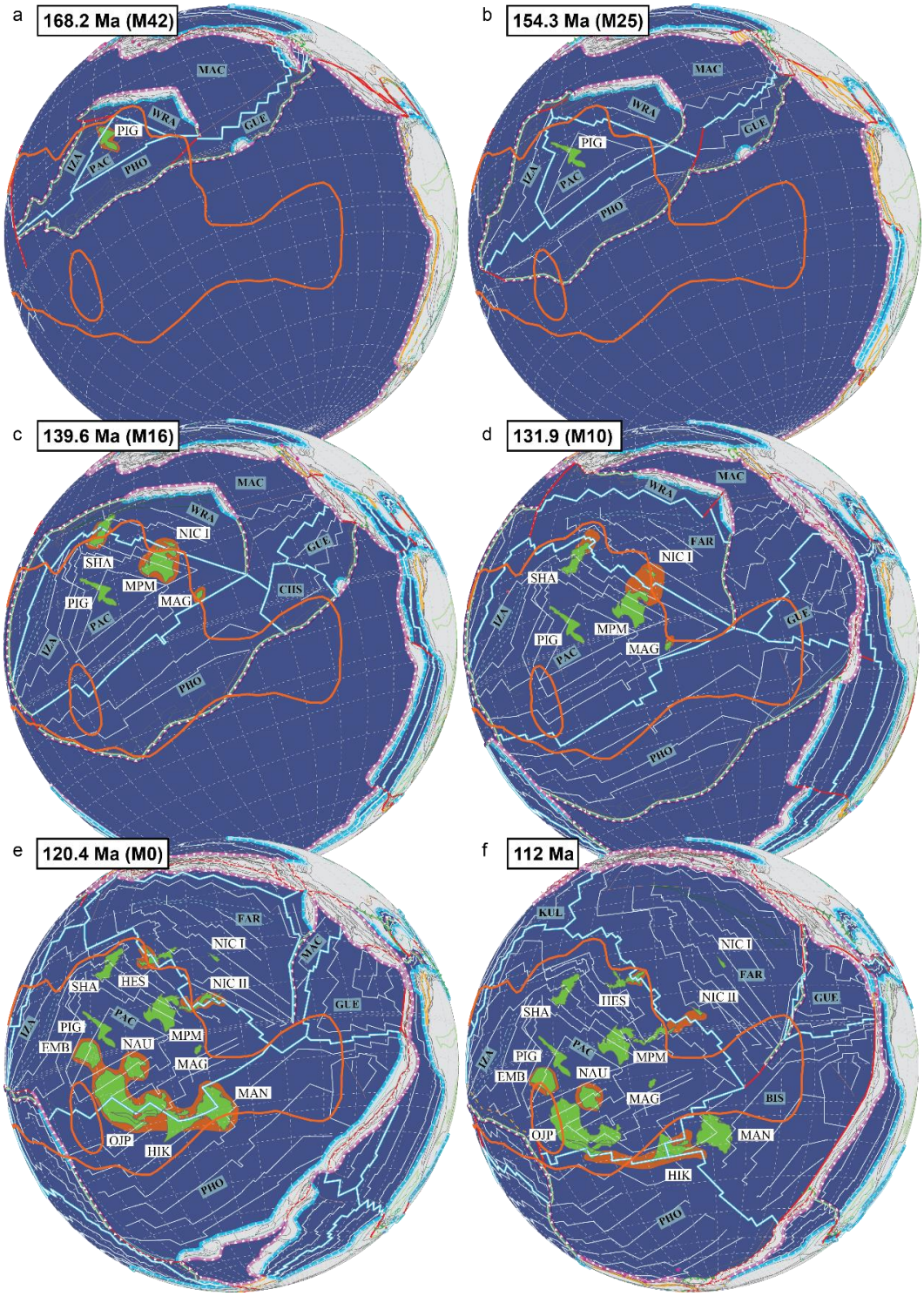
a
168.2 Ma (M42)
MAC
WRA
PIG
GUE
IZA
PAC
PHO
b
154.3 Ma (M25)
MAC
WRA
PIG
GUE
IZA
PAC
PHO
c
139.6 Ma (M16)
MAC
WRA
NIC I
GUE
SHA
MPM
CHS
PIG
MAG
PAC
IZA
PHO
d
131.9 (M10)
MAC
WRA
FAR
NIC I
SHA
IZA
MPM
GUE
PIG
MAG
PAC
PHO
e
120.4 Ma (M0)
FAR
NIC I
MAC
SHA
HES
NIC II
GUE
IZA
PIG
PAC
MPM
EMB
NAU
MAG
MAN
OJP
HIK
PHO
f
112 Ma
KUL
NIC I
FAR
HES
NIC II
GUE
SHA
IZA
PIG
PAC
MPM
EMB
NAU
MAG
BIS
OJP
MAN
HIK
PHO

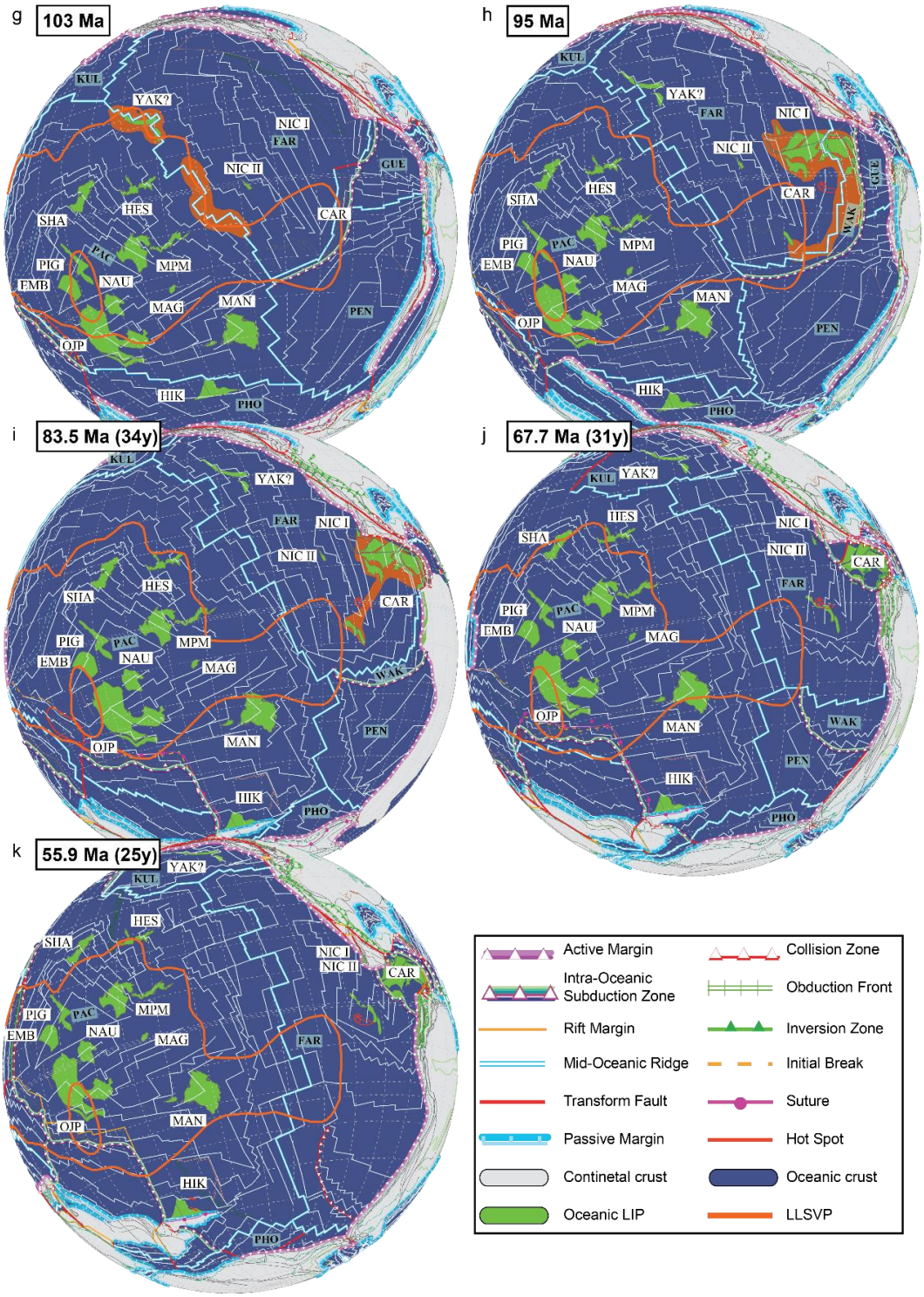

Figure 2.4. Kinematic plate tectonic reconstructions at a-168.2 Ma (M42), b- 154.3 Ma (M25), c- 139.6 Ma (M16), d- 131.9 Ma (M10), e- 120.4 Ma (M0), f- 112 Ma, g- 103 Ma, h- 95 Ma, i- 83.5 Ma (34y), j- 67.7 Ma (31y) and k- 55.9 Ma (25y). Notations in parenthesis refer to established magnetic anomalies. Tectonic plate abbreviations BIS (Biscoe), CHS (Chonos), FAR (Farallon), GUE (Guerrero), IZA (Izanagi), KUL (Kula), MAC (Mackinley), PAC (Pacific), PEN (Penas), PHO (Phoenix), WAK (Washikemba), WRA (Wrangellia). See text for further descriptions.

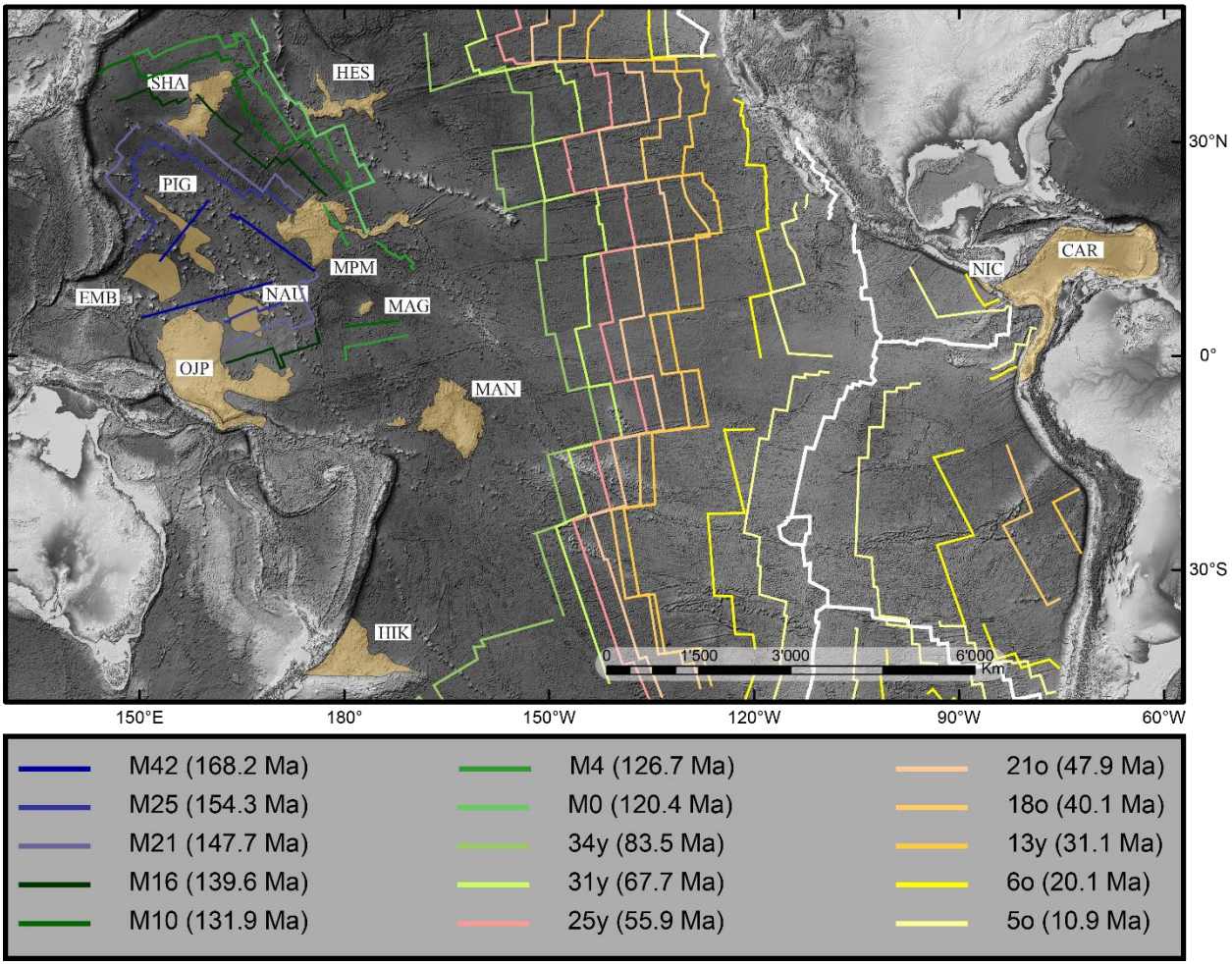

Figure 2.5. Central Pacific Ocean seafloor spreading map, the color lines represent the isochrones used for our kinematic model. Letters, numbers and ages correspond to magnetic isochrons after Müller et al. (1997) and Müller et al. (2008).

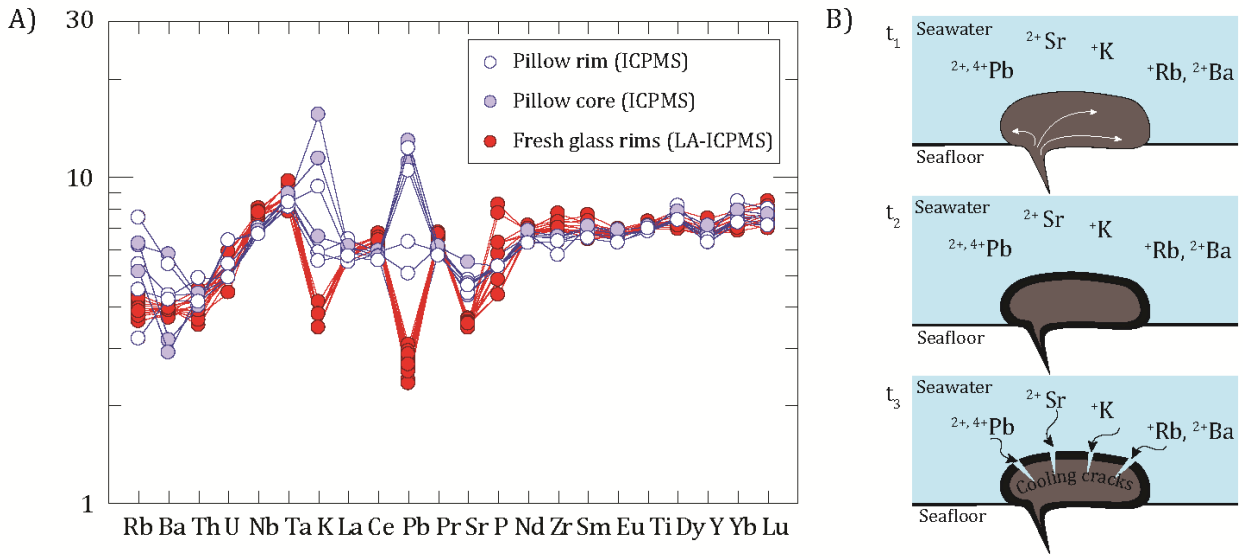

Figure 2.6. Geochemistry of Nicoya basaltic glasses. A) Multielement diagram showing the marked differences in fluid mobile element contents between analysis made in-situ on pillow basalt glass rims (red symbols) by LA-ICP-MS and on whole rock analyses from the pillow cores (blue close symbols) and the pillow rims (blue open symbols). Elements like K, Pb and Sr show a clear enrichment in the inner parts of the pillow due to cation mobilization during seawater interaction. Elements like Rb and Ba do not show a clear trend; however, note how the analyses in fresh glass samples account for less variability (better precision in the analyses) than its counterparts. B) Schematic representation of the seawater-pillow basalt interaction at eruption on the seafloor. At t_1 the pillow basalt erupts (at temperatures ~1000 °C) at the seafloor where immediately gets in contact with cold seawater (~1 °C). In t_2, the thermic shock results in the instantaneous quenching of the lava, which creates a rim surrounding the pillow basalt. At t_3 the pillow basalt starts to cool down it contracts creating radial fractures that allow the entrainment of seawater. Hence, cations dissolved in seawater like Pb, Sr, K, Rb and Ba can percolate and react with the hot core of the pillow basalt, which consequently will get geochemically enriched in such cations.

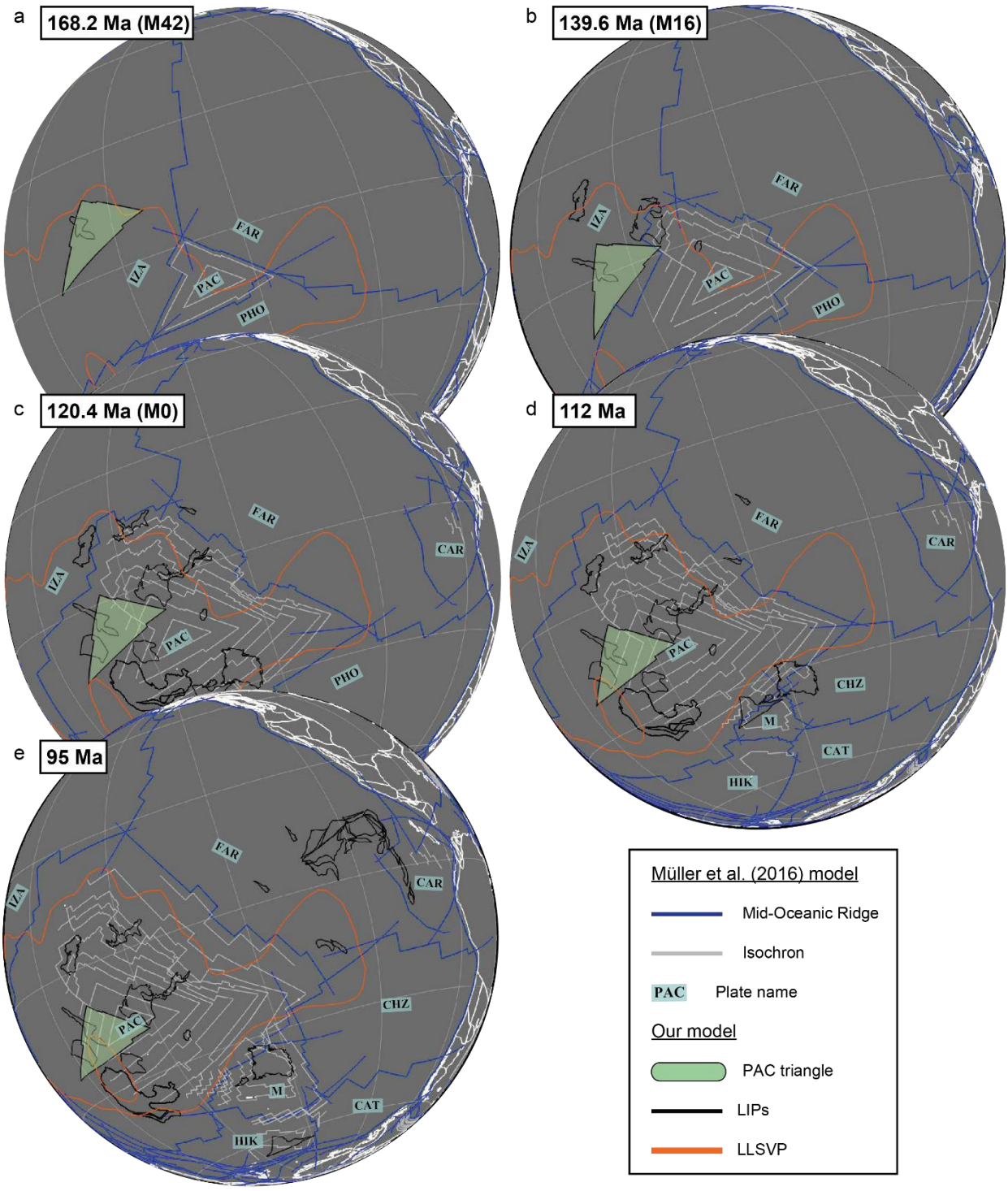

Figure 2.7. GPlates-based plate tectonic reconstructions after Müller et al. (2016) compared to the positions of the LLSVP edge, Large Igneous provinces (LIPs), and the Pacific plate triangle given by our kinematic reconstructions. Note the both models do not dramatically differ on the position of the Pacific plate for the given times. Tectonic plate abbreviations from Müller et al. (2016).CAR (Caribbean), CAT (Catequil), CHZ (Chazca), FAR (Farallon), HIK (Hikurangi), IZA (Izanagi), M (Manihiki), PAC (Pacific), and PHO (Phoenix).

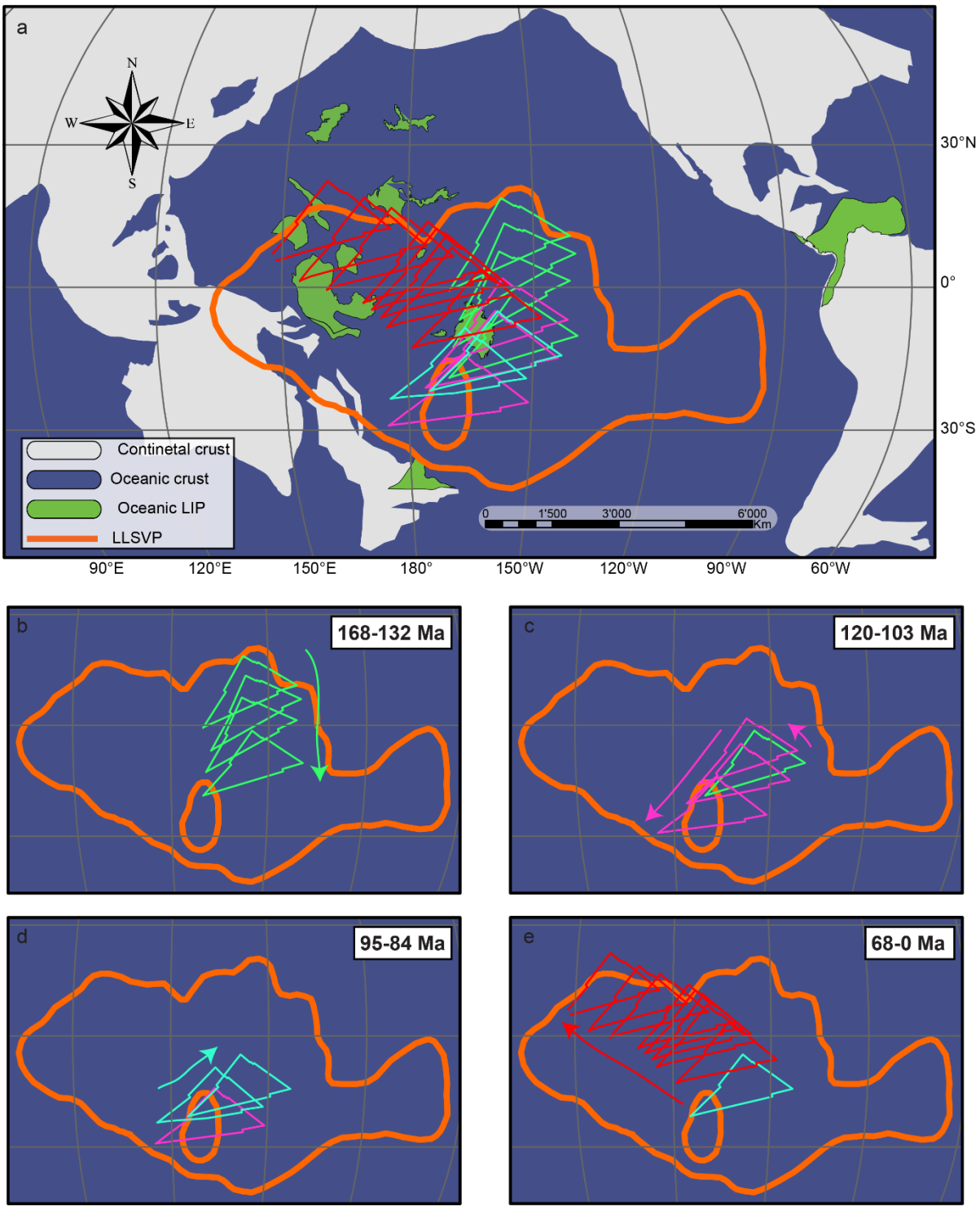

Figure 2.8. Rotational evolution of the Pacific plate triangle based on our kinematic plate tectonic model. Note how the migration paths describe a relative motion towards the south at ~168-132 Ma, changing towards southwest at ~120-103 Ma, then towards northwest at ~95-84 Ma and finally to the current northwest rotational path at ~68-0 Ma.

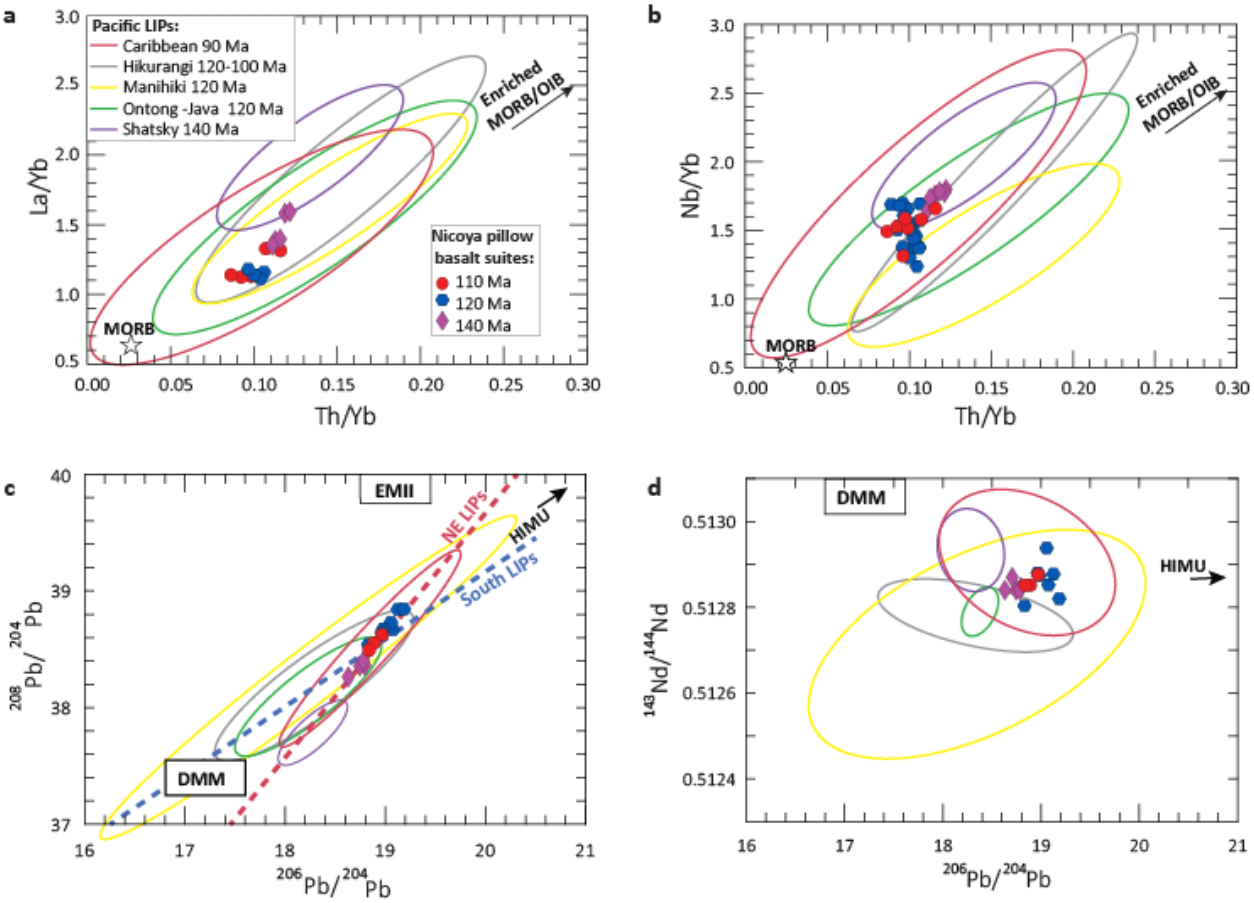

Figure 2.9. Geochemistry of the Nicoya accreted LIPs compared to contemporaneous Pacific LIPs. Data density ellipses for the Pacific LIPs were calculated at the 95% confidence level. (a) La/Yb vs. Th/Yb. (b) Nb/Yb vs. Th/Yb. All the LIP trace element data can be described as the result of different amounts of mixing of an enriched end-member (Enriched MORB/OIB; McDonough and Sun, 1995) and a depleted MORB endmember (Gale et al., 2013). (c) $^{208}Pb/^{204}Pb$ vs. $^{206}Pb/^{204}Pb$. (d) $^{143}Nd/^{144}Nd$ vs. $^{206}Pb/^{204}Pb$ isotope systematics for the basalts of the different LIPs compared to the accreted terranes of Nicoya I and II showing distinct trends for LIPs originated at the northeastern edges of the LLSVP (Shatsky, Caribbean, Nicoya I and II) and for the southern edge LIPs (Ontong-Java, Manihiki, Hikurangi). All Pacific LIPs show a clear mixing relations between DMM and HIMU end-members, although Manihiki samples also require a third component to explain the low Nd isotopes at a given Pb isotopes.

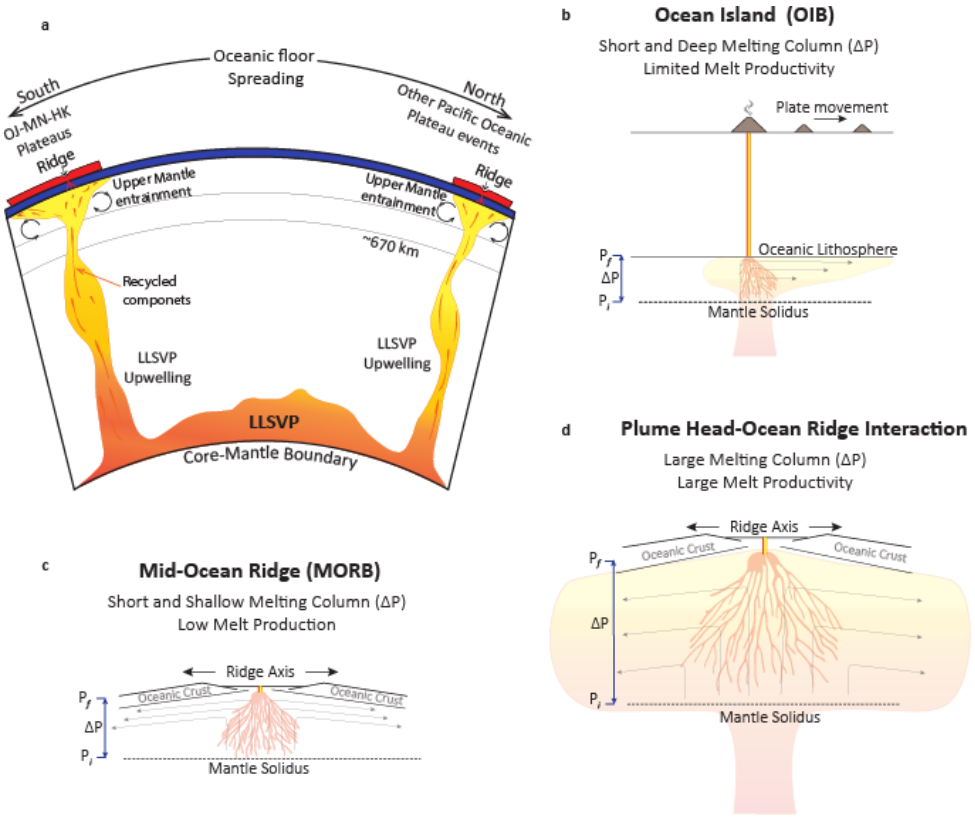

Figure 2.10. Comparison of melting processes and sources at different melting environments. (a) Schematic representation of the Pacific LLSVP. Hot heterogeneous material from the core-mantle boundary (CMB) rises through the mantle as a result of instabilities and positive buoyancy. The ascending material carries the geochemical signature of the stagnant reservoirs at the CMB; ancient subducted oceanic slabs, sub-continental lithosphere or sediments. (b) At ocean island chains feed by a mantle plume, initial and final melting pressures (P_i) will occur at higher depths; however, the melting column (ΔP) will be limited due to lithospheric thickness (P_f). (c) In the case of mid-ocean ridges both P_i and P_f occur at shallow levels. (d) And in the case of a plume head impacting at a mid-ocean ridge a combination of conditions occur where P_i will be deep and P_f shallow; consequently, the melting column (ΔP) and melt production are large, making the conditions for the emplacement of a LIP ideal.

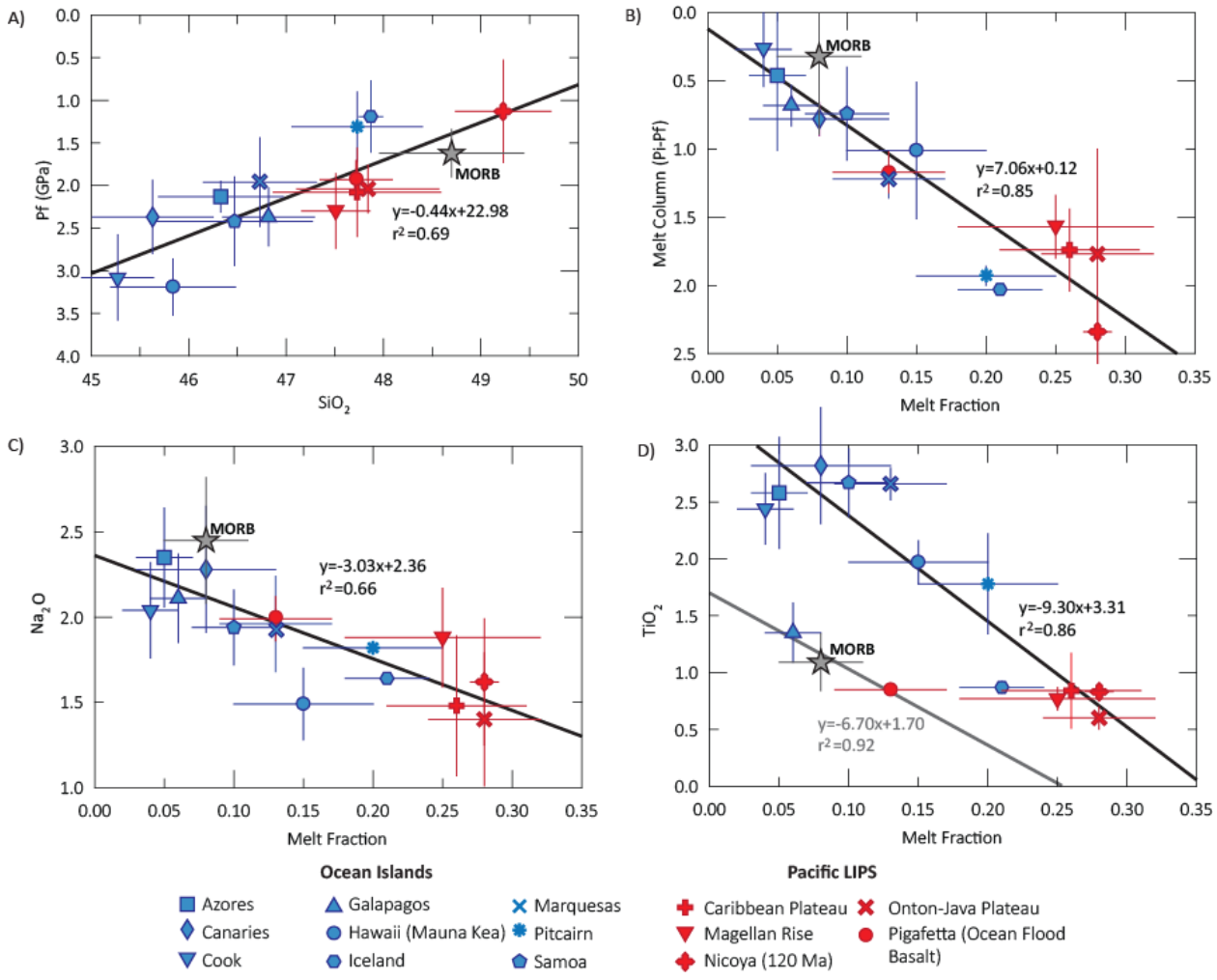

Figure 2.11. Correlation diagrams showing the different trends for average petrological constraints and primary magma compositions of modern oceanic islands (OIB), LIPs and MORB. (a) Final melting pressures (P_f) plotted against SiO_2 content. LIP primary magmas are characterized by low pressure values and high SiO_2 contents, similar to MORB. (b) Melt column ($P_{initial}$-P_{Final}) plotted against melt fraction; LIPs display more extended melt columns that resulted in higher melt productivity, compared to MORB and OIB. (c) Average Na_2O content vs. melt fraction. Note how overall LIPs have the highest melt fractions and lowest Na_2O contents. (d) Average TiO_2 contents against melt fraction. Two distinct trends can be identified where LIPs show the lowest TiO_2 contents and the highest melt, but in in the same correlation with most OIB primary magmas. Average MORB, Pigafetta, Galapagos and to some extend Iceland define another trend. The error bars denote the standard deviation from the average.

Chapter 3: Recycling seamounts: Implications for Upper Mantle Source Heterogeneities

Abstract

Intraplate magmatism provides with a window into the composition of mantle heterogeneities, nevertheless, the origin of these heterogeneities are still a matter of debate. Radiogenic isotopes (Sr-Nd-Pb) from present-day ocean island basalts (OIB) produced by intraplate magmatism can help establish the source compositions of these chemically and isotopically enriched reservoirs. Here we present evidence that suggests that a highly enriched mantle reservoir can originate from OIB-type subducted material that gets incorporated and stirred throughout the mantle. We explore this hypothesis using a restricted set of data from non-plume related OIB volcanism; focusing on isolated seamounts with no apparent age progression and interpreted to be related to either plate flexure, shear driven convection and/or edge convection. Our results suggest that an enriched mantle reservoir composed by recycled seamount materials can be formed in a shorter time period that than ancient subducted oceanic crust (>1 Ga) thought to be the forming agent of the HIMU mantle reservoir endmember. A "fast-forming", enriched reservoir could explain some of the enriched signatures commonly present in intraplate magmas not related with an active mantle plume upwelling.

1. Introduction

Intraplate volcanism is responsible for the occurrence of magmatism away from tectonic plate boundaries and accounts for the generation of diverse styles of volcanism like hotspot volcanic chains, isolated seamounts, and isolated volcanic edifices within continents. These magmatic processes are characterized by low volume basaltic melts predominantly alkaline in

composition that provide a window to mantle heterogeneities and the mechanisms that control melting in such environments (Hofmann and White, 1982; Ringwood, 1990; Schilling, 1991; White et al., 1993; Hofmann, 1997; Niu and O'Hara, 2003; Campbell, 2007).

Some occurrences of intraplate volcanism can be explained by mantle plumes (Morgan, 1971; White, 2010), deep thermochemical anomalies that remain in a near fixed location and create seafloor swelling and volcanic chains (Thorne et al., 2004; French and Romanowicz, 2015). These chains are easy to recognize as they show a clear age progression from the active site towards the older and more eroded parts of the volcanic chain (Hofmann and White, 1982; White, 2010). Nevertheless, a significant number of seamounts, especially in the Pacific Ocean, seem to be isolated or show no age progression whatsoever with adjacent volcanic edifices (Hillier and Watts, 2007). These isolated seamounts are unlikely related to deep mantle anomalies; instead they probably are the product of low volume melting of shallower upper mantle heterogeneities making them ideal locations to study the composition, age, and extent of these less characterized reservoirs of recycled material.

Another mechanism often invoked to explain intraplate volcanism is edge-driven convection. The process of edge-driven convection can be described as a convective cell fueled by the increased temperature found beneath cratons due to continental insulation which flows towards the cooler areas beneath the adjacent, thinner, and younger oceanic lithosphere (King and Anderson, 1998). This flow pattern will create a weak upward flow near the limits of the distinct lithospheric provinces that may result in decompression melting of upper mantle material. Small scale flow velocities of ~30 mm/yr (King and Ritsema, 2000) and in this case the melt productivity is tied to the difference in mantle viscosity and lateral temperature contrast at the lithospheric discontinuity instead of the velocity of the separating plates. This mechanism is used to explain

the Bermuda Rise and some of the hotspot upwellings in the eastern Atlantic Ocean, where isolated volcanic centers can be found at around 1000 km away from the cratons edges.

Alternatively, shear driven-convection produced by the rapid shearing of the asthenosphere during convection may be another mechanism inducing upwelling and melting of upper mantle heterogeneities. The necessary conditions for shear driven convection to occur are: having rapid shearing of the asthenosphere (>3.0 cm/yr) flowing towards a progressively thinner lithosphere, presence of viscosity heterogeneities in the sheared upper mantle, and the occurrence of near-solidus asthenosphere (Conrad et al., 2011). Channelized pressure-driven flow in the asthenosphere can transport enriched source materials from the upper mantle over large horizontal distances (Ballmer et al., 2013) Asthenospheric shear-driven upwellings would be the cause of intraplate volcanism in the south East Pacific Rise (SEPR) where the Pukapuka ridge, Hotu-Matua and Sojourn ridge seamounts are found (Natland and Winterer, 2005). Sublithospheric flow causes this shear and might be responsible for mantle heterogeneities that are reflected in the more enriched MORB present in the SEPR.

Finally, a third possible mechanism related with mantle upwelling triggered by plate flexure have been evoked for the formation of small volume, monogenetic seamounts throughout the Pacific known as “petit-stop” (Hirano et al., 2006). In this scenario the tensional field of the lithosphere caused by the plate flexure as it approaches the subduction trench, allow the formation of small pockets of decompression melting. Such kind of magmatism favors the generation of low melt fractions that tap upper mantle recycled materials and resulting in compositionally enriched lavas, similar to OIB signatures (Hirano et al., 2006; Valentine and Hirano, 2010; Hirano, 2011).

Independent of their origin, ocean island basalts (OIB) are more radiogenic and enriched in incompatible elements than Mid-ocean ridge basalts (MORB). In order to produce the range in

isotopic values found at OIB is necessary to tap into at least four different isotopic mantle reservoirs: EMI, EMII, HIMU and Depleted Mantle. EMI reservoirs are characterized by unradiogenic $^{206}Pb/^{204}Pb$ and moderately high $^{208}Pb/^{204}Pb$ and $^{87}Sr/^{86}Sr$; event though there is no consensus on its origin, recent work associate it to a combination of recycled sediments and oceanic crust (Willbold and Stracke, 2006; Garapić et al., 2015). EMII has intermediate values of $^{206}Pb/^{204}Pb$ and high $^{87}Sr/^{86}Sr$ and is commonly accepted that it represents recycled marine sediments (Workman et al., 2004; Jackson and Dasgupta, 2008; Willbold and Stracke, 2010). The HIMU domain represents the most enriched and radiogenic reservoir and is characterized by high $\mu=^{238}U/^{204}Pb$ and is related to the recycling of oceanic crust (Stracke et al., 2003; Stracke et al., 2005).

Our study presents new geochemical and geochronological data from accreted seamounts found at the NW Pacific coast of Costa Rica. Previous works (Frisch et al., 1992; Hauff et al., 2000; Buchs et al., 2013) have suggested that these series of seamounts belong to intraplate volcanism unrelated to hotspot activity. Using samples from these accreted seamounts as a proxy for subducted materials, we modeled the isotopic composition in time of the potential reservoir that they consolidate once incorporated into the mantle and into the stirring processes of mantle flow, in order to contribute to the understanding of the evolution of deep heterogeneities. Our working hypothesis is that in order to create "HIMU-like signatures" as the ones found in certain intraplate locations that are clearly not related with an active mantle plume upwelling (i.e. New Zealand, Basin and Range, western US, Virginia, etc.) and possibly tapping upper mantle sources, it is necessary to recycle an enriched source in the first place. An unexplored possibility for this enriched source could be recycling already enriched seamounts by subduction. Here we present projections of the isotopic composition of different seamounts as potential recycled enriched

material to model their evolution in time and to discuss their potential as source components in the mantle.

2. Geotectonic setting

Costa Rica is situated today near the triple junction of the Cocos, Caribbean and Nazca plates (DeMets, 2001). Across the Middle American Trench, the Cocos plate is being subducted underneath the Caribbean plate resulting in an active volcanic front (Fig. 3.1). Several oceanic complexes have been accreted onto the Caribbean Plate along the Pacific side of Costa Rica (Hauff et al., 2000; Denyer and Gazel, 2009; Tournon and Bellon, 2009). The Santa Elena peninsula, in the northwestern Pacific coast, contains the oldest of these oceanic complexes and it is constituted by a cretaceous peridotite nappe obducted on top of an autochthonous tectonic basement with mid-Jurassic to mid-Cretaceous accreted oceanic lithologies. The Santa Rosa Accretionary Complex (Santa Rosa) is the footwall of the nappe that emplaced the Santa Elena Ophiolite in its current location. It outcrops along the southern coasts of the peninsula and in the Rio Potrero Grande tectonic window inland in the peninsula (Fig. 3.1b). The Santa Rosa Complex comprises an oceanic assemblage of alkaline basalts (pillow and lava flows), polymictic breccias of mafic and ultramafic rocks, and radiolarian cherts of Aptian to Cenomanian ages (Meschede and Frisch, 1994; Tournon, 1994; Bandini et al., 2011), pelagic limestones at playa Naranjo, alkaline pillow lava flows at Playa Carrizal, radiolarian cherts cut by alkaline dikes in Santa Rosa, a sequence of massive and pillow lava flows, dikes, trachytes and tuffs in playa el Respingue and sequences of sandstones and micro-conglomerates of felsic volcaniclastic composition (Baumgartner and Denyer, 2006; Madrigal et al., 2015).

The alkaline basaltic lava flows and intrusions have been interpreted as sections from small-volume volcanic edifices that became accreted at the continental margin (Frisch et al., 1992;

Hauff et al., 2000; Buchs et al., 2013). From the base to the top they are constituted by basal lava flow, dike sequences and thick radiolarite deposits that denote deep sedimentation. In addition, as described by Buchs et al. (2013) the accreted section that includes the seamounts also contains series of trench-fill sediments that also support this interpretation. Their geochemical composition is in agreement with a low melt fraction magma production, characteristic of intraplate volcanism and similar to that of petit-spot volcanoes. $^{40}Ar/^{39}Ar$ geochronology of these seamounts yielded ages of formation of 173.9 ± 0.5 Ma, 177.0 ± 0.8 Ma (Buchs et al., 2013) while Bandini et al. (2011) estimated an age of accretion to the margin of ~110 Ma. Based in their geochronology and composition Buchs et al. (2013) interpreted the origin of the Santa Rosa seamounts to be formed by low melt fraction magmas formed in response to tectonic stress from fracture zones during the onset of the Pacific Plate.

Although the Santa Rosa seamounts are located in proximity to other accreted sequences found throughout Central America, their age and geochemical signature do not correlate to other accreted of the Galapagos-related hotspot tracks (Geldmacher et al., 2008; Buchs et al., 2013) or to fragments of the accreted Caribbean Large Igneous Province (CLIP) (Hauff et al., 2000). Detail lithostratigraphic sequences described in Buchs et al. (2013) suggest that these accreted seamounts are similar to those from the Japan Trench and the Line Islands chain, supporting the interpretation of a non-plume origin for the accreted Santa Rosa seamounts.

3. Analytical Methods

Fresh samples were collected directly from coastal outcrops along the Santa Elena Peninsula (Fig. 3.1). We cut the best samples using a water-lubricated rock saw and then crushed them in a jaw rock crusher to a gravel size. The gravels were cleaned with de-ionized water. Using

a stereoscope microscope, we hand-picked the rock chips that show absence of alteration mineral phases. Then, selected gravels were powdered using an alumina mill for major and trace element analysis.

Major element (wt%) concentrations were measured by X-ray fluorescence (XRF; Siemens SR3000 spectrometer) at the University of Auckland following the methods described by Norrish and Hutton (1969). In general, precision for each major element is better than ±1% (1σ) of the reported value as described by Norrish and Hutton (1969). Trace elements were measured by laser-ablation inductively-coupled-plasma mass-spectrometry (LA-ICP-MS) at the Research School of Earth Sciences, Australian National University, using Excimer LPX120 laser (193 nm) and Agilent 7500 series mass spectrometer following the method of Eggins et al. (1998). Samples were run in batches of 15 using the NIST612 glass standard at the beginning and end of each run to calibrate. USGS glass standard BCR-2 was also run as a monitor analytical performance. Repeat analyses of standard BCR-2 indicate precision of <4% (RSD) and accuracy better than 5% at the 95% confidence level. Radiogenic isotopes analyses were conducted in the Lamont-Doherty Earth Observatory TIMS facility and following the methods described in Jweda et al. (2016).

To obtain the $^{40}Ar/^{39}Ar$ data, unaltered rock chips of 425-300 μm in diameter were hand selected from each sample. The groundmass (matrix) separates were irradiated for 60 hours at the Oregon State University TRIGA-type reactor in the Cadmium-Lined In-Core Irradiation Tube. At the University of Wisconsin-Madison Rare Gas Geochronology Laboratory, incremental heating experiments were conducted using a 25 Watt CO_2 laser. Each step of the experiment included heating at a given laser power, followed by an additional 10 min for gas cleanup. The gas was cleaned with two SAES C50 getters, one of which was operated at ~450 °C and the other at room temperature. Blanks were analyzed after every second laser heating step, and were less than 5 x

10^{-20} mol/V for 36Ar and 2 x 10^{-17} mol/V for ^{40}Ar, respectively. Argon isotope analyses were performed using a MAP 215–50, and the isotope data was reduced using ArArCalc software version 2.5 (http://earthref.org/ArArCALC/). Ages were calculated from the blank-discrimination and decay-corrected Ar isotope data after correction for interfering isotopes produced from potassium and calcium in the nuclear reactor. Ages are reported with 2σ uncertainties (includes the J uncertainty) and are calculated relative to a Fish Canyon standard age of 28.201 ± 0.046 Ma (Kuiper et al., 2008) and a value for λ^{40}K of 5.463 ± 0.107 x 10^{-10} yr^{-1} (Min et al., 2000).

4. Results

4.1. Geochronology and geochemistry of the Santa Rosa alkaline dikes

The geochronological analyses made on fresh dike samples yielded ^{40}Ar/^{39}Ar ages of 132 ± 4.3 Ma (measured on amphibole) and 155.8 ± 0.2 Ma (measured on groundmass). These ages are much older than the diabase intrusions that cross-cut the peridotite nappe of Santa Elena which range from 126- 116 Ma (Madrigal et al., 2015).

For this study we report 13 new major and trace element analyses for the Santa Rosa dikes. Major element data show that our samples are classified as alkaline basalts and their composition range from basanites to phonolites (Fig. 3.2). They present olivine (sometimes altered to iddingsite), clinopyroxene, plagioclase, hornblende and magnetite. These intrusions are characterized by their composition range from picro-basalts to tephri-phonolite and basaltic trachy-andesite however a large set of samples are categorized as basanites. Decreasing values of FeOt and TiO_2 with decreasing MgO contents suggest the differentiation of magnetite during crystallization. The correlation of the major element oxides and MgO suggest and olivine control fractionation trend, that evolves towards crystallization of clinopyroxene and plagioclase. The

alkaline dikes of the Santa Rosa Complex present high concentrations in incompatible elements in comparison with other Pacific intraplate volcanic seamounts.

Trace element data of the alkaline dikes were normalized to primitive mantle (McDonough and Sun, 1995) (Fig. 3.2) and it show an evident OIB pattern with a relative enrichment in the LREE, especially Nb and Ta, compared to HREE. Depletions in the HREE, like Dy, Y, Yb, and Lu, suggest the presence of a garnet-bearing peridotite source (Kay and Gast, 1973; Johnson, 1998). Small negative anomalies in K and Sr may be due to the mobility of these elements in fluids during seafloor alteration. The presence of garnet in the source is confirmed by trace element ratios like Gd/Yb (Fig. 3.3a) and Dy/Yb (Fig. 3.3b) as Yb is fractionated from the MREE. The Santa Rosa alkaline dikes show a significantly more enriched signature than other seamounts interpreted by as non-plume origin; nevertheless, a similar trend can be observed in samples from Davidson seamounts (Castillo et al., 2010), Vesteris seamount (Haase and Devey, 1994), the Japan Trench seamounts (Hirano, 2011). As expected the Santa Rosa seamounts plot close to the OIB extreme of the mantle array defined by the Th/Yb vs. Nb/Yb diagram (Pearce, 2008) (Fig. 3.3c). Depletions in Th and enrichments Nb can be regarded as proxies for recycled material, as Th is prone to be carried by subduction fluids during sediment recycling and Nb is retained by residual phases in subducted slabs (Wood et al., 1979; Pearce, 2014).

4.2. Radiogenic Isotopes

We report 8 new radiogenic isotope analyses (Sr, Nd, and Pb) for the alkaline dikes of the Santa Rosa. Even though we used the freshest samples available, these samples were surely exposed to seawater alteration through their geologic past, thus, we focused the data discussion

and interpretations on the more reliable results from Nd and Pb systematics to avoid uncertainties related to the spread on the Sr ratios data. The measured isotope ratios range from 0.70390 to 0.70513 in $^{87}Sr/^{86}Sr$; 0.51264 to 0.51281 in $^{143}Nd/^{144}Nd$; 19.364 to 20.049 in $^{206}Pb/^{204}Pb$; 15.643 to 15.6.97 in $^{207}Pb/^{204}Pb$; and 39.587 to 39.953 in $^{208}Pb/^{204}Pb$ (Fig. 3.4).

Compared to isotopic values from global MORB (Gale et al., 2013), the Santa Rosa seamounts have lower ratios of $^{143}Nd/^{144}Nd$ and similar contents of $^{87}Sr/^{86}Sr$ as the more enriched (EMORB) values (Fig. 3.4a), while showing more radiogenic Pb-isotopes. Values for the East Pacific Rise (EPR) are outlined in figure 3.4; note that even though these seamounts are interpreted to be of Pacific origin, the isotopic differences between the Santa Rosa dikes and MORB from EPR are significant and correspond to different sources. Isotope values from the Caribbean Large Igneous Province (CLIP) (Hauff et al., 2000; Hoernle et al., 2004; Trela et al., 2015) which are in proximity to the Santa Rosa seamounts are also plotted as red field, nevertheless, their values are higher in $^{143}Nd/^{144}Nd$, lower in $^{207}Pb/^{204}Pb$, and comparable in $^{206}Pb/^{204}Pb$ and $^{208}Pb/^{204}Pb$.

5. Discussion

5.1. Geochronology

Our new plateau $^{40}Ar/^{39}Ar$ ages contrast with the previously published ages for the alkaline basalts of the Santa Rosa Complex (Buchs et al., 2013). Buchs et al. (2013) reported two $^{40}Ar/^{39}Ar$ plateau ages of 173.9±0.5 and 177.0±0.8 Ma analyzed on amphiboles and three whole rock analyses that yielded integrated ages of 104.3, 109.7 and 126.5 Ma, however they are less precise as the samples were affected by alteration and Ar loss and recoil (Buchs et al., 2013). For this reason, hereafter we will only consider the plateau ages. Our two new $^{40}Ar/^{39}Ar$ plateaus yielded younger ages, at 132 ± 4.3 Ma (amphibole separate) and at 155.8 ± 0.2 (groundmass) Ma,

nevertheless, because of low K content in the amphibole, the former age presents less certainty than the latter.

We attribute the differences in ages to the chaotic configuration of the accretion complex and to the strong possibility that we are sampling different accreted seamounts. Also, while most of the ages were obtained from samples that belong to Playa Colorada (Fig. 3.1b), in the southern coast of the Santa Elena Peninsula, we present a new age for the Potrero Grande tectonic window (132 ± 4.3 Ma) where, most definitely, we sampled a different seamount fragment. Interestingly, the ages of these seamounts span from ~175 Ma, ~155 Ma, and ~132 Ma, suggesting that perhaps a series of different accretion pulses became accreted in this location.

5.2. Geochemistry of non-plume seamounts

The mechanisms of seamount formation can be arguably diverse and this is reflected in the variability of compositions of OIB suites worldwide. However, some characteristics are common to these seamounts like high K, Ti, Ba and Rb contents, interpreted as the results of low degrees of partial melting (<1%) and enriched isotopic compositions.

Petit-spot lavas, as described by Hirano et al. (2006), have enrichments in incompatible elements like Rb, Ba, U, Th and Nb, depleted HREE suggesting a garnet-bearing deep source (~90 km), possibly the base of the lithosphere. Isotopic compositions for petit-spots yield low $^{143}Nd/^{144}Nd$ (0.5125-0.5127) and $^{206}Pb/^{204}Pb$ (16.87-17.93) with relatively high $^{87}Sr/^{86}Sr$ (0.7042-0.7047) which can be similar to some OIB (Machida et al., 2009), nevertheless their noble gas isotopic compositions are indicative of a depleted mantle source as opposed to a deep mantle source (Hirano, 2011). As the Santa Rosa seamounts, petit-spot lavas plot close to the EM-1 isotopic endmember (see Fig. 3.3). Machida et al. (2009) suggest that EMI and DMM are the major

components during petit-spot magmatism, similar to EMI-type OIB (e.g. Pitcairn), however the main difference between both is that during petit-spot magmatism the volume of EMI is several orders of magnitude less than in EMI-type OIB.

Metasomatism must play an important role in the resulting enriched signatures found at intraplate volcanism, particularly in the instances where non-plume related magmatism taps upper mantle refertilized peridotite. Mantle metasomatism refertilizes the surrounding peridotite to create zones enriched in incompatible elements. Fluids responsible for this metasomatism are likely to come from the interface between the low velocity zone and the lithosphere (Niu et al., 2002). Alkalic and highly alkalic OIB are characterized by ~1-5% degrees of partial melting when the source is a fertile peridotite (Dasgupta et al., 2007). The heterogeneities of mantle reservoirs suggest different proportions or recycled materials; these heterogeneities ultimately control the dynamics of melt production and extraction. Machida et al. (2009) suggested that these heterogeneities are small-scaled which supports the idea of widespread upper mantle heterogeneities. These heterogeneities will melt preferentially with respect of DMM and EM-1 components are incorporated into the magma during melt migration (Machida et al., 2009).

Carbonated source, such as a carbonated peridotite could also be responsible of producing melts enriched in highly incompatible elements (Dasgupta and Hirschmann, 2006). Moreover, the effect of carbonate in the peridotite is to decrease the solidus during partial melting (~150 ˚C less than normal peridotite), allowing melting processes to occur deeper in the upper mantle (Dasgupta et al., 2007), thus forming the characteristic trace element patterns that denotes garnet in the residue and observed in OIB (Fig. 3.2b). On the other hand, a pyroxenitic fertile mantle-source can contribute to the formation of some EMORBs and OIB (Sobolev et al., 2007) as ubiquitous upper mantle heterogeneities caused by small amounts of recycled materials (<1 km^3). This persistent

small-scale heterogeneity is probably masked in areas of higher degrees of partial melting such as MORs (~8-10% partial melting) where the enriched signatures become diluted (Machida et al., 2009). Although pyroxenitic and carbonated peridotite may contribute as a source for HIMU-like alkalic lavas, none of them can be the sole component, instead they need to be mixed with other reservoirs to satisfy the composition of HIMU (Jackson and Dasgupta, 2008). Perhaps it may be a reservoir composed of recycling of alkali basalts from subducted seamounts (Hémond et al., 2006) and altered oceanic crust (Stracke et al., 2003).

Using PetDB and GEOROC databases, we compiled the available data for non-plume related seamount occurrences in the Pacific, focusing in the alkaline basalt to basanite samples to compare them to our Santa Rosa samples, that included both trace elements and isotopic compositions. These data points are plotted for comparison in Figures 3.4-3.6 and include the Northeast Pacific seamounts like Juan de Fuca and Kodiak-Bowie seamounts (Eaby et al., 1984; Cousens et al., 1985; Cousens, 1988; Hegner and Tatsumoto, 1989; Desonie and Duncan, 1990), Tuzo Wilson seamounts (Cousens et al., 1985; Allan et al., 1993), Lamont seamounts (Fornari et al., 1988; Allan et al., 1989; Danyushevsky et al., 2000), Seamounts on and off-axis of EPR (Batiza and Vanko, 1984; Aggrey et al., 1988; Graham et al., 1988; Hekinian et al., 1989; Allan et al., 1994; Chauvel and Blichert-Toft, 2001; Brandl et al., 2012; Jenner and O'Neill, 2012), Oshawa seamount (Cousens et al., 1999), continental margin of California seamounts (i.e. San Juan, Rodriguez seamounts; Davis et al., 1995; Davis et al., 2002), Japan Trench seamounts (Koppers et al., 1995; Shimoda et al., 2011), Ruru, Cloud and Hotu seamounts (Hall et al., 2006; Salters et al., 2011), Pito seamount (Hekinian et al., 1996; Verati et al., 1999), MIT Guyot (Koppers et al., 1995), Graham seamount (Cousens et al., 1999), Shimada seamount (Graham et al., 1988), and Davidson seamount (Castillo et al., 2010).

5.2. Modeling of the heterogeneity evolution in time: implications for mantle endmembers

By projecting the measured isotopic ratios to a given time t, we can model the resulting composition after that temporal lapse of recycling within the mantle. This can be calculated using the equations of decay of each of the isotopic species. For instance, in the case of Nd the equation will be based on the decay of ^{147}Sm, as follows:

$$\left(\frac{^{143}\text{Nd}}{^{144}\text{Nd}}\right)_t = \left(\frac{^{143}\text{Nd}}{^{144}\text{Nd}}\right)_i + \frac{^{147}\text{Sm}}{^{144}\text{Nd}}\left(e^{\lambda t} - 1\right)$$

Where $\left(\frac{^{143}\text{Nd}}{^{144}\text{Nd}}\right)_t$ indicates the P/D values at the time t (in years) that we wish to calculate; $\left(\frac{^{143}\text{Nd}}{^{144}\text{Nd}}\right)_i$ the initial values, which in this case, are the measured values; and λ denotes the decay constant of ^{147}Sm (λSm=6.5x10^{-12} yrs). The term $\frac{^{147}\text{Sm}}{^{144}\text{Nd}}$ is calculated from the Rb/Sr weight ratio. Given this equation, we can resolve to calculate the P/D values projected as the reservoir evolves in the mantle during a certain amount of time.

The same procedure can be used to calculate the P/D ratios at time t for ^{87}Sr/^{86}Sr, ^{206}Pb/^{204}Pb, ^{207}Pb/^{204}Pb and ^{208}Pb/^{204}Pb using the respective P decay constant: λ^{87}Rb=1.42x10^{-11} yrs, λ^{238}U=1.55125x10^{-10} yrs, λ^{235}U=9.8485x10^{-10} yrs, and λ^{232}Th=0.4948x10^{-10} yrs, as follows:

$$\left(\frac{^{87}\text{Sr}}{^{86}\text{Sr}}\right)_t = \left(\frac{^{87}\text{Sr}}{^{86}\text{Sr}}\right)_i + \frac{^{87}\text{Rb}}{^{86}\text{Sr}}\left(e^{\lambda t} - 1\right)$$

$$\left(\frac{^{206}\text{Pb}}{^{204}\text{Pb}}\right)_t = \left(\frac{^{206}\text{Pb}}{^{204}\text{Pb}}\right)_i + \frac{^{238}\text{U}}{^{204}\text{Pb}}\left(e^{\lambda 238 t} - 1\right)$$

$$\left(\frac{^{207}\text{Pb}}{^{204}\text{Pb}}\right)_t = \left(\frac{^{207}\text{Pb}}{^{204}\text{Pb}}\right)_i + \frac{^{235}\text{U}}{^{204}\text{Pb}}\left(e^{\lambda 235 t} - 1\right)$$

$$\left(\frac{^{208}\text{Pb}}{^{204}\text{Pb}}\right)_t = \left(\frac{^{208}\text{Pb}}{^{204}\text{Pb}}\right)_i + \frac{^{232}\text{Th}}{^{204}\text{Pb}}\left(e^{\lambda 232 t} - 1\right)$$

Thus we projected values from examples of seamounts associated with processes other than mantle plume upwelling (e.g. petit-spot, shear driven convection, edge driven convection) to compare with the results obtained for the Santa Rosa seamounts (Fig. 3.5, 3.6). At t=0 Ma, the Santa Rosa alkaline dikes show an isotopic composition close to the EMI endmember (Fig. 3.5, blue symbols). When projected the samples into longer periods of time t=200 Ma (Fig. 3.5, yellow symbols), t=500 Ma (Fig. 3.5, green symbols), and t=1000 Ma the isotopic values progressively become more enriched. In $^{207}Pb/^{204}Pb$ vs. $^{206}Pb/^{204}Pb$ (Fig. 3.5a), the enrichments more evident in ^{206}Pb. In Fig. 3.5b both $^{208}Pb/^{204}Pb$ and $^{206}Pb/^{204}Pb$ seem to increase in a similar manner. In $^{143}Nd/^{144}Nd$ vs. $^{206}Pb/^{204}Pb$ (Fig. 3.5c) as time progresses a spread in the data points is evident. In the three systems consistently, as the time increases the Santa Rosa seamounts approach the range of high μ values, nevertheless, once t surpasses 500 Ma the compositions become unrealistically enriched towards values not found in nature.

We calculated the age progression for other non-plume related seamounts around the Pacific using the same approach (Fig. 3.6a, b and c) and compare them to the results from Santa Rosa seamounts and isotopic values of MORB (using the isotope ratios for NMORB from Gale et al. (2013) but combining them with the trace element values from DMM of Salters and Stracke (2004)). The Santa Rosa seamounts show a sharp isotopic composition increase in time, compared to EPR seamounts, Grattam seamount in the Atlantic and Graham seamount near British Columbia to mention some examples. However, samples from Tuzo Wilson Seamount, Japan Trench petit-

spot seamounts and seamounts in front of the North American Trench have similar enrichments in time. As the Santa Rosa seamounts, most of these non-plume related seamounts reach similar values to HIMU in times between 200 and 500 Ma.

The alkaline rocks preserved in the Santa Rosa comprise the appropriate isotopic composition to create an enriched endmember that satisfies the enriched compositions seen in certain mantle plume magmatic stages in less time than recycled oceanic crust or continental crust. In fact, when calculating mixing models between a depleted mantle reservoir like DMM (Salters and Stracke, 2004) and the projected values of non-plume seamounts at 200 Ma (Fig. 3.7), using the mixing equations of Langmuir et al. (1977) which calculates the coefficients of the hyperbola equation between two endpoints (DMM and 200 Ma projections for different cases). Figure 3.7 shows how enriched signatures from intraplate volcanism like Louisville, Virginia, New Zealand, Cape Verde, the Canaries and the Cameroon line can be described as a product of mixing a depleted component like DMM and an enriched reservoir like the resulting projection of the isotopic composition of the Santa Rosa seamounts, North American Trench seamounts and Davidson seamount, at 200 Ma. Is important to note that projections at 500 Ma and 1000 Ma become extremely enriched, with values higher than HIMU that have not been observed in nature thus far, nevertheless not even the t=1000 Ma projections are appropriate to explain the extreme values of Mangaia-HIMU sources (not shown for clarity).

5.3. A reservoir from recycling seamounts?

Even though studies have shown that the Upper Mantle is intrinsically heterogeneous, contrary to what was initially thought, the composition, provenance and distribution of these

bodies of heterogeneous material are still unknown. Our data suggests that the isotopic evolution of a seamount-province type of reservoir can evolve to become sufficiently enriched to resemble a reservoir that explains some of the most enriched magmas on Earth in a time lapse of 200 to 500 Ma. (Fig. 3.8). Broadly considering spreading rates coupled with subduction rates, we can infer that 500 Ma is not sufficient time for a heterogeneity to travel along with the subducted slabs towards the lower mantle and return back in mantle plumes. This leads us to ponder on the possibility that these subducted seamounts, with their highly enriched compositions may instead remain in the upper mantle as heterogeneities. There is evidence that suggests that flat-slabs can stagnate at the mantle transition zone or bellow (Ballmer et al., 2015; Motoki and Ballmer, 2015), where if affected by thermal instabilities can begin to rise in the form of mantle upwellings. If a subducted flat-slab carries complete or fragmented low-volume, seamounts and remains stalled for tenths of millions of years (Motoki and Ballmer, 2015) before plume-like upwelling due to convective instability and ongoing thermochemical whole-mantle convection processes, it can reach the same degree of enrichment that we can observe in OIB magmatic suites.

This scenario was explored in Ulrich et al. (2012), where the authors discuss that the origin of the ubiquitous enrichment in EMORB signatures independently of the proximity, or the lack thereof, to a hotspot is related to a seamount recycling component that is pervasive in the upper mantle. The authors use seamount compositions from hotspot volcanic chains and seamounts formed at mid-ocean ridges (on and off-axis). In this study we use this precedent and expand to the recycling of non-plume related seamounts (i.e. PukaPuka, Japan Trench, Tuzo Wilson, Santa Rosa seamounts, etc). Hoernle et al. (2011) also considered the possibility that an enriched OIB-type recycled component, locally mixed with a D-MORB component is responsible for the

anomalous crustal thickness and enriched compositions of the Mid-Atlantic Ridge segment between Ascension and Bode Verde fracture zones.

Warren et al. (2009) used abyssal peridotites to assess for the isotopic composition of the upper mantle and showed that the length scales of the heterogeneities can be as small as <1km. Many of these small scale heterogeneities are related to small veins formed by recent melt crystallization instead of recycled oceanic crust. Thus, we suggest that the mixing between DMM and the non-plume seamount component should occur in a time lapse of 200 Ma to resemble the enriched signatures seen in intraplate settings such as Hawaii (Pietruszka et al., 2011), Louisville (Beier et al., 2011), Virginia (Mazza et al., 2014) and New Zealand (Hoernle et al., 2006). This is in good agreement with estimates from Dosso et al. (1999), Donnelly et al. (2004), and Ulrich et al. (2012), which suggested time constraints of ~250 Ma, ~300 Ma, and ~266-295 Ma, respectively. In addition, the age projections (Fig. 3.5 and 3.6) and the mixing plots (Fig. 3.7), suggest that recycling of these non-plume related seamounts may not be viable in the long term. A number of reasons can factor in the absence of the 500 Ma and 1000 Ma age projection enrichments in the observed range of OIB worldwide (e.g. vigor and velocity of mantle flow, density of the surrounding mantle, partial melting processes, slab stagnation, etc.). Nevertheless, from the perspective of our geochemical modelling results we interpret that the survival of non-plume seamount heterogeneities may be dependable of two scenarios (Fig. 3.8): 1. If the subducting slab carrying the seamounts stagnates at the transition zone or deeper (~660 to 1000 km; Ballmer et al., 2015) and by means of convective instability, rises with the recycled seamount heterogeneities in a time range of <200 Ma. 2. If the slab sinks further below the transition zone and the shallower upper mantle, reaching the core-mantle boundary where, either, the heterogeneity signature becomes diluted and mixed with older reservoirs or stagnates for billions

of years. In this latter scenario is probable that the signature of the seamounts becomes lost to the mantle stirring processes. Therefore, considering estimates of mantle overturn (hereafter, understood as the time needed for a subducted slab to reach the core-mantle boundary and return back to the surface) which can be as long as 250 to 750 Ma (Kellogg et al., 2002), or 400 to 500 Ma (Tackley, 2000), we interpret that a seamount-province reservoir would only survive if it remains in the upper mantle where the timing of recycling is shorter.

Although we cannot rule out preexisting upper mantle heterogeneities, the existence of small pockets of enriched recycled material that are constantly being subducted, mechanically mixed, and convectively transported along with upper mantle flow currents may explain the geochemical variations in MORB (EMORB vs. NMORB) and in OIB from intraplate magmatism both related and unrelated to deep mantle upwellings. Once in the upper mantle, a seamount reservoir can be potentially tapped by a mantle plume and incorporated to the range of compositions observed in locations like Hawaii or Louisville (Arndt et al., 1997). Nevertheless, locations where magmatism occurs in relation to upper mantle processes like delamination, and shear- and edge-driven convection decompression melting may be favorable environments for resurfacing recycled seamounts signatures.

6. Conclusions

Countless non-plume related seamounts can be identified in the seafloor throughout the Earth's oceans. Even though they are low volume volcanic edifices, once they become subducted at plate convergent margin, they are incorporated into the mantle as heterogeneities of an originally enriched composition. By modeling their isotopic enrichments in time, our data shows that in periods of time of ~200 to 500 Ma a heterogeneity originated from a seamount can reach highly

radiogenic signatures similar to values found in other OIB occurrences globally. This is remarkably less time than needed to reach HIMU-type values by recycling altered oceanic crust or continental crust (~1-2 Ga) thus raising the possibility that seamounts may play an important role in the formation of enriched mantle reservoirs.

However, the timing and composition suggest that these small scaled heterogeneities only survive in the upper mantle, given that the evolution of such reservoirs become extremely enriched in long periods of time (>500 Ma) towards values that we have not seen in nature yet. Nevertheless, subducted slabs do sink past the transition zone, most likely carrying with them the fragments of subducted seamounts. The survival of these heterogeneities in the lower mantle is an unknown and further research would be needed to assess their fate.

A highly heterogeneous upper mantle may be a norm rather than an exception. At tectonic settings like MORs and hotspots the degrees of partial melting may be masking or diluting the geochemical signal of these small-scale pockets of recycled material. Nevertheless, both MOR and hotspots have been heavily sampled in the past, hence the false impression that these heterogeneities are uncommon. A thorough research and sampling of non-plume related magmatism will be needed to characterize the nature of these low-volume ubiquitous reservoir.

7. References

Aggrey, K.E., Muenow, D.W. and Batiza, R., 1988. Volatile abundances in basaltic glasses from seamounts flanking the East Pacific Rise at 21 N and 12–14 N. Geochimica et Cosmochimica Acta, 52(8): 2115-2119.

Allan, J., Batiza, R. and Sack, R., 1994. Geochemical characteristics of Cocos Plate seamount lavas. Contributions to Mineralogy and Petrology, 116(1-2): 47-61.

Allan, J.F., Batiza, R., Perfit, M.R., Fornari, D.J. and Sack, R.O., 1989. Petrology of lavas from the Lamont seamount chain and adjacent East Pacific Rise, 10 N. Journal of Petrology, 30(5): 1245-1298.

Allan, J.F., Chase, R.L., Cousens, B., Michael, P.J., Gorton, M.P. and Scott, S.D., 1993. The Tuzo Wilson volcanic field, NE Pacific: Alkaline volcanism at a complex, diffuse, transform-trench-ridge triple junction. Journal of Geophysical Research: Solid Earth (1978–2012), 98(B12): 22367-22387.

Arndt, N.T., Kerr, A.C. and Tarney, J., 1997. Dynamic melting in plume heads: the formation of Gorgona komatiites and basalts. Earth and Planetary Science Letters, 146(1–2): 289-301.

Ballmer, M.D., Conrad, C.P., Smith, E.I. and Harmon, N., 2013. Non-hotspot volcano chains produced by migration of shear-driven upwelling toward the East Pacific Rise. Geology, 41(4): 479-482.

Ballmer, M.D., Schmerr, N.C., Nakagawa, T. and Ritsema, J., 2015. Compositional mantle layering revealed by slab stagnation at ~1000-km depth. Science Advances, 1(11).

Bandini, A.N., Baumgartner, P.O., Flores, K., Dumitrica, P. and Jackett, S.-J., 2011. Early Jurassic to early Late Cretaceous radiolarians from the Santa Rosa accretionary complex (northwestern Costa Rica). Ofioliti, 36(1): 1-35.

Batiza, R. and Vanko, D., 1984. Petrology of Young Pacific Seamounts. Journal of Geophysical Research: Solid Earth, 89(B13): 11235-11260.

Baumgartner, P. and Denyer, P., 2006. Evidende for middle Cretaceous accretion at Santa Elena Peninsula (Santa Rosa Accretionary Complex), Costa Rica. Geologica Acta, 4(1-2): 179-191.

Beier, C., Vanderkluysen, L., Regelous, M., Mahoney, J.J. and Garbe-Schönberg, D., 2011. Lithospheric control on geochemical composition along the Louisville Seamount Chain. Geochemistry, Geophysics, Geosystems, 12(9).

Brandl, P.A., Beier, C., Regelous, M., Abouchami, W., Haase, K.M., Garbe-Schönberg, D. and Galer, S.J.G., 2012. Volcanism on the flanks of the East Pacific Rise: Quantitative

constraints on mantle heterogeneity and melting processes. Chemical Geology, 298–299: 41-56.

Buchs, D.M., Pilet, S., Cosca, M., Flores, K.E., Bandini, A.N. and Baumgartner, P.O., 2013. Low-volume intraplate volcanism in the Early/Middle Jurassic Pacific basin documented by accreted sequences in Costa Rica. Geochemistry, Geophysics, Geosystems, 14(5): 1552-1568.

Campbell, I.H., 2007. Testing the plume theory. Chemical Geology, 241(3): 153-176.

Castillo, P., Clague, D., Davis, A. and Lonsdale, P., 2010. Petrogenesis of Davidson Seamount lavas and its implications for fossil spreading center and intraplate magmatism in the eastern Pacific. Geochemistry, Geophysics, Geosystems, 11(2).

Chauvel, C. and Blichert-Toft, J., 2001. A hafnium isotope and trace element perspective on melting of the depleted mantle. Earth and Planetary Science Letters, 190(3): 137-151.

Conrad, C.P., Bianco, T.A., Smith, E.I. and Wessel, P., 2011. Patterns of intraplate volcanism controlled by asthenospheric shear. Nature Geosci, 4(5): 317-321.

Cousens, B., Dostal, J. and Hamilton, T., 1999. A near-ridge origin for seamounts at the southern terminus of the Pratt-Welker Seamount Chain, northeast Pacific Ocean. Canadian Journal of Earth Sciences, 36(6): 1021-1031.

Cousens, B.L., 1988. Isotopically depleted, alkalic lavas from Bowie Seamount, northeast Pacific Ocean. Canadian Journal of Earth Sciences, 25(10): 1708-1716.

Cousens, B.L., Chase, R.L. and Schilling, J.G., 1985. Geochemistry and origin of volcanic rocks from Tuzo Wilson and Bowie seamounts, northeast Pacific Ocean. Canadian Journal of Earth Sciences, 22(11): 1609-1617.

Danyushevsky, L.V., Eggins, S.M., Fallon, T.J. and Christie, D.M., 2000. H2O abundance in depleted to moderately enriched mid-ocean ridge magmas; part I: incompatible behaviour, implications for mantle storage, and origin of regional variations. Journal of Petrology, 41(8): 1329-1364.

Dasgupta, R. and Hirschmann, M.M., 2006. Melting in the Earth's deep upper mantle caused by carbon dioxide. Nature, 440(7084): 659-662.

Dasgupta, R., Hirschmann, M.M. and Smith, N.D., 2007. Partial melting experiments of peridotite + CO2 at 3 Gpa and genesis of alkalic Ocean Island Basalts. Journal of Petrology, 48(11): 2093-2124.

Davis, A.S., Clague, D.A., Bohrson, W.A., Dalrymple, G.B. and Greene, H.G., 2002. Seamounts at the continental margin of California: A different kind of oceanic intraplate volcanism. Geological Society of America Bulletin, 114(3): 316-333.

Davis, A.S., Gunn, S.H., Bohrson, W.A., Gray, L.-B. and Hein, J.R., 1995. Chemically diverse, sporadic volcanism at seamounts offshore southern and Baja California. Geological Society of America Bulletin, 107(5): 554-570.

DeMets, C., 2001. A new estimate for present-day Cocos-Caribbean plate motion: Implications for slip along the Central American volcanic arc. Geophysical Research Letters, 28(21): 4043-4046.

Denyer and Gazel, E., 2009. The Costa Rican Jurassic to Miocene oceanic complexes: Origin, tectonics and relations. Journal of South American Earth Sciences, 28: 429-442.

Desonie, D.L. and Duncan, R.A., 1990. The Cobb-Eickelberg seamount chain: Hotspot volcanism with mid-ocean ridge basalt affinity. Journal of Geophysical Research: Solid Earth, 95(B8): 12697-12711.

Donnelly, K.E., Goldstein, S.L., Langmuir, C.H. and Spiegelman, M., 2004. Origin of enriched ocean ridge basalts and implications for mantle dynamics. Earth and Planetary Science Letters, 226(3–4): 347-366.

Dosso, L., Bougault, H., Langmuir, C., Bollinger, C., Bonnier, O. and Etoubleau, J., 1999. The age and distribution of mantle heterogeneity along the Mid-Atlantic Ridge (31–41°N). Earth and Planetary Science Letters, 170(3): 269-286.

Eaby, J., Clague, D.A. and Delaney, J.R., 1984. Sr isotopic variations along the Juan de Fuca Ridge. Journal of Geophysical Research: Solid Earth, 89(B9): 7883-7890.

Fornari, D.J., Perfit, M.R., Allan, J.F., Batiza, R., Haymon, R., Barone, A., Ryan, W.B.F., Smith, T., Simkin, T. and Luckman, M.A., 1988. Geochemical and structural studies of the Lamont seamounts: seamounts as indicators of mantle processes. Earth and Planetary Science Letters, 89(1): 63-83.

French, S.W. and Romanowicz, B., 2015. Broad plumes rooted at the base of the Earth's mantle beneath major hotspots. Nature, 525(7567): 95-99.

Frisch, W., Meschede, M. and Sick, M., 1992. Origin of the Central American ophiolites: Evidence from paleomagnetic results. Geological Society of America Bulletin, 104(10): 1301-1314.

Gale, A., Dalton, C.A., Langmuir, C.H., Su, Y. and Schilling, J.-G., 2013. The mean composition of ocean ridge basalts. Geochemistry Geophysics Geosystems, 14(3): 489-518.

Garapić, G., Jackson, M.G., Hauri, E.H., Hart, S.R., Farley, K.A., Blusztajn, J.S. and Woodhead, J.D., 2015. A radiogenic isotopic (He-Sr-Nd-Pb-Os) study of lavas from the Pitcairn hotspot: Implications for the origin of EM-1 (enriched mantle 1). Lithos, 228–229: 1-11.

Geldmacher, J., Hoernle, K., van den Bogaard, P., Hauff, F. and Klügel, A., 2008. Age and Geochemistry of the Central American Forearc Basement (DSDP Leg 67 and 84): Insights into Mezosoic Arc Volcanism and Seamount Accretion on the Fringe of the Caribbean LIP. Journal of Petrology, 49(10): 1781-1815.

Graham, D.W., Zindler, A., Kurz, M.D., Jenkins, W.J., Batiza, R. and Staudigel, H., 1988. He, Pb, Sr and Nd isotope constraints on magma genesis and mantle heterogeneity beneath young Pacific seamounts. Contributions to Mineralogy and Petrology, 99(4): 446-463.

Haase, K.M. and Devey, C.W., 1994. The Petrology and Geochemistry of Vesteris Seamount, Greenland Basin—an Intraplate Alkaline Volcano of Non-Plume Origin. Journal of Petrology, 35(2): 295-328.

Hall, L., Mahoney, J., Sinton, J. and Duncan, R.A., 2006. Spatial and temporal distribution of a C-like asthenospheric component in the Rano Rahi Seamount Field, East Pacific Rise, 15–19 S. Geochemistry, Geophysics, Geosystems, 7(3).

Hauff, F., Hoernle, K., van den Bogaard, P., Alvarado, G. and Garbe-Schönberg, D., 2000. Age and geochemistry of basaltic complexes in western Costa Rica: Contributions to the geotectonic evolution of Central America. Geochemistry Geophysics Geosystems, 1.

Hegner, E. and Tatsumoto, M., 1989. Pb, Sr, and Nd isotopes in seamount basalts from the Juan de Fuca Ridge and Kodiak-Bowie Seamount Chain, northeast Pacific. Journal of Geophysical Research: Solid Earth, 94(B12): 17839-17846.

Hekinian, R., Francheteau, J., Armijo, R., Cogné, J., Constantin, M., Girardeau, J., Hey, R., Naar, D. and Searle, R., 1996. Petrology of the Easter microplate region in the South Pacific. Journal of Volcanology and Geothermal Research, 72(3): 259-289.

Hekinian, R., Thompson, G. and Bideau, D., 1989. Axial and off-axial heterogeneity of basaltic rocks from the East Pacific Rise at 12° 35′ N–12° 51′ N and 11° 26′ N–11° 30′ N. Journal of Geophysical Research: Solid Earth, 94(B12): 17437-17463.

Hémond, C., Hofmann, A.W., Vlastélic, I. and Nauret, F., 2006. Origin of MORB enrichment and relative trace element compatibilities along the Mid-Atlantic Ridge between 10° and 24°N. Geochemistry, Geophysics, Geosystems, 7(12): n/a-n/a.

Hillier, J.K. and Watts, A.B., 2007. Global distribution of seamounts from ship-track bathymetry data. Geophysical Research Letters, 34(13): n/a-n/a.

Hirano, N., 2011. Petit-spot volcanism: A new type of volcanic zone discovered near a trench. Geochemical Journal, 45(2): 157-167.

Hirano, N., Takahashi, E., Yamamoto, J., Abe, N., Ingle, S.P., Kaneoka, I., Hirata, T., Kimura, J.-I., Ishii, T. and Ogawa, Y., 2006. Volcanism in response to plate flexure. Science, 313(5792): 1426-1428.

Hoernle, K., Hauff, F., Kokfelt, T.F., Haase, K., Garbe-Schönberg, D. and Werner, R., 2011. On- and off-axis chemical heterogeneities along the South Atlantic Mid-Ocean-Ridge (5–11°S): Shallow or deep recycling of ocean crust and/or intraplate volcanism? Earth and Planetary Science Letters, 306(1–2): 86-97.

Hoernle, K., Hauff, F. and van den Bogaard, P., 2004. 70 m.y. history (136-69 Ma) for the Caribbean Large Igneous Province. Geological Society of America, 32(8): 697-700.

Hoernle, K., White, J.D.L., van den Bogaard, P., Hauff, F., Coombs, D.S., Werner, R., Timm, C., Garbe-Schönberg, D., Reay, A. and Cooper, A.F., 2006. Cenozoic intraplate volcanism on New Zealand: Upwelling induced by lithospheric removal. Earth and Planetary Science Letters, 248(1–2): 350-367.

Hofmann, A.W., 1997. Mantle geochemistry: the message from oceanic volcanism. Nature, 385: 219-229.

Hofmann, A.W. and White, W.M., 1982. Mantle plumes from ancient oceanic crust Earth and Planetary Science Letters, 57(421-436).

Irvine, T. and Baragar, W., 1971. A guide to the chemical classification of the common volcanic rocks. Canadian journal of earth sciences, 8(5): 523-548.

Jackson, M.G. and Dasgupta, R., 2008. Compositions of HIMU, EM1, and EM2 from global trends between radiogenic isotopes and major elements in ocean island basalts. Earth and Planetary Science Letters, 276: 175-185.

Jenner, F.E. and O'Neill, H.S.C., 2012. Analysis of 60 elements in 616 ocean floor basaltic glasses. Geochemistry, Geophysics, Geosystems, 13(2): n/a-n/a.

Johnson, M.K.T., 1998. Experimental determination of partition coefficients for rare earth and high-field-strength elements between clinopyroxene, garnet, and basaltic melt at high pressures. Contributions to Mineralogy and Petrology, 133(1): 60-68.

Jweda, J., Bolge, L., Class, C. and Goldstein, S.L., 2016. High Precision Sr-Nd-Hf-Pb Isotopic Compositions of USGS Reference Material BCR-2. Geostandards and Geoanalytical Research, 40(1): 101-115.

Kay, R.W. and Gast, P.W., 1973. The rare earth content and origin of alkali-rich basalts. The Journal of Geology: 653-682.

Kellogg, J.B., Jacobsen, S.B. and O'Connell, R.J., 2002. Modeling the distribution of isotopic ratios in geochemical reservoirs. Earth and Planetary Science Letters, 204(1): 183-202.

King, S.D. and Anderson, D.L., 1998. Edge-driven convection. Earth and Planetary Science Letters, 160(3–4): 289-296.

King, S.D. and Ritsema, J., 2000. African Hot Spot Volcanism: Small-Scale Convection in the Upper Mantle beneath Cratons. Science, 290(5494): 1137-1140.

Koppers, A.A., Staudigel, H., Christie, D.M., Dieu, J.J. and Pringle, M.S., 1995. Sr-Nd-Pb isotope geochemistry of leg 144 West Pacific guyouts: Implications for the geochemical evolution of the" SOPITA" mantle anomaly. Ocean Drilling Program.

Langmuir, C., Vocke, R., Hanson, G. and Hart, S., 1977. A general mixing equation: applied to the petrogenesis of basalts from Iceland and Reykjanes Ridge. Earth Planet. Sci. Lett., 37: 380-392.

Le Maitre, R.W., Bateman, P., Dudek, A., Keller, J., Lameyre, J., Le Bas, M., Sabine, P., Schmid, R., Sorensen, H. and Streckeisen, A., 1989. A classification of igneous rocks and glossary of terms: Recommendations of the International Union of Geological Sciences Subcommission on the Systematics of Igneous Rocks, 193. Blackwell Oxford.

Machida, S., Hirano, N. and Kimura, J.-I., 2009. Evidence for recycled plate material in Pacific upper mantle unrelated to plumes. Geochimica et Cosmochimica Acta, 73(10): 3028-3037.

Madrigal, P., Gazel, E., Denyer, P., Smith, I., Jicha, B., Flores, K.E., Coleman, D. and Snow, J., 2015. A melt-focusing zone in the lithospheric mantle preserved in the Santa Elena Ophiolite, Costa Rica. Lithos, 230(0): 189-205.

Mazza, S.E., Gazel, E., Johnson, E.A., Kunk, M.J., McAleer, R., Spotila, J.A., Bizimis, M. and Coleman, D.S., 2014. Volcanoes of the passive margin: The youngest magmatic event in eastern North America. Geology, 42(6): 483-486.

McDonough, W.F. and Sun, S.s., 1995. The composition of the Earth. Chemical Geology, 120(3–4): 223-253.

Meschede, M. and Frisch, W., 1994. Geochemical characteristics of basaltic rocks from the Central American ophiolites. Profil, 7: 71-85.

Morgan, W.J., 1971. Convection Plumes in the Lower Mantle. Nature, 230(5288): 42-43.

Motoki, M.H. and Ballmer, M.D., 2015. Intraplate volcanism due to convective instability of stagnant slabs in the mantle transition zone. Geochemistry, Geophysics, Geosystems, 16(2): 538-551.

Natland, J.H. and Winterer, E.L., 2005. Fissure control on volcanic action in the Pacific. Geological Society of America Special Papers, 388: 687-710.

Niu, Y. and O'Hara, M.J., 2003. Origin of ocean island basalts: A new perspective from petrology, geochemistry, and mineral physics considerations. Journal of Geophysical Research: Solid Earth, 108(B4).

Niu, Y., Regelous, M., Wendt, I.J., Batiza, R. and O'Hara, M.J., 2002. Geochemistry of near-EPR seamounts: importance of source vs. process and the origin of enriched mantle component. Earth and Planetary Science Letters, 199(3): 327-345.

Pearce, J.A., 2008. Geochemical fingerprinting of oceanic basalts with applications to ophiolite classification and the search for Archean oceanic crust. Lithos, 100: 14-48.

Pearce, J.A., 2014. Immobile Element Fingerprinting of Ophiolites. Elements, 10(2): 101-108.

Pietruszka, A.J., Keyes, M.J., Duncan, J.A., Hauri, E.H., Carlson, R.W. and Garcia, M.O., 2011. Excesses of seawater-derived 234 U in volcanic glasses from Loihi Seamount due to crustal contamination. Earth and Planetary Science Letters, 304(1): 280-289.

Ringwood, A.E., 1990. Slab-mantle interactions: 3. Petrogenesis of intraplate magmas and structure of the upper mantle. Chemical Geology, 82(0): 187-207.

Salters, V.J., Mallick, S., Hart, S.R., Langmuir, C.E. and Stracke, A., 2011. Domains of depleted mantle: New evidence from hafnium and neodymium isotopes. Geochemistry, Geophysics, Geosystems, 12(8).

Salters, V.J.M. and Stracke, A., 2004. Composition of the depleted mantle. Geochemistry, Geophysics, Geosystems, 5(5): Q05B07.

Schilling, J.-G., 1991. Fluxes and excess temperatures of mantle plumes inferred from their interaction with migrating mid-ocean ridges. Nature, 352(6334): 397-403.

Shimoda, G., Ishizuka, O., Yamashita, K., Yoshitake, M., Ogasawara, M. and Yuasa, M., 2011. Tectonic influence on chemical composition of ocean island basalts in the West and South Pacific: Implication for a deep mantle origin. Geochemistry, Geophysics, Geosystems, 12(7).

Sobolev, A.V., Hofmann, A.W., Kuzmin, D.V., Yaxley, G.M., Arndt, N.T., Chung, S.-L., Danyushevsky, L.V., Elliott, T., Frey, F.A., Garcia, M.O., Gurenko, A.A., Kamenetsky, V.S., Kerr, A.C., Krivolutskaya, N.A., Matvienkov, V.V., Nikogosian, I.K., Rocholl, A., Sigurdsson, I.A., Sushchevskaya, N.M. and Teklay, M., 2007. The Amount of Recycled Crust in Sources of Mantle-Derived Melts. Science, 316(5823): 412-417.

Stracke, A., Bizimis, M. and Salters, V.J.M., 2003. Recycling oceanic crust: Quantitative constraints. Geochemistry, Geophysics, Geosystems, 4(3): n/a-n/a.

Stracke, A., Hofmann, A.W. and Hart, S.R., 2005. FOZO, HIMU, and the rest of the mantle zoo. Geochemistry, Geophysics, Geosystems, 6(5).

Tackley, P.J., 2000. Mantle Convection and Plate Tectonics: Toward an Integrated Physical and Chemical Theory. Science, 288(5473): 2002-2007.

Thorne, M.S., Garnero, E.J. and Grand, S.P., 2004. Geographic correlation between hot spots and deep mantle lateral shear-wave velocity gradients. Physics of the Earth and Planetary Interiors, 146(1): 47-63.

Tournon, J., 1994. The Santa Elena Peninsula: an ophiolitic nappe and a sedimentary volcanic relative autochthonus. Profil, 7(7): 87-96.

Tournon, J. and Bellon, H., 2009. The southern Central America puzzle: cronology and structure a review. Revista Geológica de América Central, 40(40): 11-47.

Trela, J., Vidito, C., Gazel, E., Herzberg, C., Class, C., Whalen, W., Jicha, B., Bizimis, M. and Alvarado, G.E., 2015. Recycled crust in the Galápagos Plume source at 70 Ma: Implications for plume evolution. Earth and Planetary Science Letters, 425: 268-277.

Ulrich, M., Hémond, C., Nonnotte, P. and Jochum, K.P., 2012. OIB/seamount recycling as a possible process for E-MORB genesis. Geochemistry, Geophysics, Geosystems, 13(6): n/a-n/a.

Valentine, G.A. and Hirano, N., 2010. Mechanisms of low-flux intraplate volcanic fields—Basin and Range (North America) and northwest Pacific Ocean. Geology, 38(1): 55-58.

Verati, C., Lancelot, J. and Hékinian, R., 1999. Pb isotope study of black-smokers and basalts from Pito Seamount site (Easter microplate). Chemical geology, 155(1): 45-63.

Warren, J.M., Shimizu, N., Sakaguchi, C., Dick, H.J.B. and Nakamura, E., 2009. An assessment of upper mantle heterogeneity based on abyssal peridotite isotopic compositions. Journal of Geophysical Research: Solid Earth, 114(B12): B12203.

White, W.M., 2010. Oceanic island basalts and mantle plumes: the geochemical perspective. Annual Review of Earth and Planetary Sciences, 38: 133-160.

White, W.M., McBirney, A.R. and Duncan, R.A., 1993. Petrology and geochemistry of the Galápagos Islands: Portrait of a pathological mantle plume.

Willbold, M. and Stracke, A., 2006. Trace element composition of mantle end-members: Implications for recycling of oceanic and upper and lower continental crust. Geochemistry, Geophysics, Geosystems, 7(4): n/a-n/a.

Willbold, M. and Stracke, A., 2010. Formation of enriched mantle components by recycling of upper and lower continental crust. Chemical Geology, 276(3–4): 188-197.

Wood, D.A., Joron, J.-L. and Treuil, M., 1979. A re-appraisal of the use of trace elements to classify and discriminate between magma series erupted in different tectonic settings. Earth and Planetary Science Letters, 45(2): 326-336.

Workman, R.K., Hart, S.R., Jackson, M., Regelous, M., Farley, K.A., Blusztajn, J., Kurz, M. and Staudigel, H., 2004. Recycled metasomatized lithosphere as the origin of the Enriched Mantle II (EM2) end-member: Evidence from the Samoan Volcanic Chain. Geochemistry, Geophysics, Geosystems, 5(4): Q04008.

8. Figures

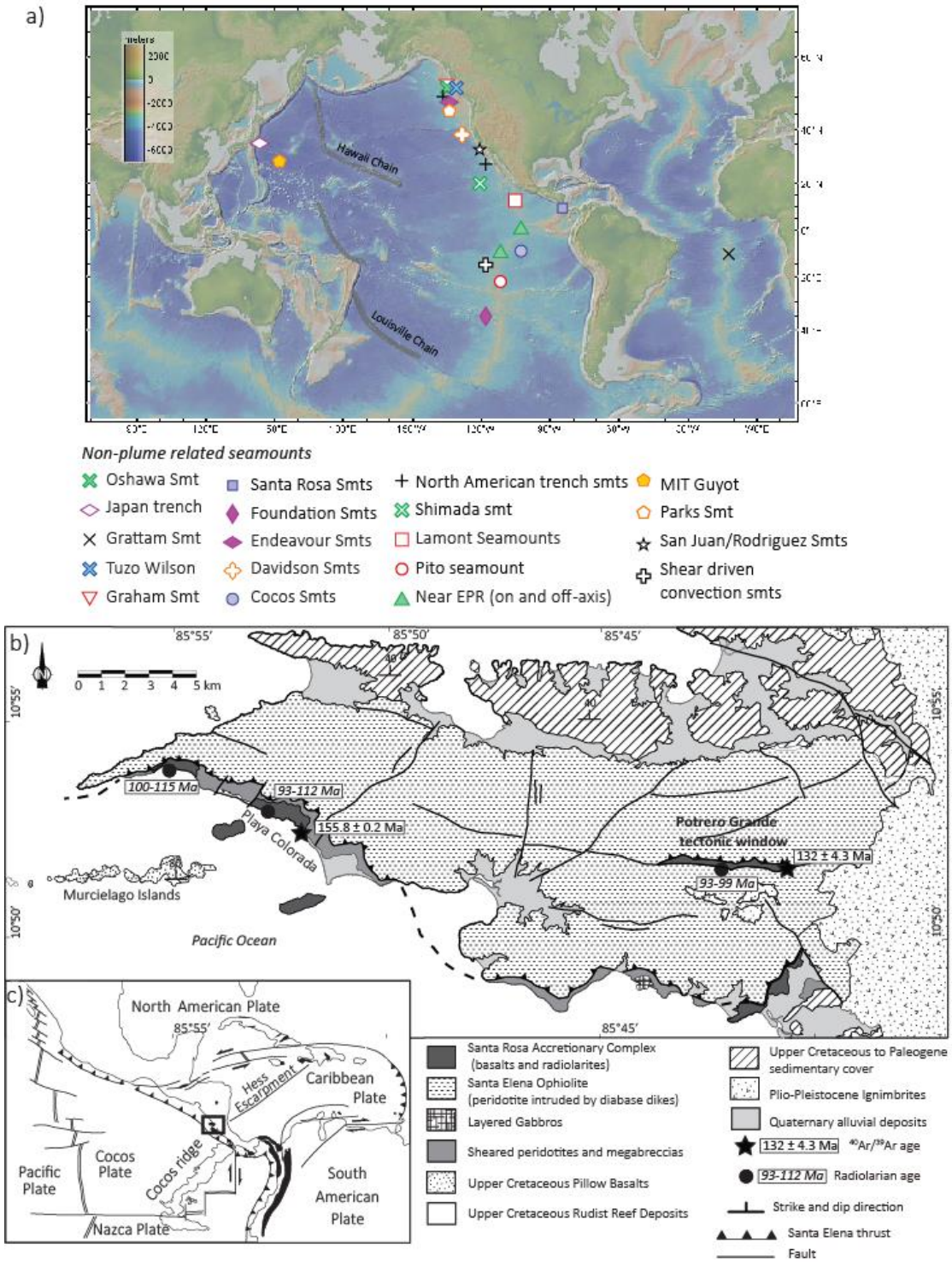

Figure 3.1. Location of non-plume related seamounts and the Santa Rosa accreted seamounts.a) Global map with the location of seamounts unrelated to deep mantle plumes. b) Geologic map of Santa Elena Peninsula, Costa Rica with sample location and ages. The circles represent show radiolarian ages (in italics) from Baumgartner and Denyer (2006) and Bandini et al. (2011). Map modified from Madrigal et al. (2015).

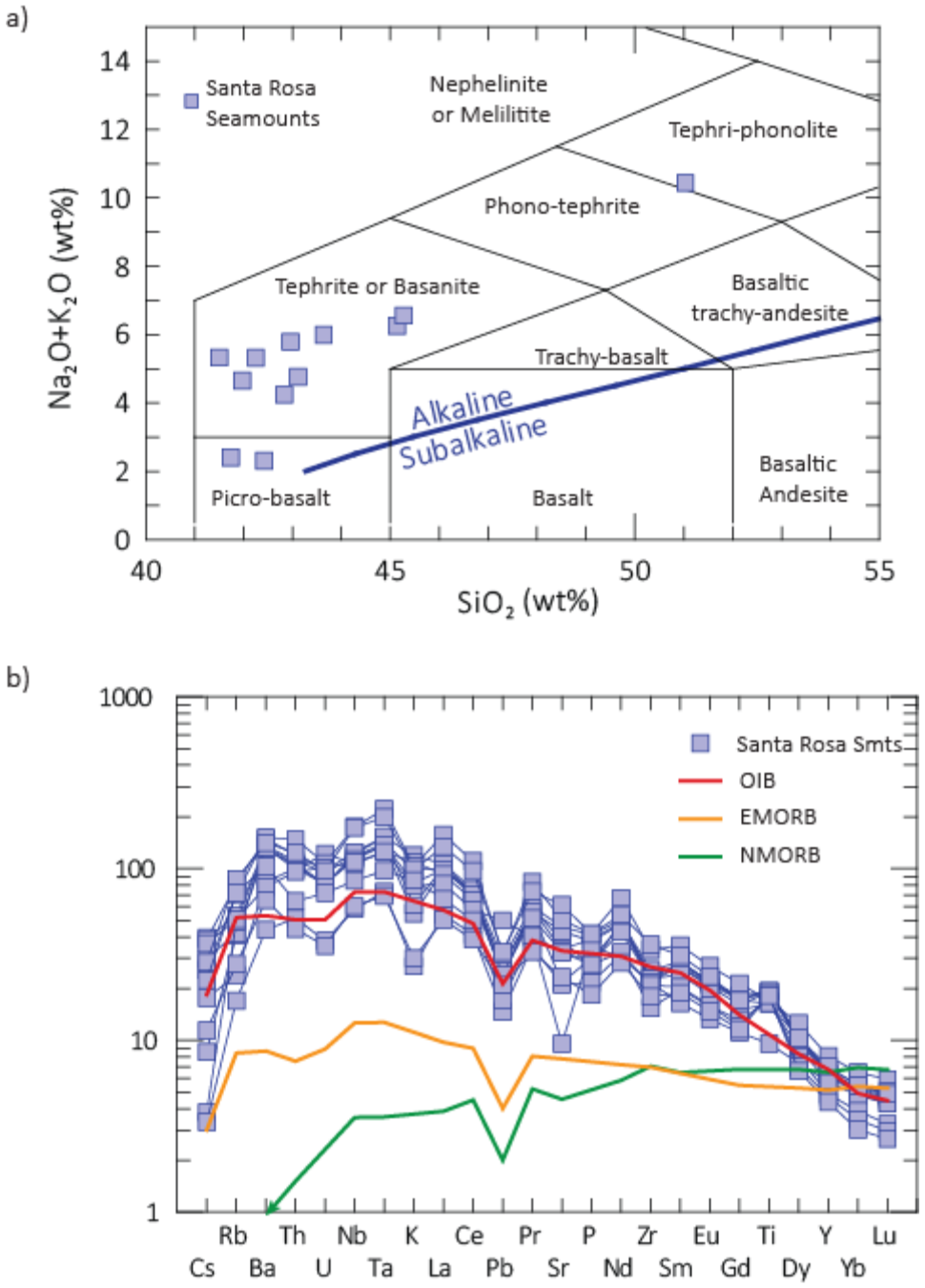

Figure 3.2. Geochemistry of the Santa Rosa alkaline seamounts. a) Total Alkalis vs silica (TAS) diagram for the Santa Elena Alkaline dikes (Le Maitre et al., 1989). Our samples compositions vary from picro-basalts to tephra-phonolite, however a vast majority plots within the basanite field. The blue line represents the alkaline-subalkaline division based on the work of Irvine and Baragar (1971). b) Trace element spider-diagram normalized to primitive mantle (McDonough and Sun, 1995) showing the composition of the Santa Rosa seamounts. Lines for NMORB (green), EMORB (yellow) and OIB (red) compositions are shown for comparison. Note the enrichments in LREE (Nb, Ta) and the depletion in HREE, indicative of presence of garnet in the source.

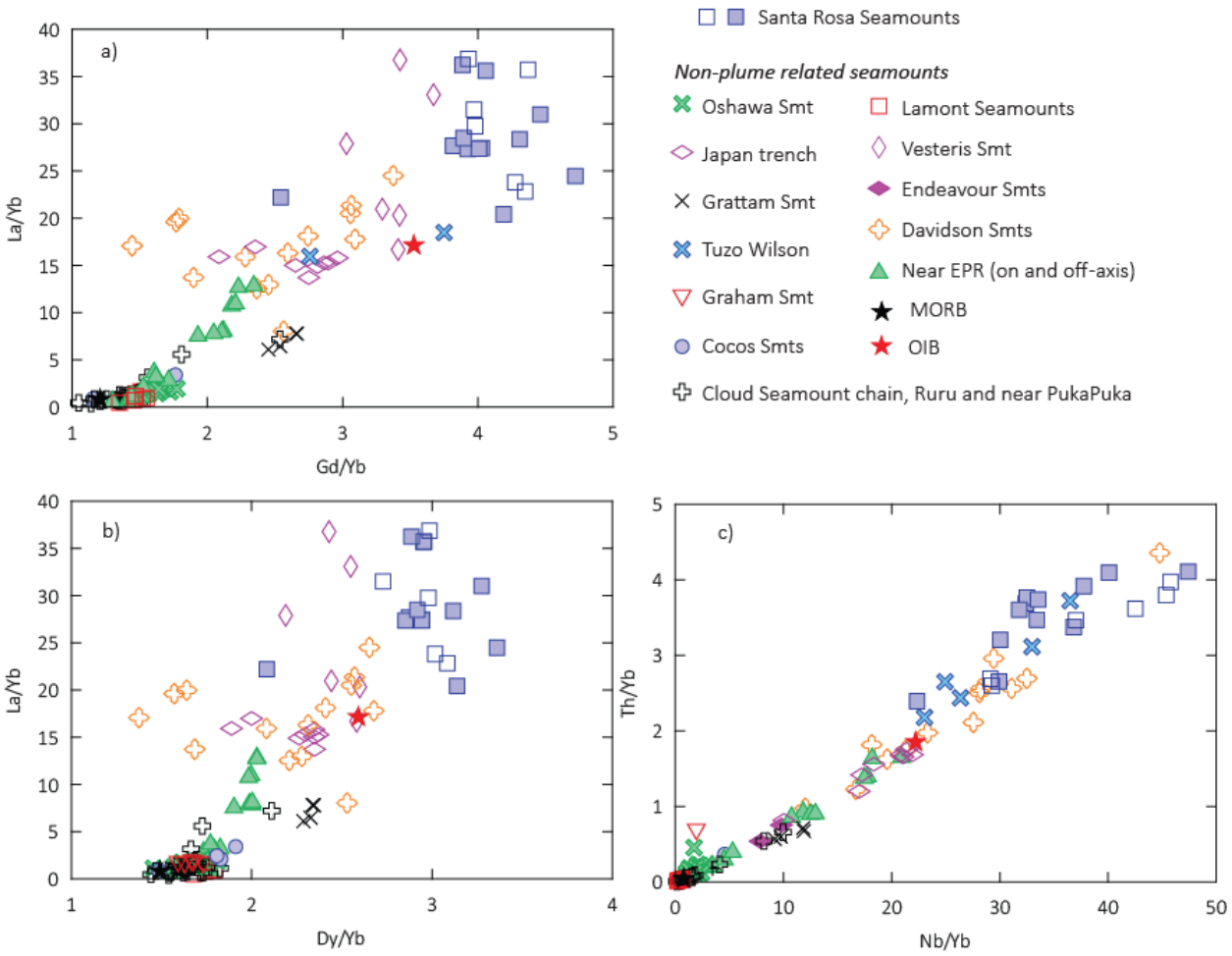

Figure 3.3. Trace element ratios for the non-plume related seamounts and the Rosa alkaline basalts. Ratios of La/Yb against Gd/Yb (a) and Dy/Yb (b) suggest the presence of garnet in the source since Yb is fractionated from the MREE during melting. (c) In the discrimination diagram of Th/Yb vs. Nb/Yb (Pearce, 2008) the Santa Rosa alkaline basalts plot in the field of OIB., towards the more enriched section of the mantle array. Note how the Santa Rosa seamounts show a marked enrichment in comparison to other non-plume related seamounts, though, sharing similarities with the Vesteris, Davidson and Tuzo Wilson seamounts.

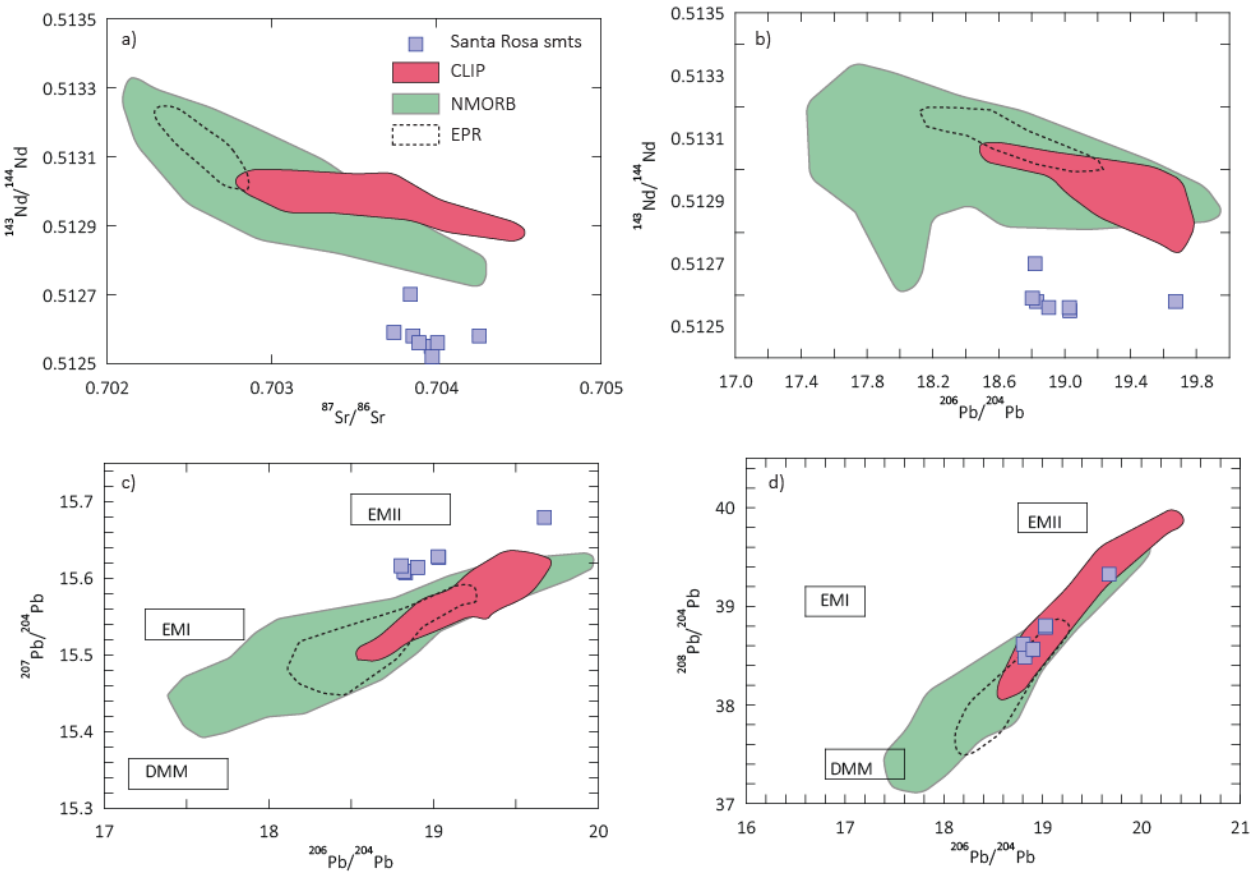

Figure 3.4. Measured isotope ratios for the Santa Rosa alkaline basalts. Values for MORB and EPR (Gale et al., 2013) as well as values for the Caribbean Large Igneous Province (CLIP) (Hauff et al., 2000; Hoernle et al., 2004; Trela et al., 2015) are outlined for comparison. Our data points plot close to an EMII reservoir and trend towards a HIMU-like reservoir. a). In $^{143}Nd/^{144}Nd$ vs. $^{87}Sr/^{86}Sr$ the Santa Rosa alkaline basalts show lower values of $^{143}Nd/^{144}Nd$ and similar contents of $^{87}Sr/^{86}Sr$ compared to MORB and the CLIP. The spread in the $^{87}Sr/^{86}Sr$ may be due to low degrees of seafloor alteration. b) In $^{143}Nd/^{144}Nd$ vs. $^{206}Pb/^{204}Pb$ space, the Santa Rosa alkaline basalts show similar $^{206}Pb/^{204}Pb$ contents as the more enriched suites of MORB and the CLIP, but at lower $^{143}Nd/^{144}Nd$ contents. c) In $^{207}Pb/^{204}Pb$ vs. $^{206}Pb/^{204}Pb$ our data show a more radiogenic Pb-isotopes trend than MORB and the CLIP. d) $^{208}Pb/^{204}Pb$ vs. $^{206}Pb/^{204}Pb$ show a similar behavior as the more enriched values of MORB and the CLIP.

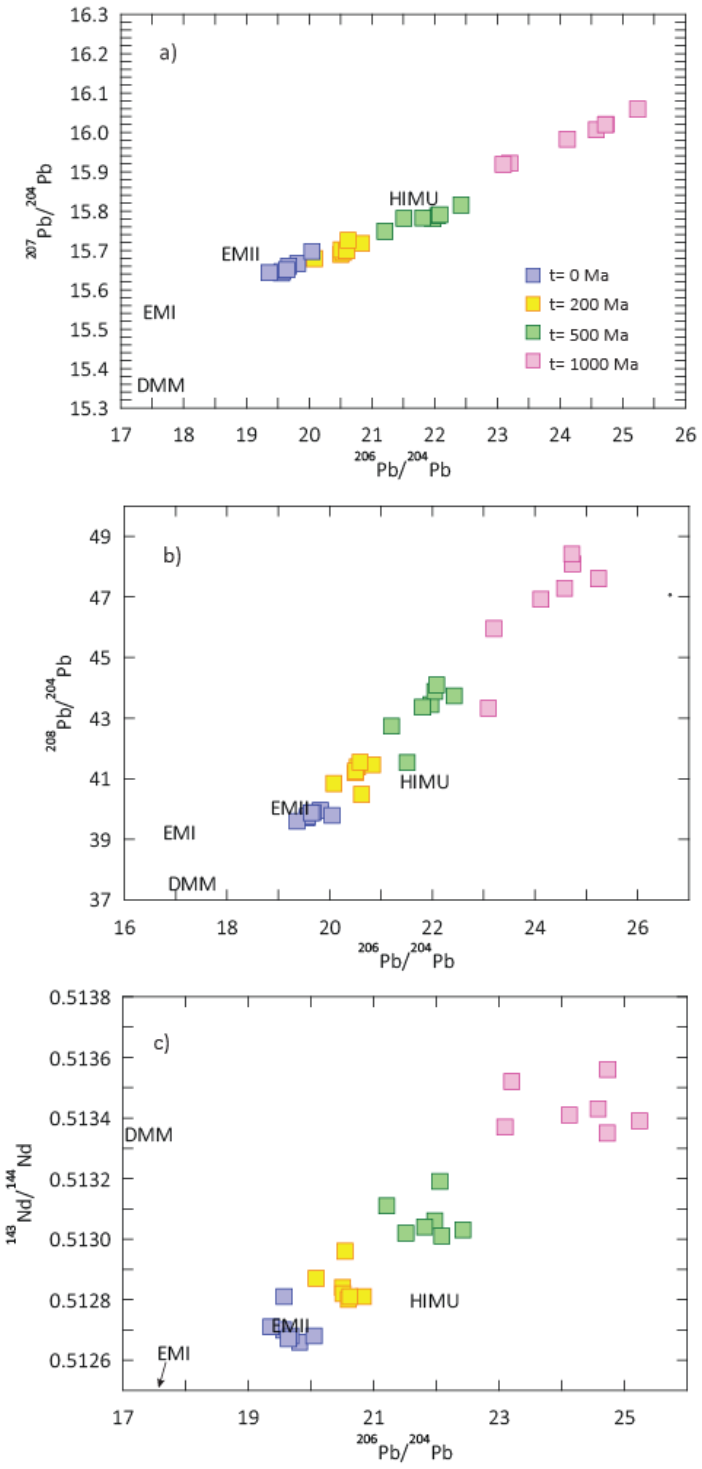

Figure 3.5. Isotopic evolution in time of the Santa Rosa seamounts. We projected the Santa Rosa isotope data in time (*t*= 200 Ma, *t*= 500 Ma, *t*= 1000 Ma) to assess for the enrichment of the seamounts during recycling. a) Using $^{207}Pb/^{204}Pb$ vs. $^{206}Pb/^{204}Pb$ systematics, the Santa Rosa alkaline seamounts start at values close to EMII and progress towards HIMU. b) $^{208}Pb/^{204}Pb$ vs. $^{206}Pb/^{204}Pb$. c) $^{143}Nd/^{144}Nd$ vs. $^{206}Pb/^{204}Pb$. Note that the data reach an enrichment similar to HIMU in a time lapse between 200 Ma and 500 Ma, however, at 1000 Ma the compositions evolve to values not found in nature thus far, suggesting that the recycling processes for this seamounts are not long-lived.

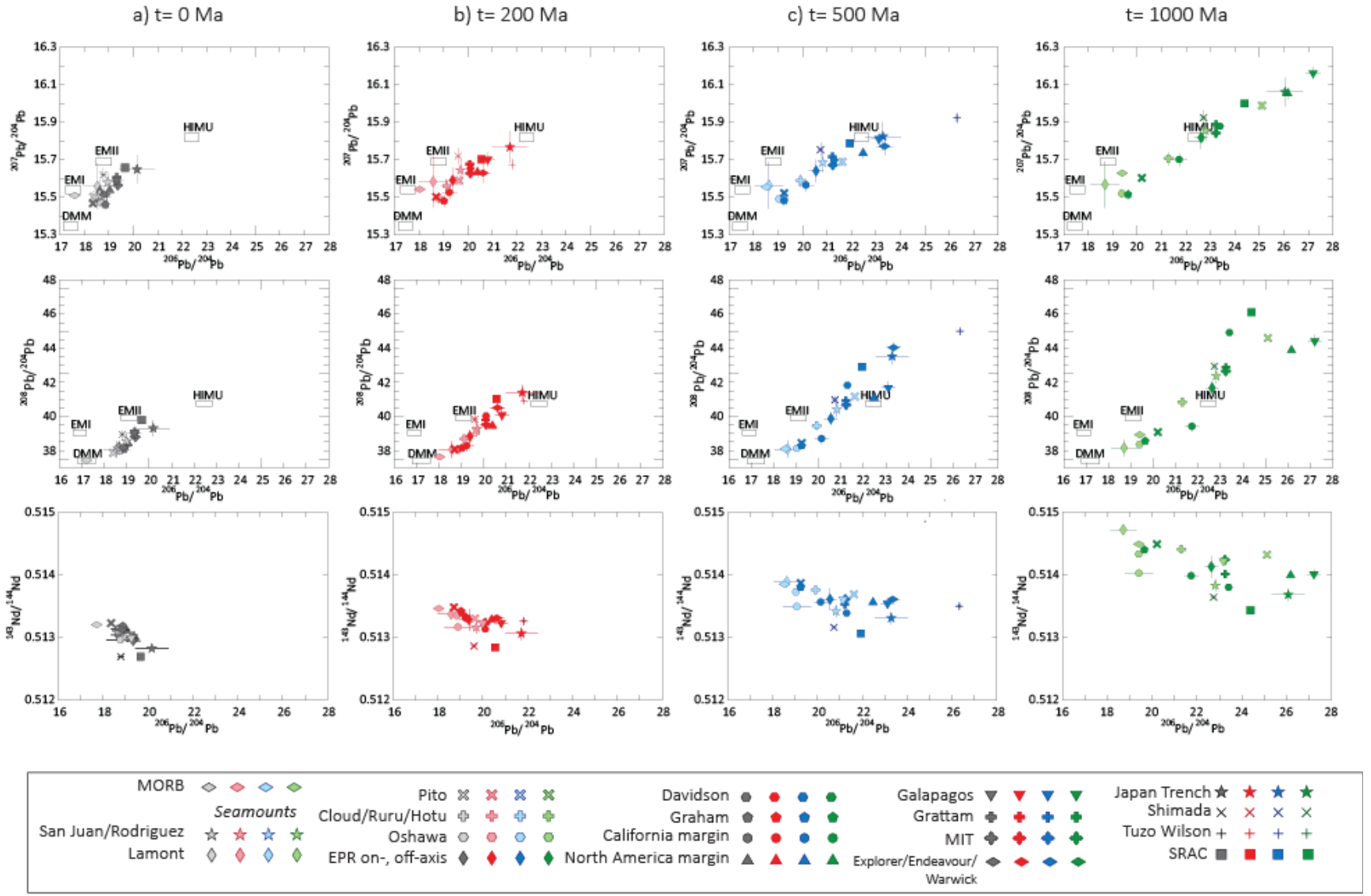
a) t= 0 Ma
b) t= 200 Ma
c) t= 500 Ma
t= 1000 Ma
HIMU
EMII
EMI
DMM
MORB
Seamounts
San Juan/Rodriguez
Lamont
Pito
Cloud/Ruru/Hotu
Oshawa
EPR on-, off-axis
Davidson
Graham
California margin
North America margin
Galapagos
Grattam
MIT
Explorer/Endeavour/ Warwick
Japan Trench
Shimada
Tuzo Wilson
SRAC

Figure 3.6. Isotope composition evolution in time for other non-plume related seamounts. Panels show the same isotope systems as in Figure 5 at a) t= 0 Ma, b) t= 200 Ma, c) t= 500 Ma, and d) t= 1000 Ma. Note that the evolution in the isotope compositions are similar to the Santa Rosa seamount enrichments, although many of the plotted seamounts start at less radiogenic compositions. Samples from Tuzo Wilson Seamount, Japan Trench petit-spot seamounts and seamounts in front of the North American Trench show the more similarities to the Santa Rosa seamounts.

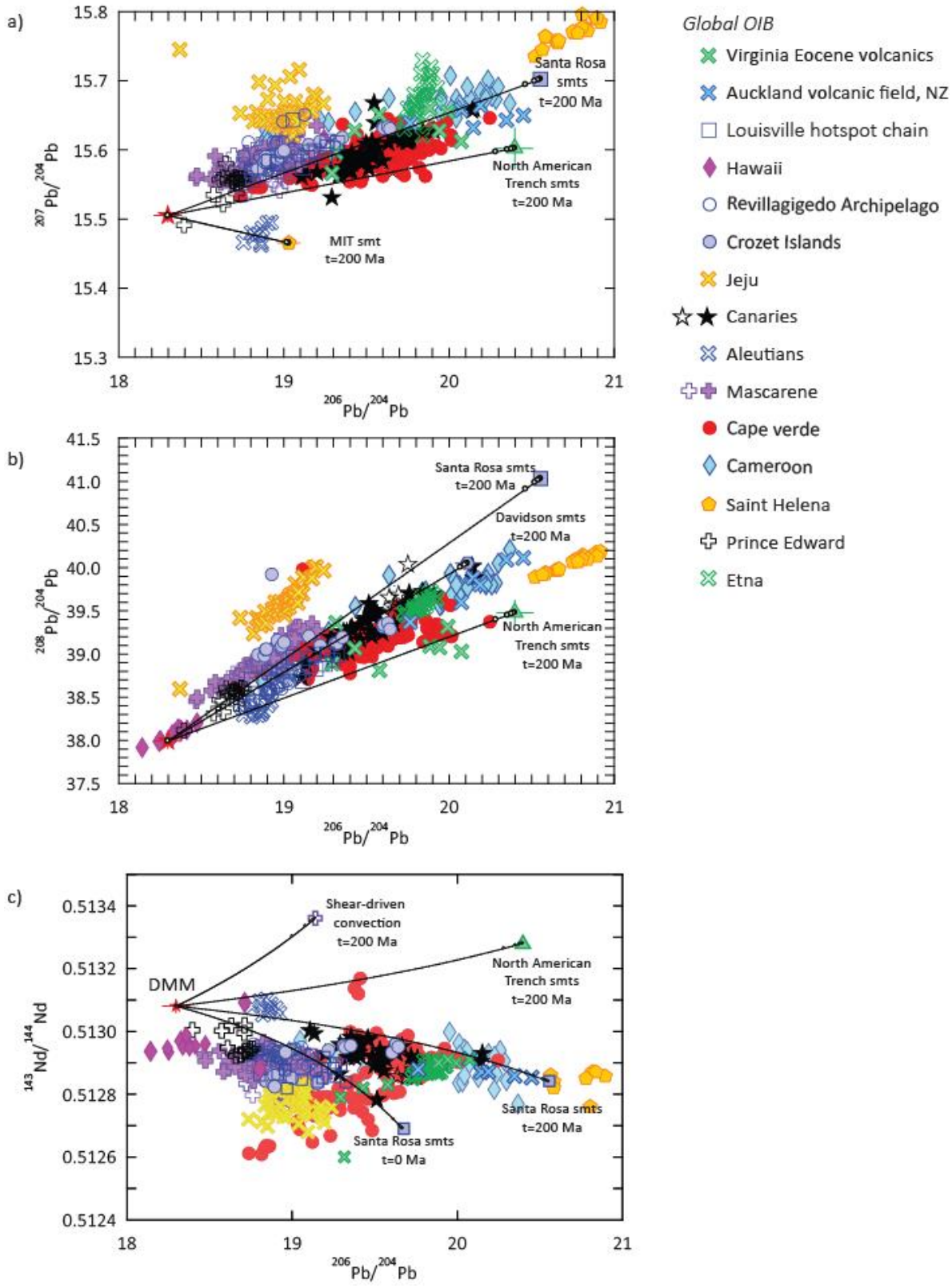

Figure 3.7. Binary mixing models using a depleted endmember (DMM) and seamounts projected data as an enriched endmember. a) In $^{207}Pb/^{204}Pb$ vs. $^{206}Pb/^{204}Pb$ the mixing lines between DMM and Santa Rosa

seamounts (t=200 Ma), and DMM and North American Trench seamounts (t= 200 Ma) successfully describe the enriched isotopic composition from global OIB (compiled from GEOROC and PetDB databases) like Cameroon Line, Virginia Eocene volcanics, Canaries, Louisville hotspot chain, and Cape Verde. b) The same applies for $^{208}Pb/^{204}Pb$ vs. $^{206}Pb/^{204}Pb$ where also, the mixing model between DMM and Davidson seamount (t= 200 Ma) describes well some of the OIB values. c) In $^{143}Nd/^{144}Nd$ vs. $^{206}Pb/^{204}Pb$ space, the models between North American Trench seamounts and shear-driven convection, with DMM do not recreate any of the global OIB however, the values of Santa Rosa at t= 0Ma and t= 200 Ma successfully model most OIB. Note that mixing models with projections at 500 Ma and 1000 Ma did not successfully recreate any of the OIB (not shown), thus, we interpret that the recycling times for the non-plume seamounts range between 200 Ma and 500 Ma.

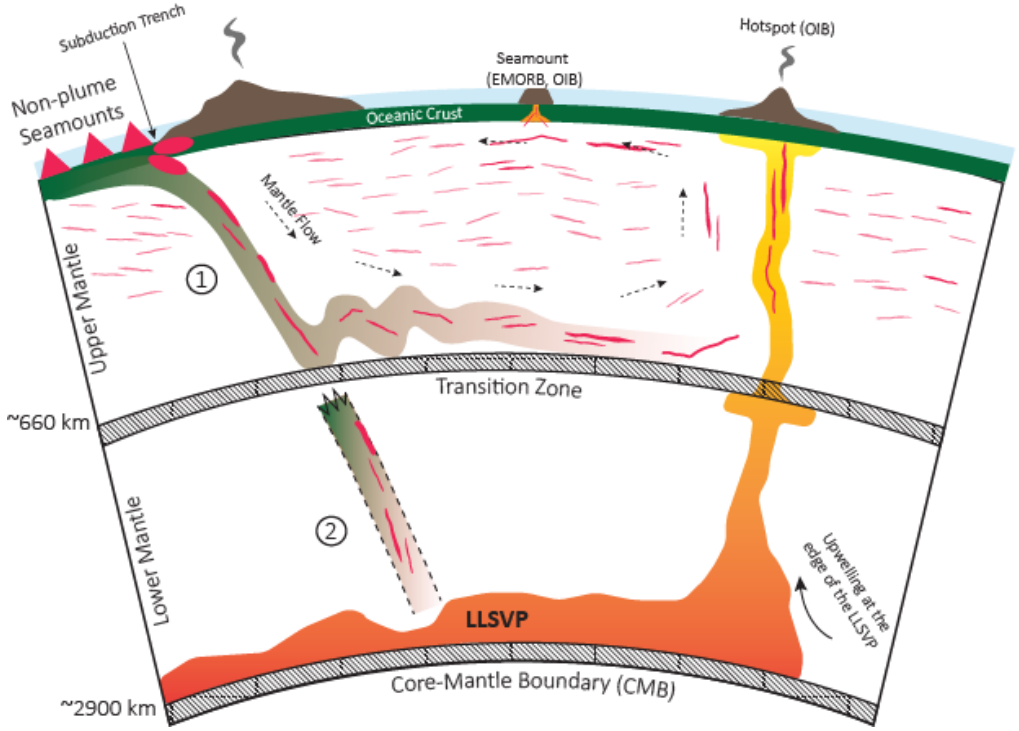

Figure 3.8. Recycling seamounts through subduction. Non-plume related seamounts traveling on top of oceanic crust arrive at a subduction trench where they become either subducted or accreted. The subducted material necessarily comprises small volumes (~1-5 km^3) thus, they become small-scaled heterogeneities travelling along with the subducted slab. When the slab arrives at the transition zone we could have two possible scenarios: 1) the slab becomes stagnant at the transition zone where, after tens of millions of years (Motoki and Ballmer, 2015), it starts upwelling due to convective instabilities that re-distributes the small-scale heterogeneities throughout the upper mantle where they can be tapped by deep mantle upwellings and/or by MORs. Or 2) the slab trespasses the transition zone and reaches the core-mantle boundary where the slab gets mechanically mixed with the surrounding reservoirs and the signature of the seamounts become diluted and lost.